Finite Element Studies and Experimental Validation of Asymmetric Incremental Sheet Forming of Extra Deep Drawing Steel

THESIS

Submitted in partial fulfilment

of the requirements for the degree of

DOCTOR OF PHILOSOPHY

by

KURRA SURESH

ID No 2009PHXF452H

Under the Supervision of

SRINIVASA PRAKASH REGALLA

BITS Pilani

Pilani | Dubai | Goa | Hyderabad

BIRLA INSTITUTE OF TECHNOLOGY AND SCIENCE, PILANI

2015

BIRLA INSTITUTE OF TECHNOLOGY AND SCIENCE, PILANI

CERTIFICATE

This is to certify that the thesis entitled "**Finite Element Studies and Experimental Validation of Asymmetric Incremental Sheet Forming of Extra Deep Drawing Steel**" and submitted by **KURRA SURESH** ID No. **2009PHXF452H** for award of Ph.D. degree of the Institute embodies original work done by him under my supervision.

Signature of the Supervisor:

Name in capital letters : **Prof. SRINIVASA PRAKASH REGALLA**

Designation : **Professor**

Date:

Acknowledgements

I wish to thank one and all who helped me to complete my Doctor of Philosophy degree in Mechanical Engineering. Firstly, I would like to express my sincere thanks to my advisor, Prof. Srinivasa Prakash Regalla for his support and guidance throughout the years of my Ph.D. program. His constant encouragement and timely guidance helped me sustain and write this thesis. I am grateful to my doctoral advisory committee members, Dr. Srinivas M and Dr. Jeevan Jaidi for their valuable advice during semester reviews.

I take this opportunity to thank Prof. Bijendra Nath Jain, Vice-Chancellor (BITS Pilani) and Prof. V.S. Rao, Director, Hyderabad campus, for allowing me to carry out my doctoral research in the institute.

I am thankful to Prof. S.K. Verma, Dean, Academic Research Division, BITS Pilani and Dr. Vidya Rajesh, Associate Dean, Academic Research Division, BITS Pilani, Hyderabad campus for their co-operation and encouragement at every stage of this work.

I would like to thank the Head of Department Mechanical Engineering Prof. YVD Rao for his kind support. I am thankful to all my colleagues of Mechanical department, Dr. Jalaiah, Dr. CP Kiran, Mr.Pavan, Mr. Nitin, Mr. Hussaini, Mr. Khalid and many others for the time they spent for me and for making my stay at the campus a memorable one. Thanks to Dr. Amit Kumar Gupta for reviewing some of my research papers and giving time slots to conduct experiments on CNC milling machine. I am also thankful to Dr. Deshmukh for his valuable suggestions during tough times.

I am really grateful to Prof. Neils Bay and Dr. Skojedt for sharing the HetoPac software for helical tool path generation. I would like to express my sincere gratitude to Prof. Swadesh Kumar Singh for his valuable suggestions and for providing the computational facility to run some of the simulations. Thanks to Dr. A Ramesh Babu, Dr. A Jagadeesh and colleagues and friends from other departments for their precious suggestions in my research work.

I am thankful to my friends Dr. Shankar Ganesh, Dr. Kurmayya, Dr. Jayakrishna, Dr. Gopi Krishna, Mr. Srihari, Ms. Rakhee, Ms. Prafulla and Mr. Koka Srikanth for their invaluable help and for the friendly ambience at BITS Pilani, Hyderabad campus. I am

very grateful to my friend Mr. Gopi Gopal for his valuable suggestions, advice and scientific discussions to conduct experiments and perform numerical simulations.

I am very thankful to Prof. Veeredhi Vasudeva Rao who groomed me in the early stage of my teaching career at SNIST. I would also like to thank Prof. Vasan who trained, encouraged and supported me to teach multi-section courses, especially Engineering Graphics with Auto CAD at BITS Pilani Hyderabad campus.

Thanks to the technical staff of workshop and Mechanical engineering department, especially Mr. Sridhar and Mr. Chandrasekhar for fabricating the forming rig and forming tools; Mr. Bhaskar and Mr. Narasimha for setting up the CNC milling machine for incremental forming experiments; Mr. Krishna Kumar and Mr. Mahindra Chari for preparing the blanks; Mr. Srinivas and Mr. Laxman for assisting in material testing; Mr. Jagadishwar Reddy and Mr. Suryanarayana for their assistance in surface roughness measurement; and Mr. Balreddy, Mr. Murali and Mr. Yadav for showing interest in my experimental works. I am also thankful to my students for their help in conducting experiments. Thanks to Mr. K Ramachandran Pillai for sparing his valuable time in proof reading some part of the thesis.

I would like to take this opportunity to thank my parents for their unconditional love and support at every stage of my life. I am always grateful and indebted for their indispensable service. I am also grateful to my grandparents who brought up and educated me in my childhood. My heartfelt thanks to my father-in-law and mother-in-law for their encouragement and inspiration to complete this task. I am also thankful to my brothers and brother-in-law for their support and understanding. Most importantly, I would like to express my deepest and dearest gratitude to my beloved family, my wife Anusha and my wonderful daughter Sri Sai Rithvika, for their support, patience, unflagging love, understanding and encouragement throughout my research.

I am always grateful and indebted to those great souls, who taught me the basic principles of human life. I am grateful to all my teachers from my childhood who is instrumental in reaching this position. Lastly, and above all, I would like to thank God Almighty; for all that he has given to me.

Kurra Suresh

Abstract

Incremental sheet forming (ISF) process has been identified as a potential and economically viable process for sheet metal prototypes and low volume production. The process is very flexible and can be carried out on a computer numerical control (CNC) milling machine, robots or specially designed machines for ISF applications. In this process, a flat sheet is held in a simple fixture and is deformed into required shape by a spherical-ended tool. The path of the tool is controlled by a part program generated using computer aided manufacturing (CAM) software. The main attractive features of this process are simple tooling, and better forming characteristics than the conventional sheet metal forming processes. The process can be carried out without any die or with a partial die setup, made up of low cost material, such as plastic or wood. The process has been demonstrated as a potential process for forming complex shapes, automotive service panels, head light casing and customized bio-medical parts, such as, ankle support, plate prosthesis, implants for arthroplasty, cranial implants etc.

Realizing the potential advantages of ISF process, the present thesis focused to investigate the behavior of Extra Deep Drawing (EDD) steel in ISF process. This material is widely used in automotive applications. The formability of EDD steel in terms of maximum formable wall angle has been evaluated using Varying wall Angle Conical Frustums (VWACF) and Varying Wall Angle Pyramidal Frustums (VEAPF). These geometries can minimize the number of experiments required for formability analysis as compared to constant wall angle conical and pyramidal frustums. The formability of the parts has also been evaluated using analytical forming limit curve and finite element simulations. The effect of process parameters on formability has been studied through systematic experiments.

The state of stresses and strains in incremental forming of VWACF and VWAPF parts have been studied through finite element simulations. The thickness distribution of these parts has been measured experimentally and compared with the results of finite element simulations. The changes in micro structure and micro-hardness due to incremental deformation have been studied through optical microscopic analysis and micro-Vickers hardness tester.

Along with the several advantages, ISF has its limitations in terms of part quality, dimensional accuracy and processing time. The experiments have been designed to understand the effect of process parameters on part quality in terms of surface roughness and manufacturing time. Mathematical models have been developed for surface roughness and manufacturing time using response surface methodology and soft computing techniques such as Artificial Neural Networks (ANN), Support Vector Regression (SVR) and Genetic Programming (GP). Optimization studies have been carried out using Genetic Algorithm (GA), Non-Sorted Genetic Algorithm – II (NSGA – II) and Grey Relational Analysis (GRA) to optimize the process performance.

The finite element simulations have been performed to understand the effect of process parameters and process mechanics. The simulations have been performed for line test, axi-symmetric part and some generalized part geometries. A methodology has been proposed to convert the part program into time-position data for finite element simulations. This procedure can enhance the accuracy of simulation results, as tool path in simulation is identical to the tool path used for the manufacturing of the part. One of the major problems with the simulations is the long processing time due to long tool paths. Different techniques, such as, time scaling, mass scaling and adaptive re-meshing strategy have been used to minimize the problems with long computational time. The consequence of these techniques on the results has been verified through a series of simulations and some guidelines have been established to carry out the numerical simulations within a reasonable time without sacrificing the accuracy.

Limited formability in single stage forming can be improved through multi-stage forming. Some preliminary studies have been performed to understand the deformation behavior of EDD steel in multi-stage incremental forming. Distribution of strains, thickness and geometric accuracy of parts in multi-stage forming has been analyzed through finite element simulations.

Keywords: Incremental forming, Finite element simulations, Formability, Thickness distribution, Surface roughness, Optimization, Multi-stage forming.

Table of Contents

List of Tables

List of Figures

List of Abbreviations

AISF	: Asymmetric incremental sheet forming
ANN	: Artificial neural network
ANOVA	: Analysis of variance
ASTM	: American Society for Testing and Materials
CAD	: Computer aided design
CAM	: Computer aided manufacturing
CNC	: Computer numerical control
DOE	: Design of experiments
EDD	: Extra deep drawing
FE	: Finite element
FFLC	: Fracture forming limit curve
FLC	: Forming limit curve
FLD	: Forming limit diagram
GA	: Genetic algorithm
GP	: Genetic programming
ISF	: Incremental sheet forming
MSIF	: Multi stage incremental forming
SPIF	: Single point incremental forming
SVR	: Support vector regression
TPIF	: Two point incremental forming
VWACF	: Varying wall angle conical frustum
VWAPF	: Varying wall angle pyramidal frustum

List of Symbols

e	: Engineering strain
E	: Youngs modulus
S	: Engineering stress
K	: Strength coefficient
n	: Strain hardening exponent
t_i	: Initial sheet thickness
t_f	: Final sheet thickness
ν	: Poisson's ratio
σ	: True stress
ε	: True strain
φ_{max}	: Maximum wall angle
$\varepsilon_1, \varepsilon_2, \varepsilon_3$	: Principal strains

Chapter 1 Introduction

1.1 Background and Motivation

Sheet metal forming is a major manufacturing process in many automobile and aerospace industries. Researchers developed many techniques over the years to form the sheet in to required shape for different applications. The manufacturing sector in 20th century focused mainly on mass production methods to reduce the manufacturing costs. Conventional sheet metal forming processes, such as, deep drawing and stamping have been very popular for mass production of sheet metal products till today. These techniques utilize heavy presses, complex dies and punches for manufacturing different sheet metal parts. In the 21st century, there is a drastic reduction in product life cycle, and many new products entered the market. Every new product requires prototype testing, and conventional mass production techniques are not economical for this due to its complex tooling and long processing times. Moreover, small batch production and custom specific production became a necessity in many industrial sectors. The industry demands intelligent, flexible and affordable technology to manufacture large complex parts in small batches with high accuracy and reproducibility.

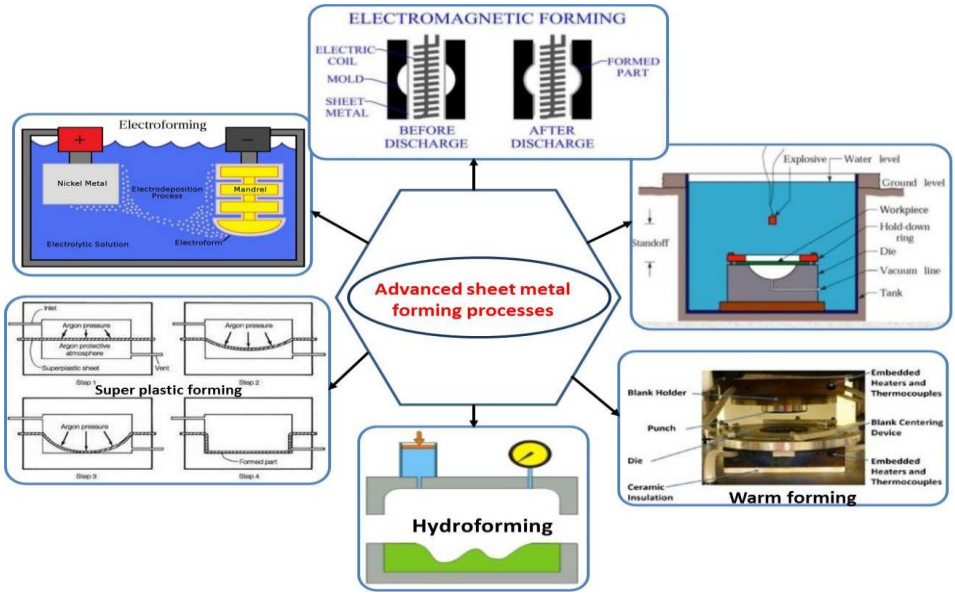

Fig. 1.1 Advanced sheet metal forming processes [Kalpakjian et al. (2009)]

Many new processes have been developed in the last decade to meet the demands from manufacturing sector (Fig. 1.1). Among them, incremental forming process seems to be promising technology for sheet metal prototyping and low volume production of complex parts. In this process, the blank is held by a simple frame and then subjected to plastic deformation locally by a punch with hemi-spherical end. The movement of the tool or the tool path is controlled by a CNC controller. During the forming process, tool moves in successive contours, this follows the final geometry and deforms the sheet into required shape incrementally. The complete computer control of tool movements enables the process as a viable option to produce complex sheet metal parts. Low setup cost, simple tooling, dieless nature and possibility to carry out the process on CNC machines, robots and parallel kinematic machines are attractive features of this process. The basic elements of incremental sheet forming are shown in Fig. 1.2.

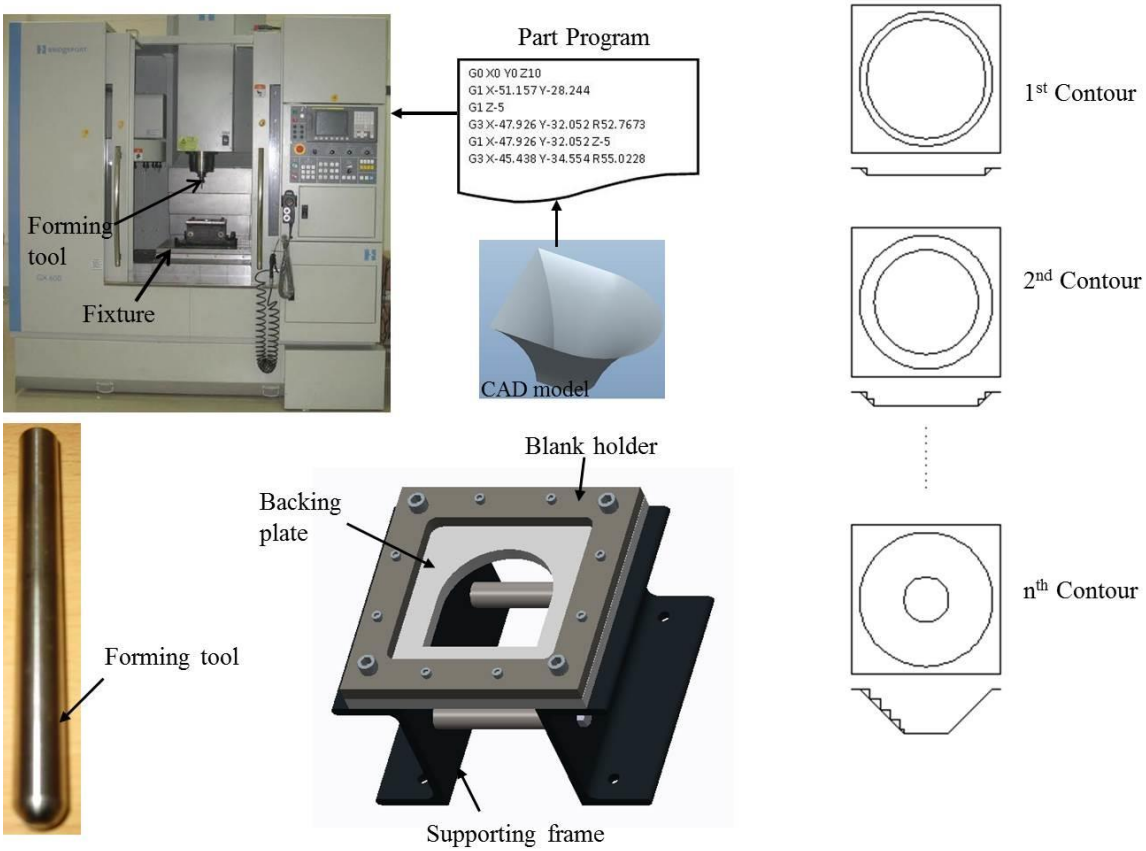

Fig. 1.2 Basic elements of incremental forming process

1.2 Incremental sheet forming

Incremental sheet forming (ISF) is a computer integrated forming technology based on layered manufacturing principles to produce complex 3-D sheet metal parts. The process is carried out on CNC milling machine with a fixture to hold the blank. The geometry of the part to be manufactured is modeled as a surface model in CAD software. In case of complex part geometries, CAD models are developed from the point cloud data collected using laser scanner. The developed model is then used to generate the profile tool path using CAM software. The tool path possesses number of contours with constant spacing between each contour. Spacing between the contours is called *step depth*. The hemispherical headed forming tool in the machine spindle moves along the generated tool trajectories and deforms the blank incrementally into the required shape of the product. The basic steps to produce the complex parts in ISF are shown in Fig. 1.3.

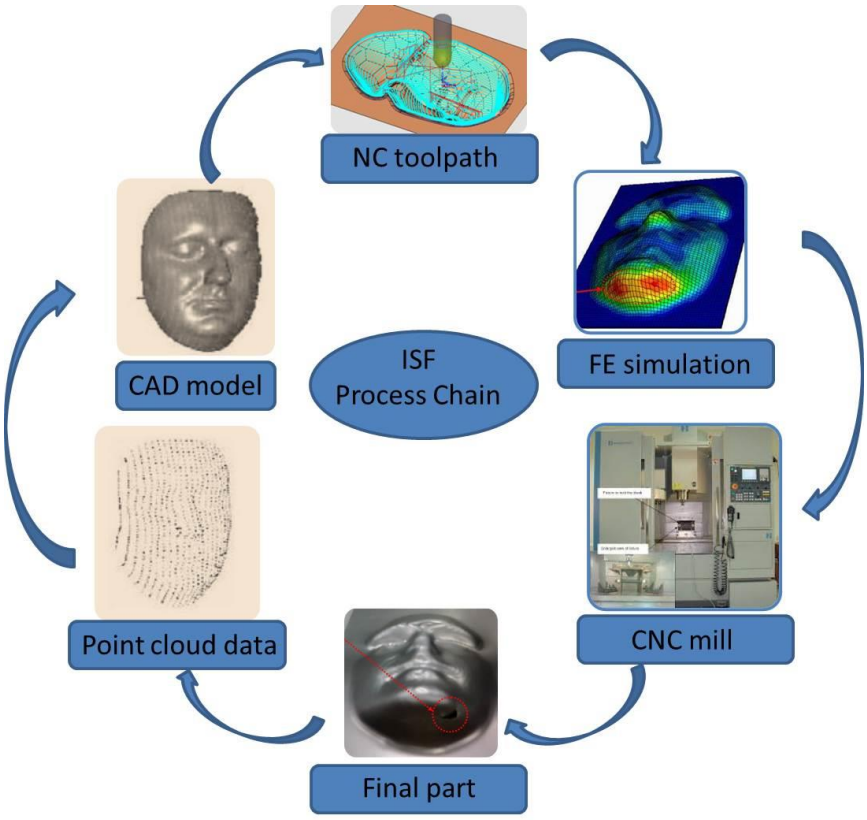

Fig. 1.3 ISF process chain

ISF processes are broadly classified in to two categories: (a) Symmetric Incremental Sheet Forming (SISF), and (b) Asymmetric Incremental Sheet Forming (AISF). Spinning and Shear Spinning are two well-known SISF processes in which only axi-symmetric features can be produced, whereas in recently innovated AISF process even asymmetric features can be produced. AISF is further classified into two types, Single Point Incremental Forming (SPIF) and Two Point Incremental Forming (TPIF). In SPIF the sheet is formed by a simple hemispherical punch without counter tools. In TPIF the sheet is formed by a hemispherical punch with partial or full support under the sheet. The process can be made more flexible by providing a counter tool that follows the top tool during forming. In SPIF the back surface of the sheet being deformed is a free unsupported surface. This creates different strain and stress patterns in the sheet as it is deformed, in contrast to TPIF. Due to this, the part quality is better in TPIF than in SPIF. Usually, a backing plate with appropriate opening is placed below the blank to improve accuracy and also to minimize the spring back in SPIF. Even though a support is used in TPIF, the process is still economical due to the fact that these supports are made of low cost material, such as, wood or resin. Different variants of AISF process are shown in Fig. 1.4.

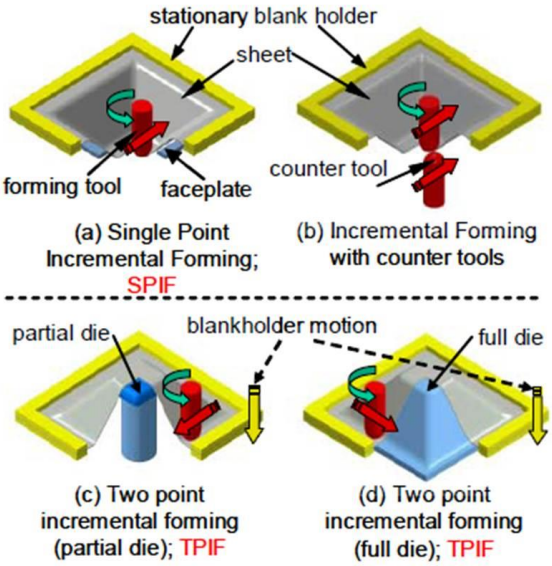

Fig. 1.4 Variants of AISF process [Jeswiet et al. (2005)]

Along with CNC machines, the process can also be carried out using robots and specially designed ISF machines. Step size, diameter of the tool, feed rate, rotational speed, thickness of the blank, friction between the punch and sheet, lubrication and tool path are some of the important process parameters in ISF process. These parameters can have significant effect on formability, surface roughness and final quality of products. Thus, a systematic study is essential to understand the effect of process parameters on forming to produce the product with required quality. Several experimental and finite element studies have been performed to understand the effect of process parameters on various aspects of ISF process and are described in subsequent chapters.

The major advantage with incremental forming is its die less nature and simple tooling. The formability of material in ISF is also far better than the conventional deep drawing and stamping processes. The process can be used for aluminum, steel, magnesium and titanium alloys. The process has potential applications in rapid prototyping, low volume production, bio-medical and automotive industries. Fig 1.5 shows some of the parts produced in ISF process. Limited geometric accuracy, low surface quality and long processing times are some of the limitations with ISF. However, these can be controlled to certain extent by careful selection of process parameters and compensation of expected deviations by modifying the imposed tool path.

Fig. 1.5 Applications of ISF process [Jeswiet et al. (2005); Pohlak (2007); Le Van Sy (2009); Skjodt et al. (2007) www.micromanufacturing.net]

1.3 Scope and Objectives of the study

Most of the studies in incremental forming were focused on aluminum and its alloys. Thus the focus of this thesis has been directed towards understanding of deformation behavior, formability, finite element simulations, surface quality and multi-pass forming of extra deep drawing steels.

Major objectives of this thesis are:

- Design and fabricate the fixture, forming tools and backing plates to carry out incremental forming experiments on CNC milling machine.
- Evaluate the mechanical properties and develop the material models to carry out finite element simulations.
- Perform preliminary simulations for the line test to understand the modeling of incremental forming process in LS-Dyna.
- Develop methodology to define the tool path for finite element simulations from the generated part programs using CAM software. This can enhance the flexibility to simulate any kind of geometry using finite element code.
- Understand the effect of process parameters on plastic strain, forming forces and thinning through finite element simulations. This provides a preliminary insight into the effect of process parameters before starting experiments.
- Study the effect of mass scaling, time scaling and adaptive meshing on the results of finite element simulations.
- Study the formability of EDD steel using varying wall angle conical and pyramidal frustums. Analyze microstructure, fracture and deformation behavior of formed parts. Validate the experimental results with finite element simulations.
- Develop the empirical models for surface roughness using RSM and soft computing techniques. Developed models are used for optimization using genetic algorithms and Taguchi based grey relational analysis.

- Investigate deformation behavior of EDD steel in multi-stage incremental forming using cylindrical shells. Perform finite element simulations to understand material flow and geometric accuracy of part.

The above goals have been achieved through carefully planned experiments, modeling and optimization procedures described in subsequent chapters of the thesis. Fig. 1.6 shows the overall research plan.

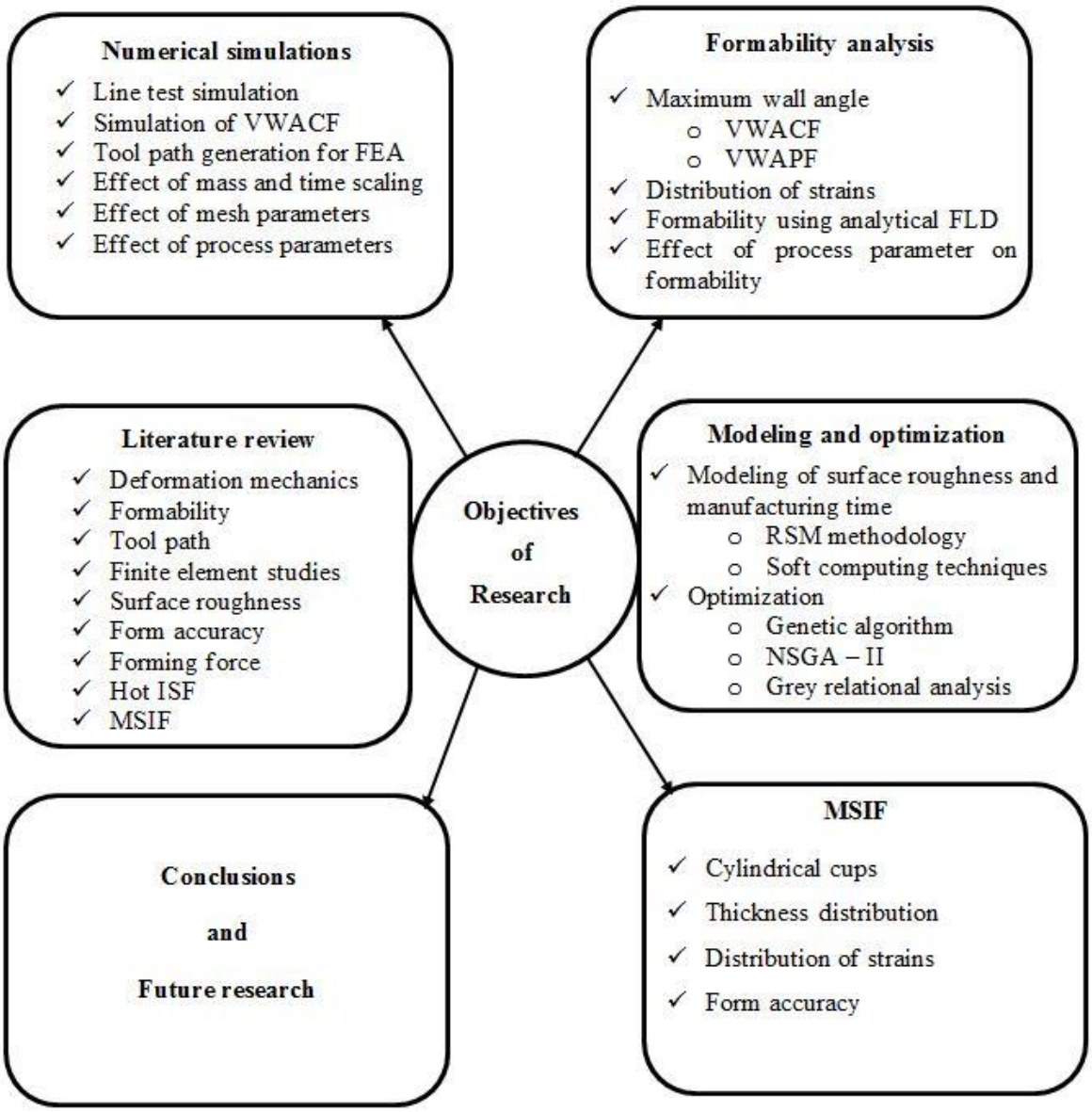

Fig. 1.6 Flowchart of overall research plan

1.4 Thesis organization

The thesis has been organized under seven chapters with the contents summarized as follows.

Chapter 1 emphasizes the importance of ISF process in the current manufacturing scenario. It describes different variants of ISF process, advantages, limitations and objectives of the current study.

Chapter 2 provides a systematic review on state-of-the-art in ISF. The literature in ISF has been organized in to six sections. It includes deformation mechanisms, formability, surface finish, form accuracy, tool path strategies, forming forces, multi-stage incremental forming and finite element simulations.

Chapter 3 presents the material characterization and preliminary simulations to understand the process mechanics. It describes the unique methodology to define the tool path for finite simulations of any complex geometry. The finite element simulations have been used to study the effect of different process parameters on selected response variables. It also discusses different methods to minimize computational time, which is the major problem in FE simulation of ISF process and studied the effect of these methods on the accuracy of simulation results.

Chapter 4 presents the formability and deformation behavior of EDD steel sheets in ISF. The study has been done using varying wall angle conical and pyramidal frustums. The effect of process parameters on formability and thickness distribution has been discussed. Further, the finite element simulations have been performed and validated with experimental results.

Chapter 5 focuses on surface roughness aspects of steel sheets in SPIF process. The effect of process parameters on surface roughness has been studied using Box-benkhen design of experiments. The surface roughness has been modeled using different soft computing techniques and response surface methodology. Further, the developed models have been used for single and multi-objective optimization using genetic algorithms. It also discusses the effect of process parameters on manufacturing time in SPIF.

Chapter 6 presents the studies related to deformation behavior of EDD steel in multi-stage incremental forming. Further, the finite element simulations have been

performed to understand the thickness distribution, distribution of strains and form accuracy of parts produced in multi-stage incremental forming.

Chapter 7 summarizes the key observations drawn from the studies discussed in this thesis. Some recommendations are also provided to extend this work to the next stage of research in future.

Chapter 2 Literature Review

Incremental forming process has got significant attention from both industry and academic institutes in the last decade. The main attractions of this process are its simple tooling and die less nature to produce complex parts from the sheet metal. Numerous papers have dealt with the process from several aspects. This chapter presents a detailed literature review on the state-of-the-art in ISF. The literature review covers studies related to deformation mechanisms, tool path generation, formability, surface roughness, geometric accuracy, forming forces, multi-stage forming and finite element studies in ISF process.

2.1 Tool path generation strategies

Tool path has significant effects on dimensional accuracy, surface roughness, processing time and thickness variation. Thus the tool path generation is an important step in incremental sheet forming (ISF). Three different methods have been used to generate the tool path for ISF in the literature (i) tool path generation using commercial CAM softwares, (ii) Cutter location (CL) based approach, and (iii) cutter contact (CC) based approach [Li et al. (2012b)]. Commercial CAM packages offer different tool paths for the machining application. One tool path among them suitable for ISF application is the profile tool path. In profile tool path, tool moves in one plane till it reaches its initial point. Thereafter it moves vertically downward direction by specified step depth. After reaching to next plane tool continues its motion in the same direction as that of earlier cycle. This process continues till the complete geometry is formed. Profile tool path can produce any complex geometry but it produces a scarring on the surface of the part. This scarring may not be permitted on parts which are aesthetically important. However, it can be minimized by diverting it to some converging surface or along the edges of the shape.

From the above view point, helical tool path is more suitable for ISF. This helical tool path completely eliminates the scarring on the surface of formed component and produces homogeneous thinning. In helical tool path, tool moves along the periphery while maintaining the gradual helix along the vertical direction (depth direction). The

distance from one point on the cycle to the corresponding point on the consecutive cycle is constant and is equal to step depth. Helical tool path option in CAM packages work with axi-symmetric objects only. To overcome this problem, Skjoedt et al. (2007) proposed a methodology to convert the profile tool path in to helical tool path. This program will generate the helical tool path for any geometry provided with its profile tool path.

Jadhav (2004) has observed twist and dent in parts formed using helical tool path. To overcome this problem, a bi-directional profile tool path has been suggested. This tool path is similar to profile tool path except that in each subsequent cycle the tool changes the direction of motion. This tool path minimizes twist and enhances geometric accuracy of the formed component. However it may not be possible to divert the scar mark to unimportant area in all cases. He also proposed bi-directional profile tool path with distributed increment, which is not in commercial CAM packages.

In the bi-directional tool path, tool completes a cycle and a quarter of tool path cycle is added before it moves to next cycle. By doing this, the position of tool changes from one cycle to another cycle and scar mark is not be visible on the part geometry. Moreover, by doing this, forming force distributes uniformly along the edge of the geometry and enhances the geometric accuracy of the part.

Blaga et al. (2011) investigated the influence of profile tool path, spiral tool path and radial tool path on strain distribution, relative thinning and forces in ISF. They observed homogeneous strain distribution and lower strain values with spiral tool path over other tool paths. Distribution of forces was also more homogeneous with spiral tool path without any local peaks and valleys. Silva et al. (2009) observed that the movement of tool (upward or downward) has significant influence on thickness distribution and feasibility of producing sound cylindrical cups with vertical walls in multistage ISF. Manco et al. (2011) considered tool path as a variable and optimized the tool path for minimum thinning. They analyzed the effect of four different tool trajectories *viz*. single slope, incremental slope, wall slope and decremental slope on thickness distribution. They found that there is a possibility to enhance the material formability by selecting appropriate tool trajectory. Azaouzi et al. (2012) optimized spiral tool path using

response surface methodology, sequential quadratic programming and finite element simulation. Their objective was to minimize the tool course subjected to the constraints on allowable thinning in the part.

Most of the researchers used machining tool paths available in commercial CAM packages for incremental forming. Some efforts were made to generate the tool path specifically for incremental forming from STL files [Li et al. (2012b), Jie et al. (2004)]. Malhotra et al. (2010) proposed a methodology to generate automatic spiral tool path with variable step depth for symmetric and asymmetric parts, by considering specified constraints on desired geometric accuracy and maximum specified scallop height while reducing the forming time. Rauch et al. (2009) proposed a new approach for tool path generation to improve accuracy of formed components. This new approach adapts the tool paths during the manufacturing of a part according to process data evaluations. Tool path adaptation was carried out by using CNC data. This ensures a high flexibility in incremental forming.

Attanasio et al. (2008) studied the effect of tool path on geometric accuracy, surface quality and thinning. They considered tool path with constant step depth and variable step depth with imposed scallop height. Lu et al. (2013) proposed feature-based tool path generation algorithm for incremental sheet forming process. In this algorithm, tool paths are generated according to specified critical edges. They tested the efficiency of proposed method with three case studies including a truncated cone with double bottoms, a non-symmetrical cone and a car fender. The results suggest that the new tool path stretches the sheet in a different way and resulted in different thickness distributions. Behera et al. (2013) used Multivariate Adaptive Regression Splines (MARS) as an error prediction tool to generate continuous error response surfaces for individual features and feature combinations. The predicted response surfaces have been used to generate compensated tool paths by systematically translating the individual vertices in a triangulated surface model of the part available in STL file format orthogonal to the surface of the CAD model, and using the translated model to generate the optimized tool paths. Paniti et al. (2014) presented a methodology for tool path generation of two point incremental forming with eccentric upper tool.

2.2 Deformation analysis

The deformation within single-point incremental forming occurs in a small region around the area of contact. Iseki (2001) studied the deformation of material in ISF by approximate calculation method based on plane-strain deformation model. The prediction by approximate deformation model and FE model was in good agreement with experimental results. Martins et al. (2008) presented the first closed-form analytical model for SPIF. The model is built upon membrane analysis. They developed the analytical equations for the state of strain and stress in the small localized deformation zone. They successfully explained the reasons for different fracture morphologies and the location of fracture. Jackson et al. (2009) examined the deformation mechanism of incremental sheet forming experimentally through forming specially prepared copper sheets. Strain distributions through the thickness of the sheets are measured for two configurations of ISF: two-point incremental forming (TPIF) and single-point incremental forming (SPIF), and a comparison was made with respect to pressing. The measurements shown that the deformation mechanisms of both SPIF and TPIF were stretching and shear in the plane perpendicular to the tool direction, with shear in the plane parallel to the tool direction.

Silva et al. (2008) developed analytical model for fracture forming limit diagram based on ductile damage mechanics. The two experimental procedures utilized for characterizing the formability in SPIF ((a) fracture forming limit in the principal strain-space (ε_1, ε_2) and (b) maximum drawing angle φ_{max} at the onset of fracture) have been merged into a single concept—the onset of fracture. Adams et al. (2014) proposed an empirical model for the contact geometry as a function of tool diameter, step depth and wall angle. Lu et al. (2014) developed the analytical model for friction in ISF process. The analytical derivation provides a better understanding of how the friction affects the stress state and corresponding forming load, as well as the formability in the SPIF process. Finally, the role of through-the-thickness-shear in the ISF process has also been discussed.

Emmens et al. (2009a) analyzed different stabilizing deformation mechanisms which are reasonable for the enhanced formability in ISF. They found six different

mechanisms that may enable stable deformation namely, contact stress, bending-under-tension, shear, cyclic straining, geometrical inability to grow and hydrostatic stress. Cui et al. (2013) modeled the deformation in ISF. They developed analytical model to study the deformation in terms of principal strain. Then proposed methodology has been validated by forming hyperbolic cone, skew cone and elliptical cone.

2.3 Formability studies in incremental forming

The formability in incremental forming of sheet metal was studied by several researchers. It is recognized that the material behavior and formability in AISF can be described by the maximum value of the draw angle φ_{max} and forming limit diagrams. As φ increases, the thickness reduction reaches a minimum value where fracture occurs as a consequence. Micari et al. (2004) used cone of base diameter 72 mm with a height equal to 40 mm as a benchmark for predicting maximum draw angle of various materials. Hussain et al. (2007b) proposed varying wall angle conical frustums to measure the maximum wall angle with minimum number of experiments. Minutolo et al. (2007) evaluated the maximum slope angle of aluminium alloy using frustum of cone and pyramid with different slope angles. The cone has been formed with top base diameter as 70 mm and depth as 39 mm, and pyramid has been formed with top side length of 70 mm and maximum depth of 35 mm.

. Ham et al. (2007) studied the effect of various process parameters on maximum wall angle using response surface methodology. Response surface plots and forming limit diagrams for different aluminium alloys were constructed. Jeswiet et al. (2002) conducted a parametric study and developed the relation between maximum draw angles to sheet thickness for aluminum alloys. Hussain et al. (2008) studied the effect of tool diameter, feed rate, step depth and lubricant type on maximum wall angle of commercially pure titanium sheet. It was observed that the maximum wall angle decreased with increasing tool diameter, feed rate and step depth. Fan et al. (2010) studied the effect of process parameters on maximum wall angle in electrically heated incremental forming of difficult to form materials. The study revealed that an increase in the electric current can increase

the temperature and formability. On the contrary, an increase in feed rate, tool diameter, or step size can decrease the temperature and formability.

Bhattacharya et al. (2011) studied the effect of tool diameter, step depth, sheet thickness and feed rate on maximum wall angle. They formed the conical shape with different wall angles till the fracture. The study indicated that tool diameter, step depth and sheet thickness have significant effect on maximum wall angle while the effect of feed rate was negligible. Hussain et al. (2010) studied the effect of process parameters on maximum wall angle of AA2024 material in the annealed and presaged conditions. The effect of process parameters have been quantified through response surface methodology called central composite design. The maximum wall angle with different process settings has been measured using varying wall angle conical frustums. Fiorentino (2011) studied the effect of step depth on forming forces, formability, form accuracy and final part thickness in single point and two point incremental forming.

Forming limit diagram in incremental forming process is quite different from that of traditional Forming Limit Diagram (FLD). It was shown to be a straight line with a negative slope in positive region of minor strain in forming limit diagram. Jeswiet et al. (2005) studied the effect of various process parameters on formability of sheet. They identified that thickness of sheet, size of step down, speed of deformation and size of forming tool have major influence on formability of sheets. Fratini et al. (2004) studied the effect of various mechanical properties on forming limit curve. The analytical equation provided in this paper is useful to predict the major strain at fracture in plane strain conditions (FLD_o) for a given material.

Filice et al. (2002) proposed frustum of cone, frustum of square pyramid and cross shape to get limiting strains under different straining conditions and consequently to the determination of forming limit diagrams for progressive forming operations. Shim et al. (2001) used triangle, square, pentagon, hexagon, octagon, circle and square shapes to construct the forming limit curves in ISF. Park et al. (2003) formed different complex shapes with and without supports to construct the forming limit curves for aluminium sheet in ISF. The forming limit curves of ISF have been compared with the forming limit diagrams of conventional stretching and deep drawing processes. Jeswiet et al. (2005)

used cone, pyramid, dome, hyperbolic and five lobe shapes to construct the forming limit diagrams of AA3003-O in incremental forming. Very high strains up to 300% have been observed in their study. Ji et al. (2008) assessed the formability of magnesium AZ31at elevated temperature in the incremental forming using plane-strain stretching and axisymmetric stretching tests. In plane-stretching, the tool moved back and forth along the center line and deepened incrementally on a rectangular specimen until a crack occurred. In axisymmetric stretching, the tool moved vertically down at the center of a square specimen until a crack occurred. Based on these forming limits, cones with different inclination angles were designed and successfully formed at different temperatures. A circular cup with a high inclination angle, which exceeds the forming limit, was formed by introducing the concept of progressive forming to the incremental forming. Kim et al. (2000) constructed the forming limit curves for double pass forming using ellipsoidal cup and clover cup. They observed improved formability in double pass forming due to improved uniformity in thickness distribution

Kim et al. (2002) investigated the effect of tool type, tool size, friction, feed rate and planar anisotropy on the forming limit curve of aluminum alloy in ISF through experimental and numerical simulation of line test. Hussain et al. (2009) proposed an analytical equation to determine major strain at fracture in plane strain conditions as a function of reduction in area at tensile fracture. Ham and Jeswiet (2006) studied the effect of process parameters on maximum wall angle of AA3003. They used fractional factorial design (2^{6-3}) for study. Ambrogio et al. (2008) studied the effect of various process parameters in warm incremental forming of AZ31 magnesium alloy. The study revealed that the temperature and step depth have significant effect on FLD_0, while the role of tool diameter was negligible in the investigated range.

2.4 Surface roughness

Hagan et al. (2004) studied the effect of step depth and spindle speed on mean peak-to-valley height in incremental forming, by forming Al 3003 sheet into 45^0 wall angle conical frustum. They observed an exponential increase in the mean peak-to-valley height with step depth but spindle speed had a very little effect. They also proposed an

analytical model to predict the peak to valley height (R_t) in CNC incremental forming based on available equation for shear forming.

Attanasio et al. (2008) studied the effect of tool path on surface quality and dimensional accuracy in two point incremental forming. For this study, they have chosen two different tool paths: (a) tool path with constant step depth and (b) tool path having variable step depth with imposed restriction on scallop height. Bhattacharya et al. (2011) studied the effect of process parameters on formability and surface finish in single point incremental forming of Al-5052. They observed a decrease in surface roughness with an increase in tool diameter and decrease in surface roughness value with increase in wall angle for all step depths. Surface roughness increased first with an increase in step depth up to a certain wall angle and then decreased. Cavaler et al. (2010) studied the effect of process parameters and tool coating on surface roughness in single point incremental forming of AISI-304L austenitic stainless steel. They observed a decrease in surface roughness with an increase in step depth. Also, higher surface roughness was observed with uncoated tools compared to coated tools. Rattanachan et al. (2010) studied the effect of tool radius on surface roughness in single point incremental forming of dome shape using DIN 1.0037 Steel. The radius of the tool was varied from 2.5 mm to 5 mm and good surface finish was observed with larger diameter.

Durante et al. (2009) studied the effect of tool rotational speed and direction of tool rotation on friction, forces, temperature and surface roughness. They found that these parameters had a negligible effect on surface roughness. Hamilton et al. (2010) investigated the effect of high feed rates and spindle speeds on orange peel effect, microstructure and thickness distribution. They proposed a mathematical model to predict the orange peel effect in ISF using measured roughness values and using forming parameters. Durante et al. (2010) developed analytical models for predicting average roughness and maximum roughness of incrementally formed parts. They validated the developed models by forming pyramidal frustums with AA7075-T0 aluminum alloy.

Hussain et al. (2008b) investigated suitable tool material and lubricant for negative incremental forming of pure titanium sheet. From the studies of surface roughness, scanning electron microscopy and energy dispersive spectroscopy they found

that HSS tool with molybdenum disulphide (MoS_2) with petroleum jelly in a specific proportion was producing good surface quality. De Bruyn et al. (2012) investigated the effectiveness of different solid state lubricants in incremental forming of Ti-6Al-4V. They found that molybdenum disulphide and graphite were good choices for significant improvement in surface finish of the parts.

2.5 Finite element studies in incremental forming

Ambrogio et al. (2005) analyzed the form accuracy of parts produced in incremental forming using explicit finite element simulations. They found very good correlation between experimental and simulation results. Yamashita et al. (2008) used dynamic explicit finite element code DYNA 3D to simulate SPIF process. The simulations were performed on a quadrangular pyramid with two different heights (5 mm and 10 mm). Four kinds of tool paths were adopted to study the deformation shape, distribution of thickness strain and the force acting on the traveling tool. Ceretti et al. (2004) used PAM-STAMP to simulate the thickness distribution in incremental forming. Henrad et al. (2011) studied the effect of different constitutive laws in predicting tool force in incremental forming of conical parts. Dejardin et al. (2010) analyzed the shape distortions and springback problems in incremental forming through numerical simulations. The simulations were performed in explicit finite code LS-Dyna. Malhotra et al. (2012b) incorporated the fracture model to predict the occurrence of fracture in incremental forming of cone and funnel shapes. Eyckens et al. (2011) studied the strain behavior of material in incremental forming through digital image correlation technique and FE simulations. Two distinct large strain FE formulations, shell and first order reduced integration brick elements were used to model the sheet during incremental forming into a truncated cone. Han et al. (2003) Han et al. (2008) investigated the effect of process parameters on distribution of stresses, strains and thickness in incremental forming through experimental and FE studies. Bouffioux et al. (2008) proposed the methodology to identify the material properties in order to enhance the quality of finite element simulations. Essa et al. (2011) developed the finite element model to investigate the effects of adding a backing plate, a supporting kinematic tool and modifying the final stage of the tool path on form accuracy of formed parts. Li et al. (

2014a) studied the effect of different contact interfaces on forming force, strain behavior and thickness distribution through finite element simulation of straight groove test. Kim et al. (2002) simulated the major and minor principal strains in straight groove test. Nguyen et al. (2010) used Oyane's ductile damage model to predict the fracture in incremental forming of complex shape (e.g human face). Ren et al. (2010) discussed the challenges in numerical simulation of freeform incremental forming using explicit finite element code LS-Dyna. It was demonstrated that the simulation results correlates very well with experimental measurements. Sena et al. (2010) studied the influence of solid and solid-shell finite element formulations (C3D8I and RESS) in forming force prediction using ABAQUS. Cui et al. (2013) analyzed strain distribution in incrementally formed hyperbolic cone, skew cone and elliptical cone through analytical, numerical and experimental results. Ma et al. (2008) used brick elements to establish whole three dimensional FE model and simplified three dimensional FE model of a truncated cone and truncated pyramid in order to analyze the deformation behavior of material in incremental forming. It was found that the simplified model was more efficient over full model. Seong et al. (2014) used FE simulations and stress based forming limit diagrams to explain the suppressed necking and enhanced formability in incremental forming process. Elford et al. (2013) compiled FE simulation results of NUMISHEET incremental forming bench mark problem with different FE softwares. It was observed that the FE simulations are good in predicting the strains, forming loads, thickness distribution and deformed profile after spring back during incremental forming.

2.6 Multi stage incremental forming

Cao et al. (2014) proposed an analytical method to predict the thickness distribution in MSIF. The methodology has been validated by forming four different geometrical shapes, i.e., conic, parabolic conic, non-axisymmetric, and hemispherical parts. Shi et al. (2014) developed forming limit diagrams for MSIF by forming the parts with different number of steps. Junchao et al. (2013) proposed area division method to manufacture car taillight bracket in MSIF with a wooden support. Liu et al. (2014a) proposed analytical models to design the intermediate passes in MSIF. Proposed methodologies have been validated by experiments and finite element simulations. Zhang

et al. (2013) used hydraulic bulging simulation to get the shape of intermediate passes for producing a cylinder with vertical walls in MSIF. Li et al. (2012a) studied the effect of number of passes on plastic strain, thickness distribution and spring back. They observed more uniform thickness distribution with increase in number of stages but the quantity of spring back was becoming larger.

Duflou et al. (2008) analyzed the sheet thicknesses and strains in MSIF. A cylindrical cup has been formed in five stages with an initial wall angle of 50^0. The number stages depend on the tool diameter and part height to avoid the folding during forming. Cerro et al. (2006) analyzed forming forces, surface roughness, thickness distribution and form accuracy in MSIF. For this, a square pyramid of 75^0 wall angle has been formed successfully in seven stage. Li et al. (2013) proposed an analytical model to determine the number of stages. This methodology has been verified with relatively complex product. Further, they analyzed thickness distribution and effective plastic strain through experiments and finite element simulation. Liu et al. (2014b) studied the effect of tool path strategies on material deformation in MSIF. They formed ellipsoidal cup and free form shape to study the influence of ramp angle, start point and travel direction on thickness distribution and formability. Further, the finite element results have been validated by experiments. Liu et al. (2013) proposed three multi-stage deformation pass strategies for forming cups with vertical walls. Those strategies and their combinations have been evaluated in terms of the process formability. The results showed that the forming strategy using more material in the forming as well as the addition of a small amount of bending can greatly improve the formability.

Malhotra et al. (2011a) proposed mixed tool path strategy to eliminate stepped features in MSIF. They developed analytical equations to design *in* to *out* and *out* to *in* tool paths for intermediate shapes. The constants in analytical model have been predicted by finite element simulations. Xu et al. (2012) extended the work in Malhotra et al. (2012a) by relating material constants in analytical formulations to yield stress and the thickness of the blank. Therefore, the required number of prior finite element analysis (FEA) simulations is reduced to only six for arbitrary material types and thicknesses, which was a significant addition to the earlier works.

Cui et al. (2010) studied the effect of different multi-step tool path strategies in hole flanging operation. Skjoedt et al. (2008) proposed five stage strategy to form cylindrical cups with vertical walls in incremental forming. They demonstrated that the distribution of strains dependent not only on the geometry of the tool path but also on the direction (downwards or upwards). Lingam et al. (2015) proposed analytical model to predict the formed geometry after every stage. They considered tool diameter, step depth, sheet thickness, tool deflections and forming forces to predict the final geometry of formed component.

2.7 Forming force

The force required to deform the sheet into required shape is one of the important factors to design the forming tools, fixture and selection of machine tool. Duflou et al. (2007) studied the effect of different process parameters on forming force by forming aluminium alloys of different thicknesses on a CNC milling machine. The three force components were measured using Kistler 9265B six-component force dynamometer. Petek et al. (2009a) also made a similar study on DC 05 steel sheets. Aerens et al. (2009); Aerens et al. (2010) formed conical cups with five different materials in incremental forming and developed regression equations for axial, radial and tangential force components. The axial force component was expressed as a function of tensile strength of material, tool diameter, sheet thickness, wall angle and scallop height. The radial force was modeled based on the contact zone parameters obtained from numerical simulations and axial force component. Bouffioux et al. (2011) calculated limiting wall angle in case of AlMgSc alloy by forming conical geometry with different wall angles. They also performed numerical simulations to study force distribution and form accuracy of the part. For this, a quarter portion of conical geometry was simulated with different wall angles and proper boundary conditions. They observed good correlation between measured, simulated and analytical force distribution. The axial force was nearly 4 times the tangential force. The radial and tangential forces were almost equal. The mesh parameters didn't have significant influence on force components. Equations developed by Aerens et al. (2009) were used to get analytical peak force estimations.

Ambrogio et al. (2006) classified the commonly observed force trends in ISF into three categories. In case of parts with low wall angle, the force increases to peak due to bending and then it becomes stable. If thinning dominates the stain hardening, the force curve decreases monotonically after reaching the peak value. In the third category of force distribution, the force reaches peak in the beginning due to bending and dips down for a while due to domination of thinning over strain hardening, but after a few millimeters of depth equilibrium achieves between thinning and strain hardening and force becomes stable. They used force as a spy variable to control the fracture during forming and formed conical cups with more depth. Bouffioux et al. (2008) modified the material model parameters based on line test along with the classical tests to improve the force prediction in ISF. They simulated line test and observed improvement in force prediction with modified material model parameters. Pérez-Santiago et al. (2011) compiled the experimental force data available in the literature under different forming conditions. This data has been used to check accuracy of analytical models available in literature and finite element models. Conical, pyramidal, biangular pyramidal frustum and varying wall angle conical frustums were simulated using LS-Dyna software. They observed that FEM models were the best choice to predict the forming force.

Bahloul et al. (2014) used design of experiments and response surface methodologies for modeling maximum force and thinning rate. Fiorentino (2013), Filice et al. (2006) and Petek et al. (2009b) used real time force data to detect the fracture during forming. Li et al. (2014b) developed analytical model for tangential force prediction based on the energy method. The effects of deformation modes from shear, bending and stretching were taken into account separately by two sub-models.

2.8 Geometric accuracy

Ambrogio et al. (2007) analyzed the form accuracy of parts produced in incremental forming and developed analytical equations to predict the spring back and pillow effect as a function of process parameters. Tanaka et al. (2008) examined the negative spring back phenomena in incremental forming through experiments and finite element simulations. The negative spring back of pure titanium material was investigated by strip cut method. The experimental results revealed that the feed rate has significant

effect on spring back, while the effect of tool radius is negligible. Dejardin et al. (2008) studied the shape distortions and spring back effects arising in single point incremental sheet forming. The spring back has been characterized through the cut rings method and verified with finite element simulations.

Ambrogio et al. (2005) proposed a strategy to improve the form accuracy based on modification of the tool path considering the spring back effects and stiffness of clamping equipment. Proposed strategy has been realized by integrating an on-line measuring system, composed of a digital inspector and a computer numerically controlled open program. The geometry obtained is sampled in particular steps and an appropriate routine modifies the coordinates of the future punch path. Meier et al. (2009) used offline model based strategy and on-line sensor based strategy to improve the accuracy of parts formed in robotic incremental forming.

Ambrogio et al. (2012) proposed high feed rate forming and back drawing strategy to reduce the processing time and also to improve the form accuracy in ISF. Malhotra et al. (2011b) proposed squeezing tool path strategy with two forming tools to improve the geometric accuracy in incremental forming. Hussain et al. (2011) investigated the effect of various process parameters on form accuracy of parts in single point incremental forming. They used central composite rotational design to plan the experiments and developed the regression equation. They further optimized the objective function for minimum profile error using Derringer-Suich multi-criterion algorithm for numerical optimization. Radu et al. (2013)studied the effect of residual stresses on form accuracy of parts in ISF. They conducted FE simulations to get distribution of residual stresses in the formed components under different process condition. These results have been correlated with form accuracy. Micari et al. (2007) discussed state of art and future trends on shape and dimensional accuracy in SPIF. Setti et al. (2012) proposed a methodology for measuring the shape of the component formed in incremental forming by using trinocular vision and random pattern. Ashgar et al. (2014) observed that the sheet deflection due to axial force and tool deflection due to radial force are the two main factors leading to the geometric deviation in wall as well as base regions. An analytical model has been developed for estimating these two deflections. These deflection values are incorporated in the tool path generation, and the components formed using the

compensated tool path resulted in acceptable dimensional accuracy in the wall region. Wei et al. (2011) proposed spring back evaluation method in SPIF. They found that the geometric accuracy of the formed parts can be improved significantly by adopting compensation method.

2.9 Summary

This chapter provides a comprehensive review on different aspects in incremental forming process. The literature study demonstrated that the process is very economical for sheet metal prototyping and low volume production due to its flexibility, simple tooling, die less nature and enhanced formability. The literature study also revealed that most of studies in incremental forming have been performed on aluminium and its alloys. Very limited studies have been made to understand the behavior of steel blanks in SPIF. Thus, the present thesis focuses mainly to understand the formability, deformation behavior, surface roughness in single stage and multi stage incremental forming processes of EDD steel blanks. EDD steel possesses excellent formability and widely used in automotive applications involving simple and complex parts requiring high formability. The subsequent chapters provide detailed discussions on evaluation of formability, effect of process parameters on formability & surface roughness and finite element simulation of the process.

.

Chapter 3 Numerical Simulations

This chapter discusses the methods adopted for material characterization and finite element simulation of ISF process. The flow stress behavior of EDD steel has been obtained from uni-axial tensile test. The preliminary simulations have been performed in commercial finite element code LS-Dyna to understand the mechanics of ISF process. Various aspects for efficient simulation of ISF process have been discussed in detail.

3.1 Material characterization

EDD steel is a low carbon steel with maximum 0.08 % carbon and possesses excellent formability. It is widely used in automotive sector for door inners, dash panels, body side inners and floor pans. The chemical composition (*wt %*) of the material is given in Table 3.1. Uni-axial tensile test has been conducted to get flow curves of the material for numerical simulations. The tensile test specimens have been cut on wire cut EDM as per ASTM E8M standards. The experiments are performed with a cross-head velocity of 2 mm/min. The load-displacement data obtained from computer controlled universal testing machine have been used to calculate engineering stress (S) and engineering strain (e) using relations (3.1) and (3.2). The stress–strain data have been used to get the true stress (σ) – true strain (ε) data using Eqs. (3.3) and (3.4) assuming constant specimen volume. The elastic region is removed from true stress – true strain data to get the true stress – true plastic strain and shown in Fig. 3.1a. In sheet metal forming operation, the material generally undergoes the stresses beyond yield point and below the ultimate stress point. In this region, the material undergoes the strain hardening and stress–strain curve has been approximated by the Hollomon power law Eq. (3.5).

Table 3.1 Chemical composition of EDD steel

C	Si	Mn	S	P	Cr	Sn	Cu	Ni	Mo	Fe
0.044	0.78	0.17	0.01	0.01	0.024	0.005	0.021	0.051	0.025	Rest

$$S = \frac{P}{A_0} \tag{3.1}$$

$$e = \frac{\Delta l}{L_0} \tag{3.2}$$

$$\sigma = S(1+e) \tag{3.3}$$

$$\varepsilon = \ln(1+e) \tag{3.4}$$

$$\sigma = K\varepsilon^n \tag{3.5}$$

$$\log\sigma = \log K + n\log\varepsilon \tag{3.6}$$

In the above equations A_0,L_0 and Δl represent the original cross-sectional area, gauge length and elongation of tensile test specimen respectively. Eq. 3.6 is a straight line with *x*-axis as a log of true stress and *y*-axis as log of true strain (Fig. 3.1b). Slope of this line gives the strain hardening exponent (*n*) and y-intercept of the line gives the log of strength coefficient (*log K*). Strain hardening exponent (*n*) measures how rapidly the material becomes harder and stronger. The formability of the material increases with the increase in *n* value.

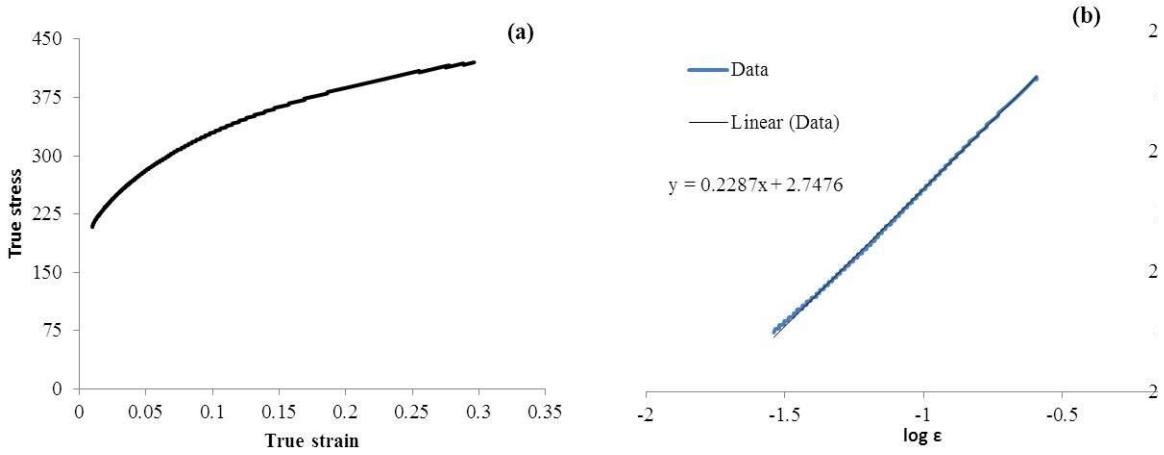

Fig. 3.1 True stress - True plastic strain curve of EDD steel

The anisotropic co-efficient of the material has been obtained from the tensile tests carried out on the specimens of 0^0, 45^0 and 90^0 to the rolling directions. The tests have been conducted as per ASTM E517 standards. The flow stress data and anisotropic

coefficients can be used to develop different yield criteria. In addition to uni-axial tensile test, Ericson cupping test is performed to get limiting dome height of the blank material. The erichsen cupping test uses a hemispherical headed punch to deform the blank between the blank holder and die till the occurrence of fracture. The test has been performed as per ASTM E643 standard. The limiting dome height of 1 mm thick EDD sheet has been found to be 13.65 mm.

3.2 Line test simulation

Line test or groove test is a simple method to study formability, forces and friction in ISF process. It requires simple 2-D tool path to form a groove of required depth in the blank. A 2-D tool path is easy to define in the finite element software, italso takes less time for computation due to its short length. In the present section, line test has been simulated using explicit finite element code LS-Dyna to study forming force, total strain distribution and principal stains. The material properties for different simulations are given in Table 3.2. The results from finite simulations are validated with the experimental data available in the literature.

Table 3.2 Material properties for finite element simulation of forces and strains

Simulation	Hardening co-efficient (K) (in Mpa)	Strain hardening exponent (n)	Youngs modulus (in Gpa)	Density (in (Kg/mm^3)	Thickness (in mm)	Poisson's ratio
Major and Minor strains	524	0.185	200	7860	0.5/0.9	0.25
Total strains	180	0.21	72.6	7850	1.2	0.36
Forces	180	0.229	72.6	7850	1.5	0.36

3.2.1 Force modeling in incremental forming

Force modeling is useful to predict the amount of force acting on CNC machine spindle while forming different materials. It is also used for adaptive control and predicting the fracture in formed geometries. For simulation, the spherical ended tool is moved in vertical direction by 5 mm and then 100 mm in horizontal directions, it again descends by 5 mm and travel back 100 mm in horizontal direction as shown in Fig. 3.2.

Bouffioux et al. (2008) measured the forces when the tool travels according to the said tool path. A numerical model has been built to simulate the process using LS-Dyna and results are compared with available data in literature.

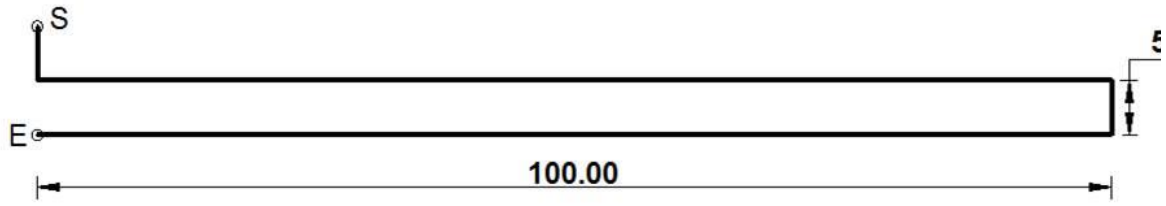

Fig. 3.2 Tool path for finite element simulation of force in line test

Finite element model based prediction of the force acting on the tool in Z-direction is shown in Fig. 3.3. The force in Z-direction increases continuously until the tool moves to maximum depth as shown in Fig. 3.3b. During its horizontal travel, force is slightly reduced and is almost constant until second step depth. During second vertical travel, again force reaches its maximum value. In this step finite element simulations are slightly over predicting the forces compared to experimental values.

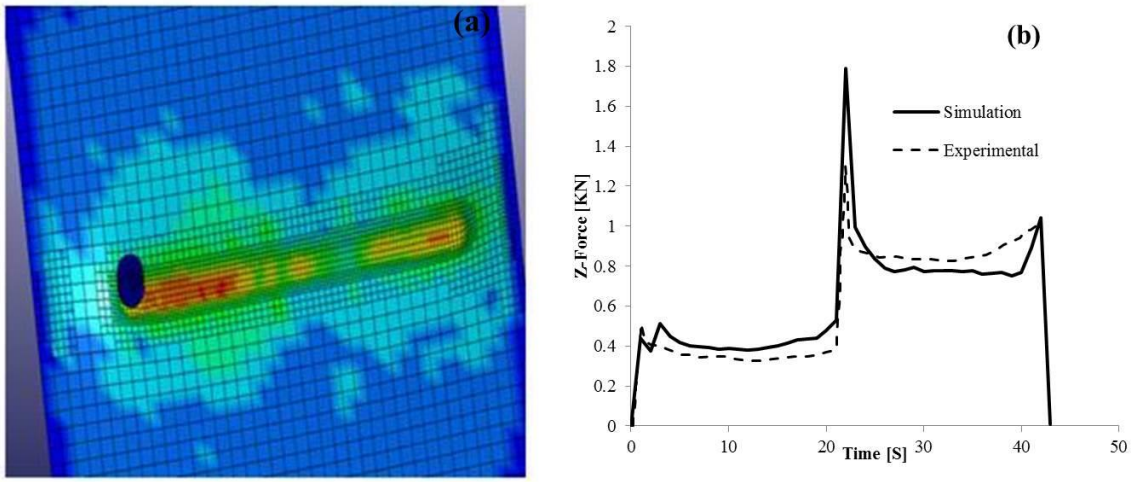

Fig. 3.3 Force distribution in the line test

At the end of the second vertical step and during the subsequent horizontal travel of the tool, the force comes down from peak value and remains stable till the end of line test. The results of present work show very close correlation with experimental work of literature as shown in Fig. 3.3 except a slight excessive force during vertical travel of the tool at the beginning of second step.

3.2.2 Total strains in incremental forming

Watzeels et al. (2005) simulated total strain distribution in incremental forming for first stroke using finite element code called Lagamine. Evolution of total strains was studied at start, middle and end of the stroke. A numerical model has been built in explicit finite element code LS-Dyna to compare total strains obtained at middle and end of the straight groove test with Lagamine in three principal directions. The material properties for simulation are shown in Table 3.2 and the tool path is shown in Fig. 3.4. Shell element with adaptive meshing and time scaling is used in building finite element model.

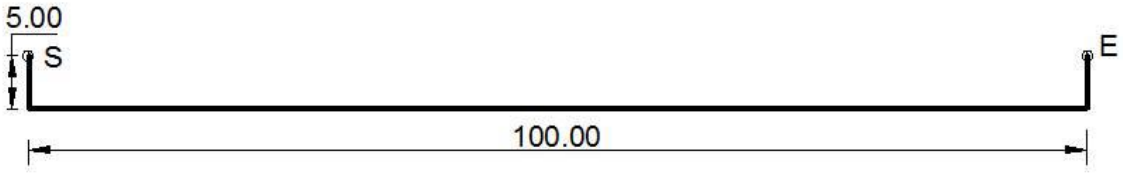

Fig. 3.4 Tool path for finite element simulation of total strains in line test

The finite element model and distribution of total strain components are shown in Fig. 3.5 and 3.6 respectively. The results obtained from LS-Dyna simulations have been compared with the results in literature [Watzeels et al. (2005)]. The strain in *x*-direction at the middle element is nearly negligible until the tool comes closer to the element as shown in Fig. 3.6. The strain is increasing slowly from the beginning and reaches maximum when tool approaches to that element. After tool crosses it, there is slight decrease in the strain due to elastic spring back. Distribution of strains in Y and Z directions has the same trend as shown in Fig. 3.6.

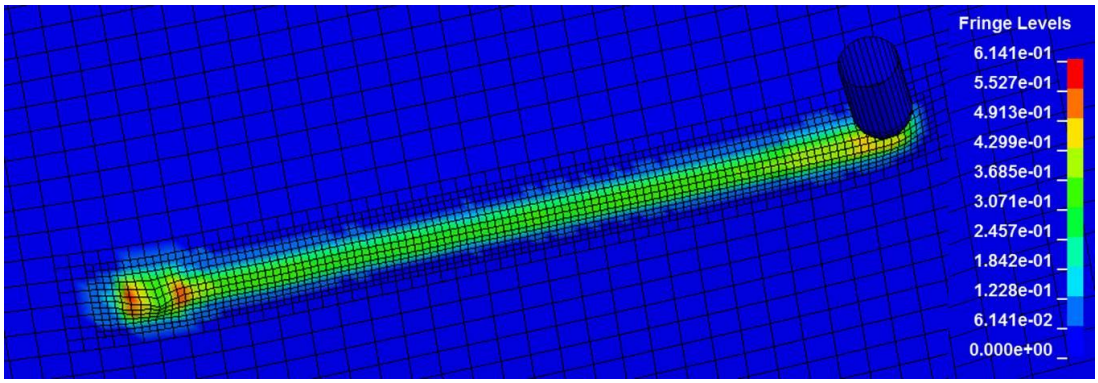

Fig. 3.5 Finite element model of line test for total strains

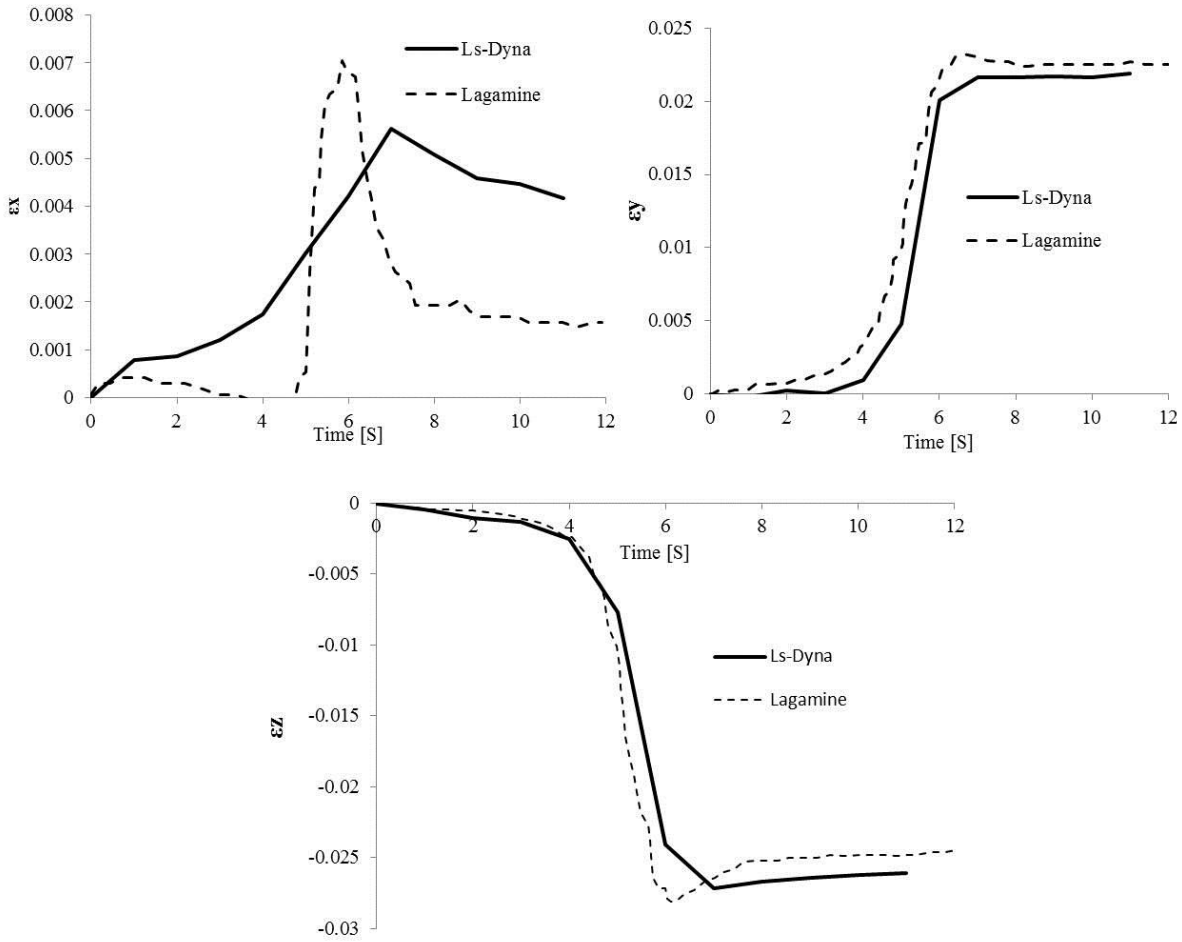

Fig. 3.6 Distribution of total strains in the element at the middle of the groove

Strains are negligibly small in Y and Z directions until the tool approaches the middle element. This is due to the localized deformation which is the nature of incremental forming. Strain in the element at the end of straight groove (at Point C) is shown in Fig. 3.7. Strain at the end point in X direction is negligible until the tool reaches middle element. When the tool crosses middle element and approaches the end point, there is gradual increase in strain and it reaches maximum values when tool reaches end point. The trend of strain in Y and Z directions is almost same as shown in Fig. 3.7 except a small deviation towards the end. This may be because of the fact that the tool has not been retracted from the end position to home position in the LS-Dyna simulations, thus ignoring the elastic springback only at this point.

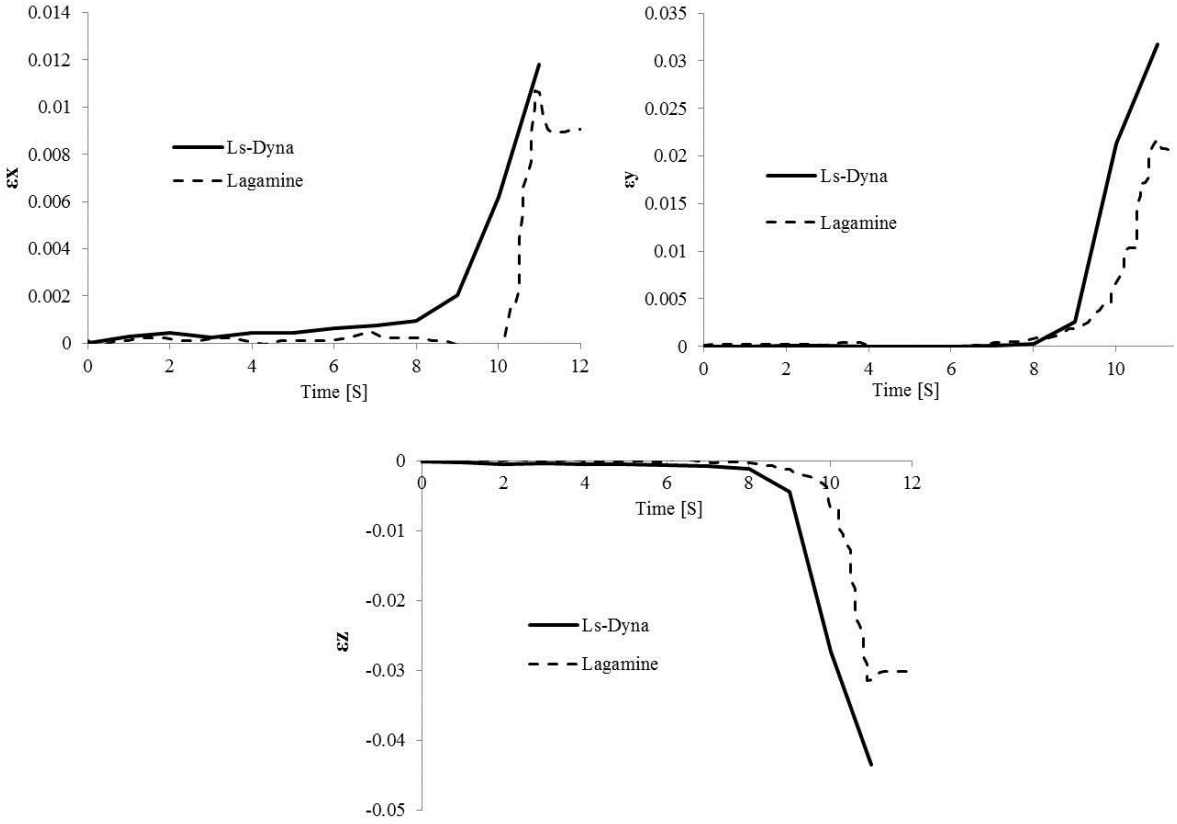

Fig. 3.7 Distribution of strain in the element at the end of the groove

3.2.3 Major and Minor Principal Strains

Numerical simulations are performed to study the distribution of major and minor principal strains in straight groove test. Fully integrated shell elements are used to model

the blank with five integration points in thickness direction. Nodal displacements and rotations are constrained at all edges of the sheet. Material is assumed to be isotropic and elasto-plastic. Its properties are modeled with power law plasticity given by the relation $\sigma = K\varepsilon^n$. To minimize the simulation time, scaling is adopted simulating the process 1000 times faster than the actual experiments. Movement of the tool in the simulation is identical to the experiments as shown in Fig. 3.8. During simulation, punch is moved in *z*-direction by an amount equal to step depth and then travels 40 mm in *x*-direction. When it reaches the end, it moves in *z*-direction with step depth and comes back in *x*-direction 40 mm. This process continues until total depth reaches 6 mm.

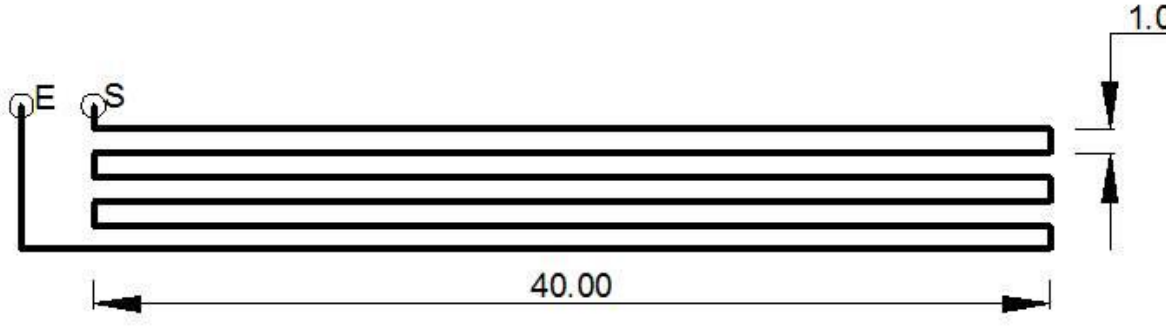

Fig. 3.8 Tool path for the simulation of major and minor principal strains

Table 3.3 Summary of minor and major principal strains in straight groove test

S.no	D (in mm)	T (in mm)	P_z (in mm)	ε_1 max	ε_2 max	ε_1 max	ε_2 max	ε_1 max	ε_2 max
				Experimental		Simulation		% Error	
B2	6	0.9	1	0.334	0.145	0.2936	0.1626	12.09	-12.13
B4	6	0.5	1	0.264	0.1737	0.27	0.1493	-2.27	14.04
B6	10	0.9	1	0.258	0.1105	0.2312	0.1271	10.38	-15.02
B8	10	0.5	1	0.236	0.109	0.2126	0.118	9.91	-8.25

The results of major and minor principal strains are summarized in Table 3.3. It shows that there is a good agreement between experimental results and numerical results.

In simulations major principal strains are under predicted while minor principal strains are over predicted. An error of maximum 12.09% is observed in measuring major strains and 15.02% in measuring minor strains.

From the line test simulations it can be concluded that the total strain distribution results obtained by using Legamine and LS-Dyna shows that the choice of finite element code doesn't have significant effect on the results. Major and minor principal strains from numerical simulations are in good agreement with experimental results. Results from numerical simulation of punch force indicate that the 2D shell element is good enough to simulate the incremental forming process accurately and much improvement may not be gained by using more computationally expensive 3D brick element. Adaptive meshing worked well in line test simulation. Adaptive meshing and time scaling seemed to have no effect on strain and force results.

3.3 Simulation of VWACF

Varying wall angle conical frustums are very popular in ISF process to predict the limiting wall angle with minimum number of experiments. In this section, VWACF with circular generatrix has been simulated in LS-Dyna to study the effect of tool path on thinning in SPIF process. The details of the part geometry are given in the appendix.

3.3.1 Tool Path generation

In incremental forming, the accuracy of final part geometry largely depends on adopted tool path for forming the sheet. Thus tool path plays a very vital role in incremental forming. Tool path can be generated either from commercial CAM packages or from MATLAB. Tool paths can also be generated from STL files. In commercial CAM systems tool paths are broadly divided in to two categories, namely, profile tool path and spiral tool path. In profile tool path, tool completes one contour and then moves down to next contour. Spiral tool path is defined by a single continuous helix from start point to endpoint. The effect these two tool paths on the thinning behavior of the part under consideration has been studied in this section. Profile tool path is generated using MATLAB program and it is converted in to spiral tool path using HeToPac [Skjoedt et al. (2007)]. MATLAB program provides the time-tool position data which can be used as an

input in simulation package. Schematic diagrams of profile and spiral tool paths are shown in Fig. 3.9.

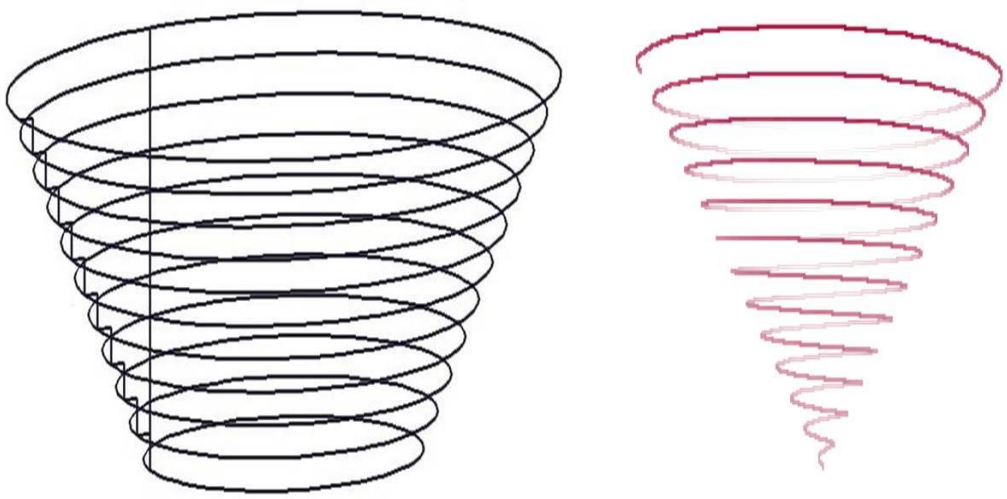

Fig. 3.9 Schematic diagram of profile and spiral tool paths

3.3.2 Finite element modeling

For finite element simulations, the blank is modeled as a square of 150 mm X 150 mm X 0.91 mm in size and is fixed at its four edges. This sheet is discretized using quadrilateral shell elements. Initial element size is taken as 4 mm and adaptive meshing option in LS-Dyna is enabled. Adaptive meshing option will take care of excessive distortions in the mesh by subdividing the elements in to smaller size. A hemi-spherical punch of 8 mm diameter is modeled and meshed with shell elements. Punch is defined as rigid and blank material properties are defined using power law plasticity. The material properties are elasticity modulus E=72 Gpa and poission's ratio ν=0.25, while the strength coefficient K=300 Mpa and hardening coefficient n=0.2283. Time scaling and mass scaling are used to minimize the computational time. Mass scaling is done by increasing the density of material and time scaling is done by artificially increasing the velocity of tool.

Since the part under study has variable wall angles, the thickness will also vary according to the sine law along its depth. It was also observed in measured parts after experiments. Thickness of part varies according to sine law up to some depth and it deviates from sine law nearer to the fracture zone. The point of deviation was treated as

transition point and used as a thinning limit in incremental forming. The average thinning limit of 63.32% was obtained at a depth of 46.29 mm for aluminium [Hussain et al. (2007)].

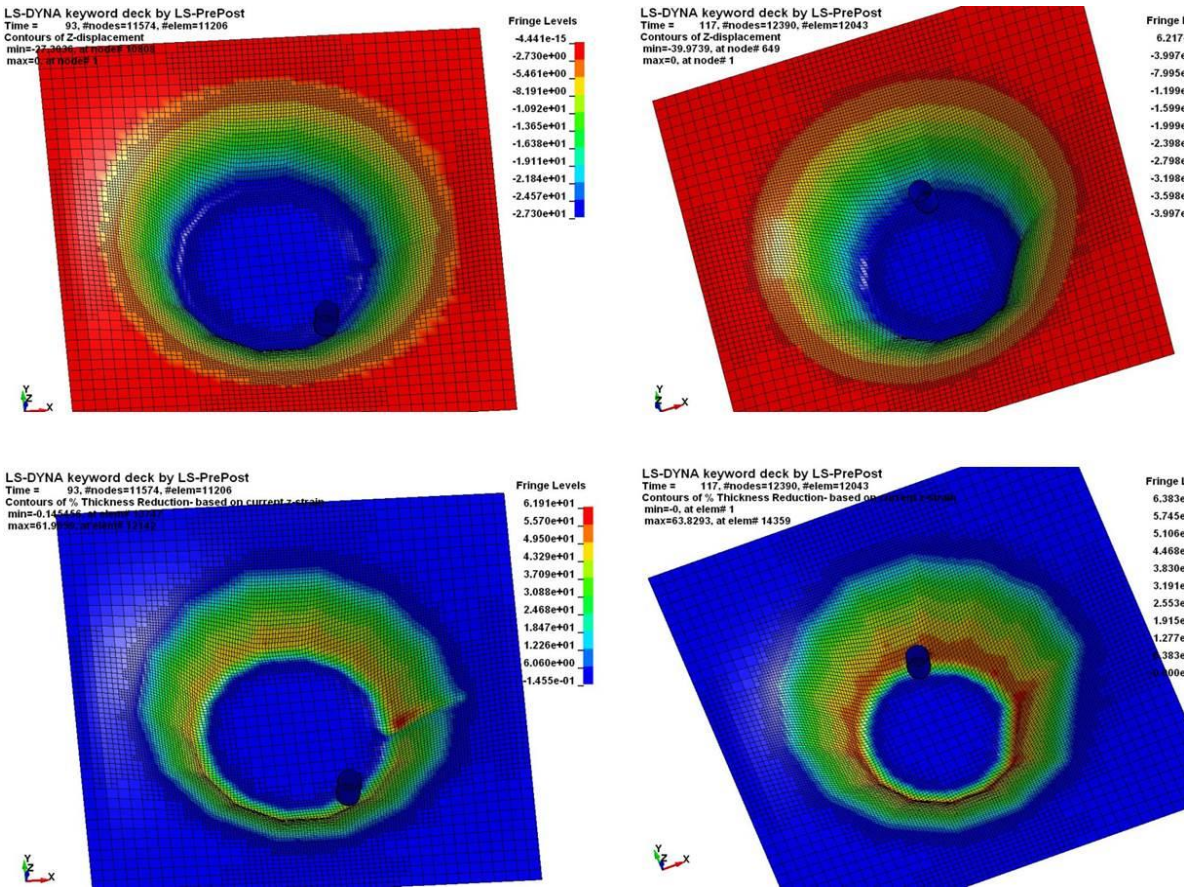

Fig. 3.10 Contour plots of Z-displacement and thickness

For analyzing numerical results, maximum allowable thinning is taken as 63.32%. Depth of the part corresponding to this thinning limit is obtained from the simulations. Depth of the part corresponding to critical thinning limit is observed as 40.97 mm in spiral tool path and 28.26 mm in profile tool path. The finite element results for the depth corresponding to critical thinning and thinning behavior of the blank with the profile and spiral tool path are shown in Fig. 3.10. Uniform thinning has been observed across the cross section in spiral tool path while in profile tool path maximum thinning is observed at the transition point from one contour to another contour. Maximum wall angles in spiral and profile tool paths are 65.82^0 and 58.65^0 respectively. Variations in spiral tool path results may be due to higher step depth (0.5 mm) used in simulations and lack of

baking plate below the sheet in simulation. In profile tool path, in addition to step depth and backing plate, non-uniform thinning restricted the maximum formable angle. Numerical solutions can be improved further by using actual experimental tool path and a baking plate.

3.4 Tool path definition for FE simulations

For numerical simulation of the ISF process tool has to follow the same path as in experimental work. But numerical simulation softwares normally do not accept the G-code file generated using CAM packages directly. In this section a methodology has been proposed to input the tool path trajectories generated using CAM packages in to numerical simulation softwares, such as, ABAQUS and LS-Dyna. For certain sample symmetric and asymmetric shapes, this methodology has been implemented in MATLAB and LS-Dyna.

3.4.1 Methodology

Different steps in numerical simulation of a general sheet metal forming process are shown in Fig. 3.11. Same steps are followed for numerical simulation of ISF also. But the tool path definition in ISF is very complex compared to other sheet metal forming operations. In conventional deep drawing and stamping this tool path is one dimensional and thus the punch/tool moves in one of the principal directions. In case of spinning, tool path will have number of cycles which are two dimensional in nature, since only symmetric parts can be made by this process, whereas, in incremental forming, sheet is formed by continuous three dimensional motion of the tool.

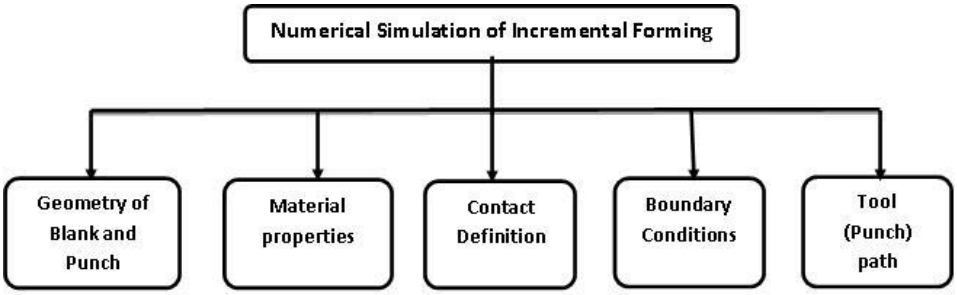

Fig. 3.11 Steps in numerical simulation of ISF

Tool path generated by CAM package includes the position of tool center point followed by linear (G01) and circular interpolation (G02/G03). Circular interpolation can be clockwise (G02) or counter-clockwise (G03). If tool moves in linear path, it is represented as G01 followed by the destination point in the part program. If tool moves in circular path, it is represented as G02/G03 followed by destination point co-ordinates and radius of the arc.

The part program generated using CAM package cannot be given as input for tool path in numerical simulation softwares. For numerical simulation, tool path should be defined in terms of position *vs* time or velocity *vs* time, or acceleration *vs* time. In this section a methodology is proposed to convert part program into position vs time data in order to provide an input file for numerical simulation of incremental forming.

Linear interpolations are easy to assign whereas in circular interpolations, tool center point must be rotated around other center points generated by CAM software, which seems impossible to assign to the tool. Therefore in this study, the circular segments are divided into linear segments with chosen allowable error. The tool path in incremental forming is generally very long and it is difficult to do position *vs* time calculations manually. Therefore, in this study, Python is used to generate the ordered file from the part program generated using CAM package. This ordered file is an array of *nX5* possessing type of interpolation, co-ordinates of tool position and radius of the arc. This ordered file is given as input to MATLAB to generate position *vs* time data.

The lines of *nX5* matrix are read one by one by MATLAB program. Depending on the value of first element of row, it is decided whether the interpolation is linear, clockwise or anticlockwise circular interpolation. For linear interpolation, distance *D* between two points say (x_i,y_i,z_i) and $(x_{i+1},y_{i+1},z_{i+1})$ is calculated using Eq. 3.7.

$$D = \sqrt{(x_{i+1} - x_i)^2 + (y_{i+1} - y_i)^2 + (z_{i+1} - z_i)^2} \tag{3.7}$$

For circular interpolation, the center of the circle is determined from the two given end points in the ordered file. In circular interpolation only *x* or *y* coordinate or both will change. The *z* coordinate always remains same. For the given two end points, there are two possibilities of arcs. One corresponds to clockwise circular interpolation

and other corresponds to counter clockwise interpolation. Accordingly, the center to be used is changed depending on the sense of interpolation. For example, as shown in the Fig. 3.12, there are two arcs having the same end points (x_1,y_1) and (x_2,y_2) but when seen with respect to the center, one is clockwise and the other is anticlockwise. The successive points on the circle are calculated using parametric equation of the circle given by Eq. 3.8.

$$\begin{aligned} x_{i+1} &= x_0 + r\cos(\theta_i + i\delta\theta_i) \\ y_{i+1} &= y_0 + r\cos(\theta_i + i\delta\theta_i) \\ 0 &\le i \le n \end{aligned} \tag{3.8}$$

where (x_0,y_0) is center of the circular arc, r is the radius of circle, θ_i is the angle with the positive x-axis measured in anticlockwise sense, $\delta\theta$ is the incremental angle calculated using Eq. 3.9 and n is number of divisions that satisfies the allowable error.

$$\delta\theta = \frac{\theta_f - \theta_i}{n} \tag{3.9}$$

where θ_f is angle subtended by the end point of the arc with x-axis. Methodology of dividing the arc segment into number of linear segments is shown in Fig. 3.12. The length of each line segment can be calculated using Eq. 3.7. The time required to cover each segment is calculated by multiplying the distance (D) with the average velocity of tool (V). Fig. 3.13 shows the flowchart to generate the input file for numerical simulation of ISF using part program generated by CAM software.

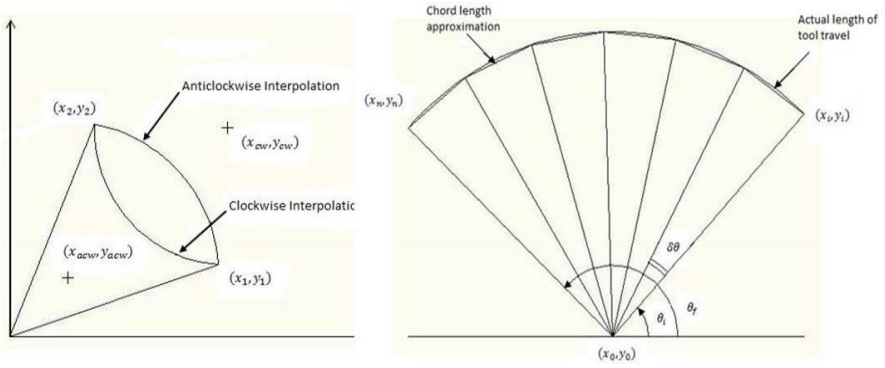

Fig. 3.12 Schematic showing arc sub division process

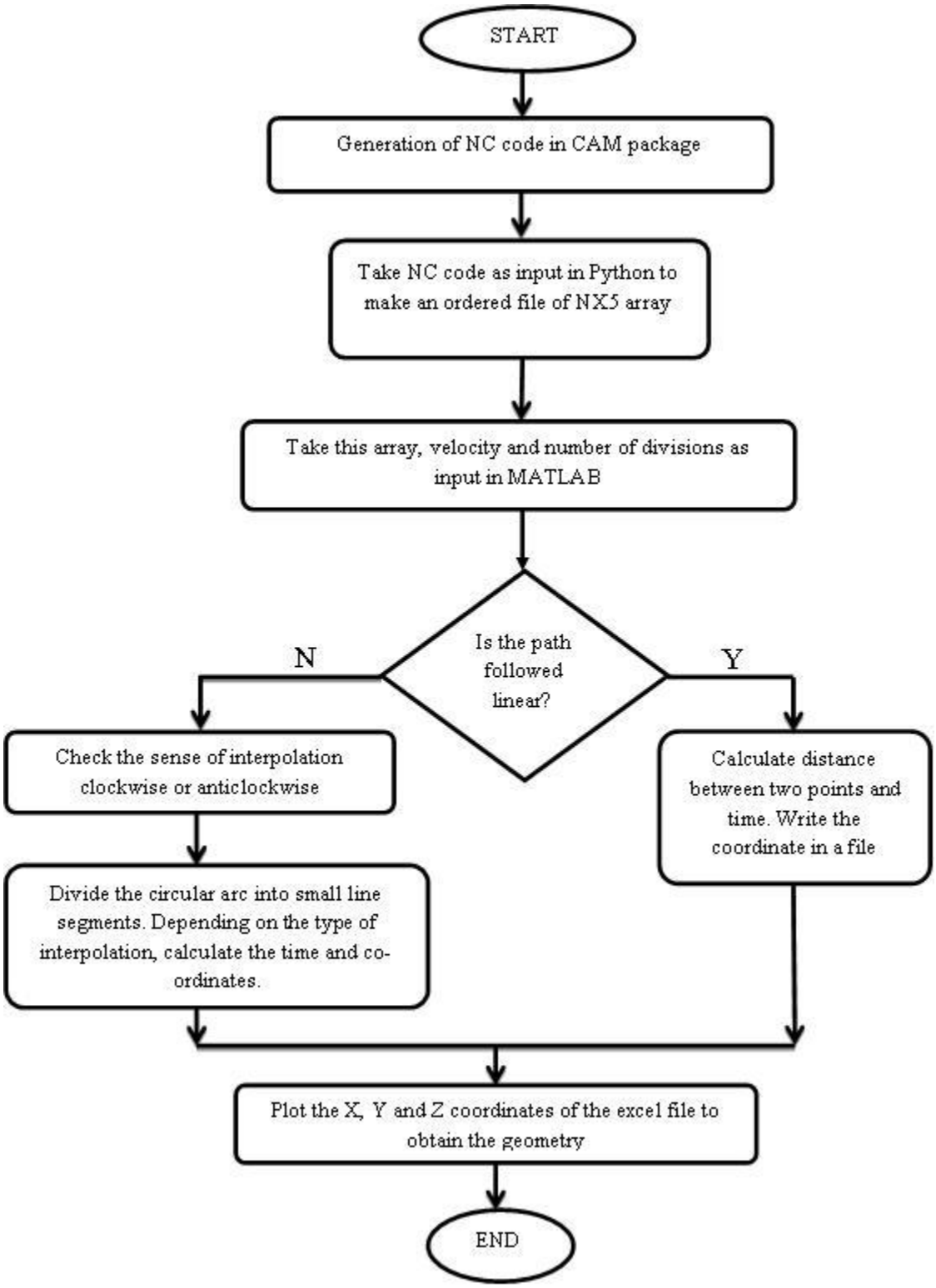

Fig. 3.13 Flowchart of proposed methodology for input file generation

3.4.2 Verification

Four different geometries are used for implementation of proposed methodology. First one is, part with planar surfaces (pyramid), second is part with curved surface (cone), third is part with curved & planar surfaces, and fourth one is asymmetric geometry. The geometries are chosen so as to verify the current methodology for a variety of geometric shapes. Geometry of parts and generated tool paths are shown in Fig. 3.14 and Fig. 3.15 respectively.

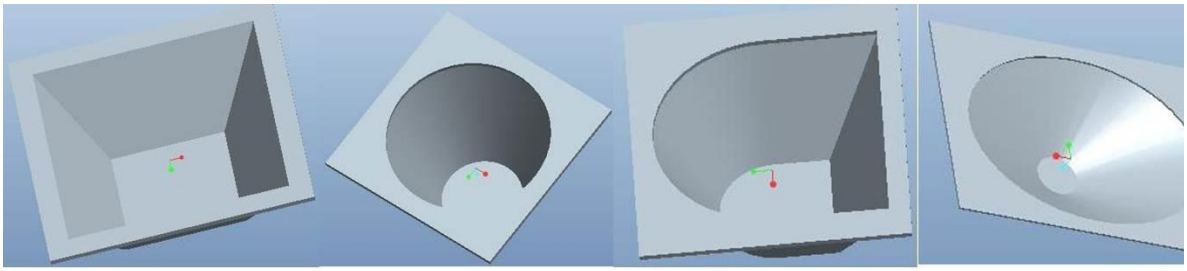

Fig. 3.14 Geometries used for testing proposed methodology

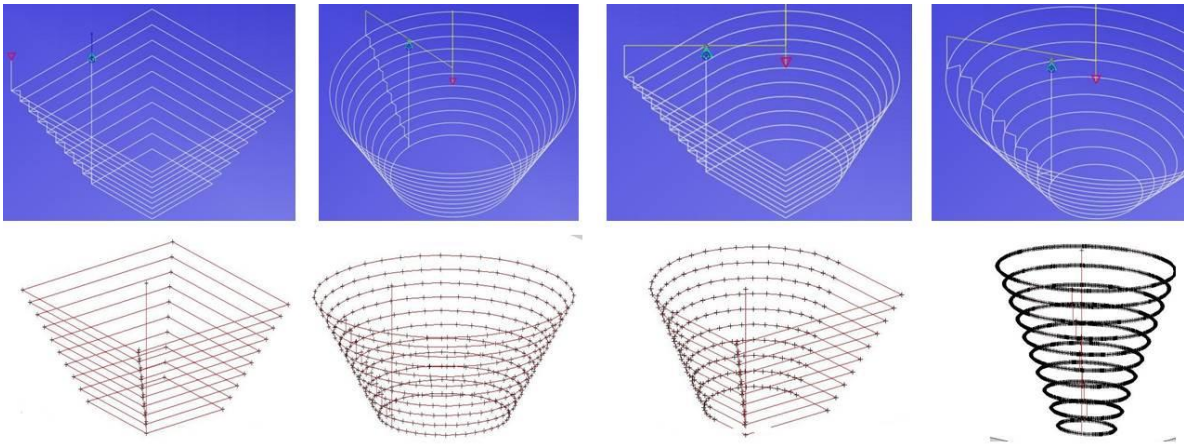

Fig. 3.15 Tool path generated using CAM software and proposed methodology

The position *vs* time data of tool, generated using current methodology is given as input to LS-Dyna software to simulate the incremental sheet metal forming. Blank is defined as a deformable body and meshed with shell elements. The punch is defined as a

rigid body and meshed with shell elements. The blank is fixed along its periphery. Two geometries are chosen to verify the tool path in numerical simulation. The deformed shape of sheet metal at the end of the simulation in LS-Dyna is shown in Fig. 3.16. It is evident from the Fig. 3.16 that the current methodology of tool path definition for numerical simulation works successfully.

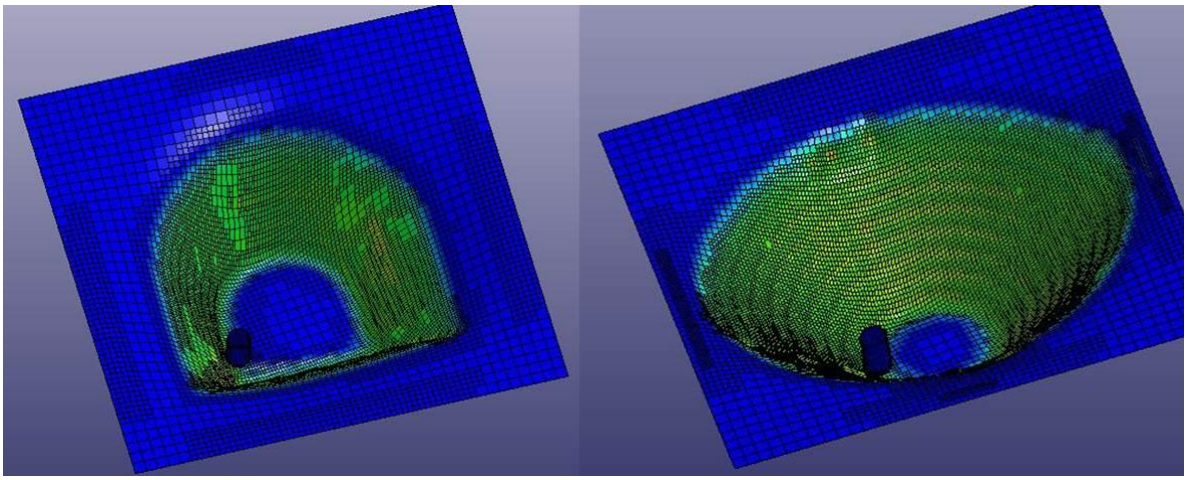

Fig. 3.16 Deformed shape of the part in FE simulation

3.5 Effect of process parameters

This section discusses the effect of various process parameters on forces, plastic strain and thinning through numerical simulations. Three important process parameters, namely, punch diameter, step depth and wall angle are used as input parameters. Taguchi orthogonal arrays are used to plan the number of simulations to study the effect of process parameters on the response variables. The numerical simulations are performed using finite element software LS-Dyna. Initially, tool path is generated using Pro-manufacturing software and is modified into suitable format for numerical simulations using Python and MATLAB programming. The results show that the wall angle is having maximum influence on all three response variables.

3.5.1 Taguchi orthogonal arrays

Taguchi is a robust design technique to analyze the process to improve the productivity and quality of the product. This technique provides a well balanced set of minimum experiments in the form of orthogonal array to analyze the effect of input

variables on output. In the present study L_9 (3^3) orthogonal array is used to study the effect of three process parameters on three output parameters. The input parameters are tool diameter, step depth and wall angle. Three levels were considered for each parameter to capture the non-linear effects. In this study it is assumed that no interaction exists between the process parameters. Table 3.4 shows the selected process parameters and their levels for numerical study.

Table 3.4 Factors and levels for three level Taguchi design

Parameter	Low	Middle	High
Diameter (A)	10 (A1)	15(A2)	20 (A3)
Step depth (B)	0.5(B1)	1(B2)	1.5(B3)
Wall angle (C)	30(C1)	50(C2)	70(C3)

In Taguchi methods different S/N ratios are used to analyze the results. S/N ratio represents both average and variation of the experimental results. In the present study low tool force, low strains and low thinning are the main objectives so smaller-the-better S/N ratio has been chosen. For this objective S/N ratio is defined by Eq. 3.10 according to Taguchi method.

$$S/N = -10\log(MSD) = -10Log\left[\frac{1}{n}\sum_{1}^{n} y_i^2\right] \tag{3.10}$$

3.5.2 Finite element modeling

A 3-D finite element model is developed in explicit finite element code LS-Dyna for numerical simulation of incremental sheet forming process. The blank, die and forming tool are modeled with Belytschko-Tsay type shell elements. Fine mesh was used for blank with element edge length of 1mm. Total five integration points are defined in thickness direction. The blank is Extra Deep Drawing (EDD) steel sheet of size of 222 mm X 222 mm X 1.6 mm and is modeled using power law plasticity (MAT 18). The die and punch are modeled using the rigid material model (MAT 20). The strength

coefficient and strain hardening exponent of blank are defined as 688 MPa and 0.305 respectively [Singh et al. (2010)]. The contact between the tool and blank, blank and die is modeled using forming one-way-surface-to-surface algorithm. Coulomb's friction law was applied with a friction coefficient of 0.01 between different contact surfaces. The finite element model of different tools is shown in Fig. 3.17.

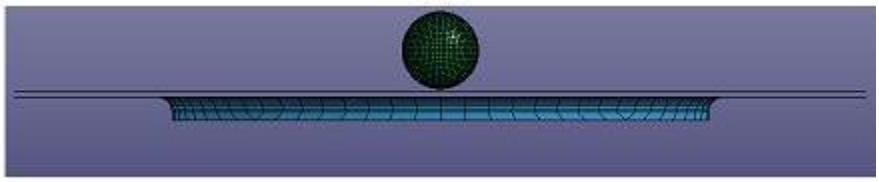

Fig. 3.17 Finite element model for numerical simulation

.

A conical part with top base diameter 140 mm and different wall angles are simulated with specified step depth and given diameter of tool. The results obtained with different combination of input parameters are summarized in Table 3.5.

Table 3.5 Summary of results from numerical simulations

Ex. No	A (mm)	B (mm)	C (deg)	Force (KN)	Plastic Strain	Max. Thinning (%)
1	A1	B1	C1	2.87	0.95	21.2
2	A1	B2	C2	4.29	1.33	48.55
3	A1	B3	C3	4.99	3.51	85.09
4	A2	B1	C2	4.61	1.53	45.47
5	A2	B2	C3	5.60	3.67	83.87
6	A2	B3	C1	3.46	0.87	27.55
7	A3	B1	C3	5.96	4.52	90.96
8	A3	B2	C1	3.75	0.78	27.48
9	A3	B3	C2	5.45	1.14	53.85

3.5.3 Punch force

Punch force in experiment 1 along X, Y and Z directions is shown in Fig. 3.18a. Fig. 3.18 (b-d) shows the evaluation of resultant punch force in different experiments.

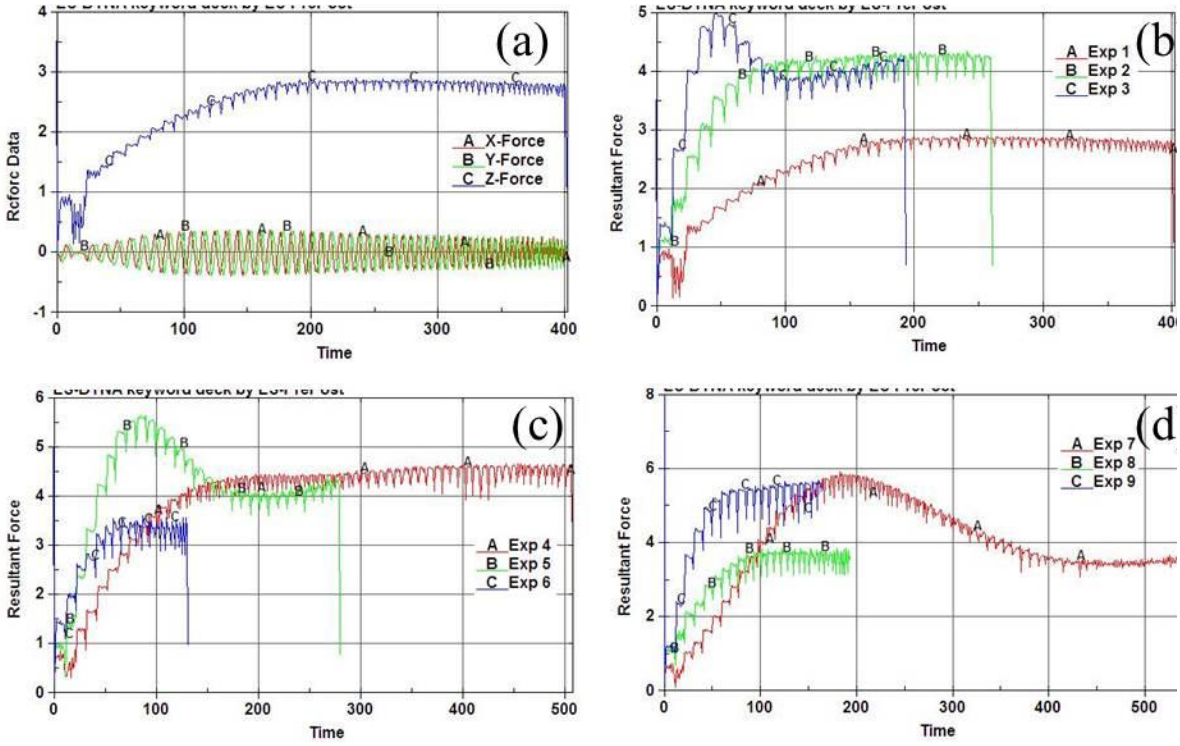

Fig. 3.18 Distribution of punch force in FE simulations

Maximum punch force is observed in parts with maximum wall angle. The force reached to maximum value and became stable in case of parts with 30^0 and 50^0 wall angles. In case of 70^0 wall angle parts, force has dropped after reaching peak value due to plastic instability and maximum thinning. Same kind of trend was observed by Duflou et al. (2007) during experiments with aluminium alloy at different wall angles, confirming that wall angle plays vital role in ISF. On the other hand, step depth and diameter of the tool have moderate effect on punch force.

3.5.4 Effective plastic strain

The amount of plastic strains in ISF is very high compared to other conventional processes. Maximum effective plastic strains are observed in parts with maximum wall angle. Among all the experiments, maximum strain is observed in experiment 7 i.e with maximum wall angle and maximum diameter. From experiments 1, 6 and 8, it is clear

that at lower wall angles the effect of diameter and step depth have negligible effect on plastic strains. Distribution of plastic strain in experiment 4 is shown in Fig. 3.19 (a).

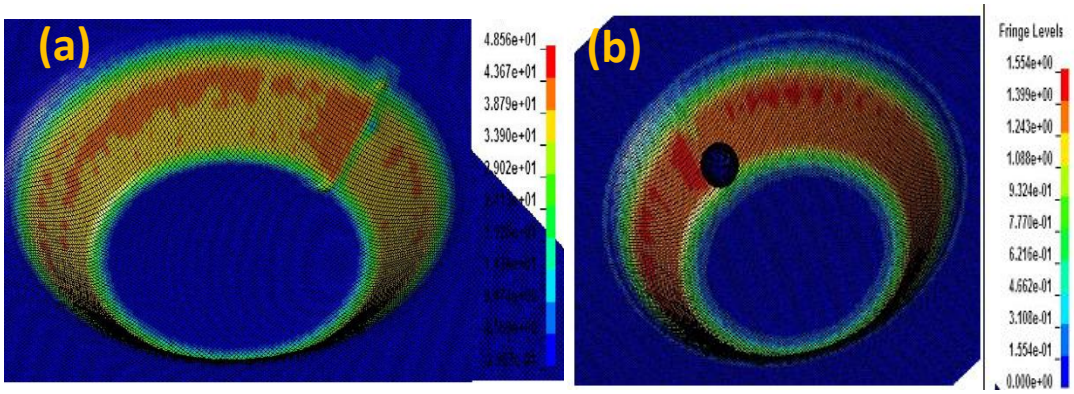

Fig. 3. 19 Contour plots of effective plastic strain and thinning percentage

3.5.5 Thinning

Theoretically the thickness distribution in ISF follows the sine law given by the following equation.

$$t_f = t_i \sin(90 - \theta) \tag{3.11}$$

In this equation, θ is the wall angle of the part. This shows that wall angle will have major effect on thinning. The same effect can be observed from simulated results. On average 20-25% thinning has been observed in parts with 30^0 wall angle. 45-50% in parts with 50^0 wall angle and 85-90% in parts with 70^0 wall angle respectively. Step depth and diameter of the tool may produce around 5% variation in thinning. Contour plot of thinning in experiment 2 is shown in Fig. 3.19 (b).

3.5.6 Statistical analysis

The Taguchi method uses S/N ratio to find the optimum process parameters. To determine optimum combination, the mean S/N ratio is calculated for each level of parameters. This mean S/N ratio for different response variables is shown in Fig. 3.20 and Table 3.6. Process parameter with maximum difference in mean S/N ratio will have maximum effect on the response variable and is given rank 1 in Table 3.6.

Table 3.6 S/N ratio values by factor level

	Resultant force			Effective plastic strain			Maximum Thinning		
Level	A	B	C	A	B	C	A	B	C
1	4.05	4.48	3.36	-4.32	-5.46	1.22	-32.95	-32.95	-28.04
2	4.55	4.54	4.78	-4.62	-3.88	-2.45	-33.48	-33.66	-33.83
3	5.05	4.63	5.51	-4.05	-3.65	-11.77	-34.19	-34.01	-38.75
Delta	1.00	0.15	2.15	0.56	1.81	13	1.24	1.06	10.71
Rank	2	3	1	3	2	1	2	3	1

Table 3.7 ANOVA results for maximum effective plastic strain

Source	DF	Seq SS	Adj Ms	P	P.C (%)
DIA	2	0.0736	0.0368	0.725	0.44
DEPTH	2	0.4154	0.2077	0.318	2.48
ANGLE	2	16.0156	8.0078	0.012	95.91
Error	2	0.1938	0.0969		
Total	8	16.6984			

Table 3.8 ANOVA results for maximum thinning

Source	DF	Seq SS	Adj MS	P	P.C (%)
DIA	2	60.65	30.32	0.214	1.04
DEPTH	2	14.14	7.07	0.538	0.24
ANGLE	2	5714.54	2857.2	0.003	98.42
Error	2	16.5	8.25		
Total	8	5805.82			

Table 3.9 ANOVA results for maximum resultant force

Source	DF	Seq SS	Adj MS	P	P.C (%)
DIA	2	1.5101	0.755	0.035	17.123
DEPTH	2	0.0355	0.0177	0.61	0.402
ANGLE	2	7.2149	3.6074	0.008	81.84
Error	2	0.0554	0.0277		
Total	8	8.8158			

Analysis of variance (ANOVA) quantitatively estimates the percentage contribution of different input parameters on output. For this ANOVA uses S/N ratio responses. The contribution of input parameters on various response variables is summarized Table 3.6-3.8.

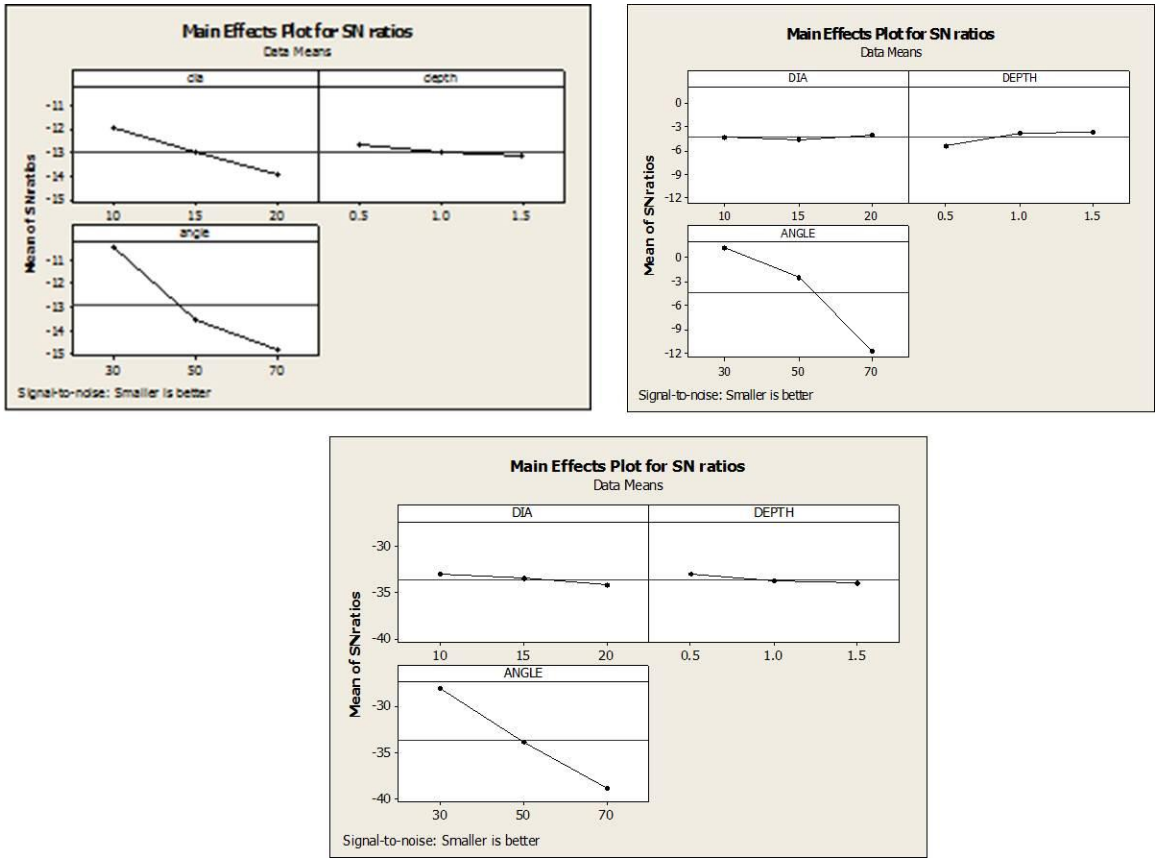

Fig. 3.20 Main effects plot for S/N ratios

According to ANOVA, the importance of different process parameters are determined by P-value and percentage of contribution (P.C) respectively. If P-value is less than 0.05 in the ANOVA table, that parameter is considered to be statistically significant at 95% confidence level. The Table 3.9 shows that wall angle and diameter of the tool have significant effect on resultant force. Wall angle and diameter of the tool affect the force by 81.84% and 17.12% respectively. Effective plastic strain and thinning are affected much by wall angle. Other two parameters have negligible effect on thinning, while step depth affects effective plastic strain by 2.48%.

In this section, effect of wall angle, step depth and diameter of the tool on maximum resultant force, plastic strain and thinning are analyzed through numerical simulations and Taguchi orthogonal array. From the results, it is found that the wall has most significant effect on all response variables. It has 98.42% effect on thinning, 95.91% effect on plastic strain and 81.84% on resultant force. Diameter has 17.12% effect on forming force due to increased contact area and negligible effect on other two response variables. Step depth has 2.48% on plastic strain and negligible effect on other two response variables.

3.6 Effect of mesh parameters

This section focuses on some investigations related to the effect of element size and adaptive re-meshing technique in numerical simulation of ISF process. The tool path for ISF process is generally very long and thus increases the computational time. Therefore, in this section the effect of element edge length and adaptive re-meshing technique has been studied to minimize the computational time without sacrificing the accuracy of the results. For this a varying wall angle conical frustum has been simulated using shell elements with different element edge lengths and adaptive mesh. Effects of these mesh parameters on plastic strain, punch force and form accuracy of deformed geometry have been studied. The necessary simulations for this study have been performed using explicit finite element code LS-Dyna.

3.6.1 Finite element modeling

The ISF process is simulated using explicit finite element code LS-Dyna. The blank is square in shape with 250 mm X 250 mm X 1 mm in size. The blank is discretized with Belytschko-Tsay shell elements (Type -2) with two integration points in thickness direction. In this study, the element with edge length of 1 mm, 2 mm, 4 mm and 4 mm with adaptive re-meshing are considered to study their effect on various response variables. The nodes along all four edges of the blank are constrained to simulate the blank holder. The blank material is modeled using power law plasticity (MAT 17). The forming tool is modeled as a cylindrical rod with hemi-spherical head of 10 mm diameter. A backing plate is provided below the blank to avoid bending and to improve the accuracy of final part. The backing plate has a hole of 110 mm diameter in the center

with 5 mm corner radius. Both forming tool and backing plate are meshed with shell elements and assigned with rigid material model. The contact between blank and backing plate, blank and forming tool is defined using master-slave contact algorithm. The friction between different contact surfaces is defined using coulomb's friction law.

A varying wall angle conical frustum has been chosen as a goal shape to study the effect of mesh parameters. To get this shape the tool has to move in three dimensional space and should deform the sheet in to required geometry. To define this complex tool path in numerical simulation, the part program has been generated using Pro-Manufacturing software for the selected geometry. This part program has been converted to time position data (*x*,*y*,*z*,*t*) using MATLAB routine as described in section 3.4. The time position data has been given as an input to the simulation software using *BOUNDRY_PRESRIBED_MOTION_RIGID keyword to control the motion of forming tool. To minimize large computational time due to long tool paths in ISF simulation, punch velocity has been increased to 40 m/s and density has been increased by 10 times.

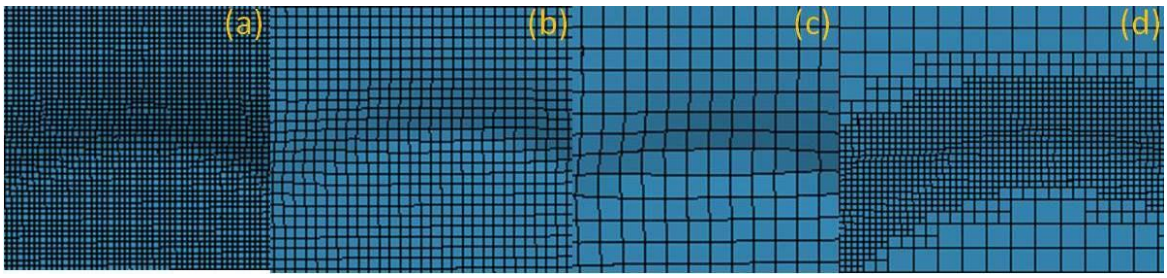

Fig. 3.21 Different mesh topologies used for numerical simulation of ISF

The effect of four different meshes with element edge length of 1 mm, 2 mm, 4 mm and 4 mm with mesh adaptivity has been tested (Fig. 3.21). In the first three meshes the number of elements is constant till the end of simulation, while in the fourth simulation (simulation with adaptive mesh) the elements are subdivided in to small elements based on total angle change in degrees relative to the surrounding element for each element to be refined. In each refinement, element is divided in to 4 elements and maximum number of refinement levels is set to 3.

3.6.2 Effect on plastic strain

Simulations are performed in LS-Dyna to study the effect of mesh topologies on evolution of effective plastic strain, punch force and final shape of the part. Fig. 3.22 shows the distribution of maximum effective plastic strain with different meshes. The effect plastic strain with adaptive mesh is almost same as that of fine mesh with element edge length 1 mm. However, the strain distribution with coarse mesh is deviated more from the strain distribution with fine and adaptive mesh. Besides, from the Fig. 3.23 it is clear that the element with edge length 4 mm undergoes plastic strain after 150 sec, while the element in the model with fine mesh undergoes plastic strain after 350 sec. Coarse mesh undergoes more plastic strain and this strain occurs earlier compared to fine mesh. Moreover, it is observed that the elements with edge length 4 mm (coarse mesh) are undergoing more distortion during the simulation.

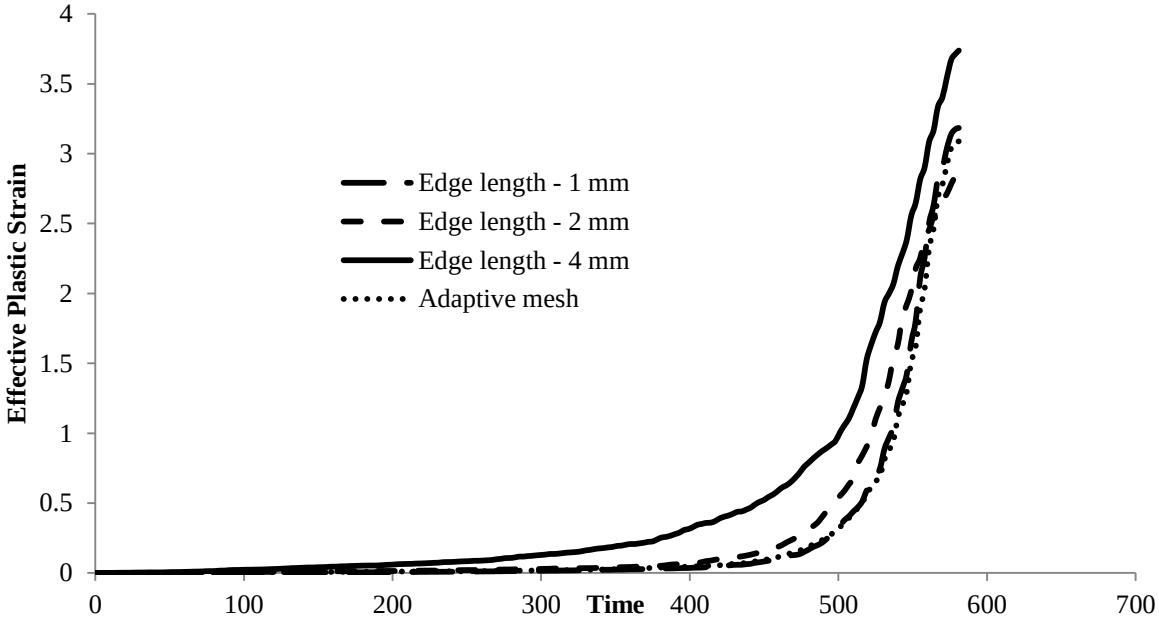

Fig. 3.22 Distribution of effective plastic strain with different mesh topologies

3.6.3 Effect on punch force

The distribution of punch force in Z-direction is shown in Fig. 3.23. This figure illustrates that the punch force with adaptive mesh is almost same as that of fine mesh with element edge length of 1 mm, while the force with element edge length of 2 mm is

slightly deviating. The force distribution with coarse mesh (element edge length of 4 mm) was deviated more compared to the results obtained with element edge length of 1 mm and 2 mm. Moreover, the estimated force with coarse mesh is lesser compared to fine mesh and has large peaks.

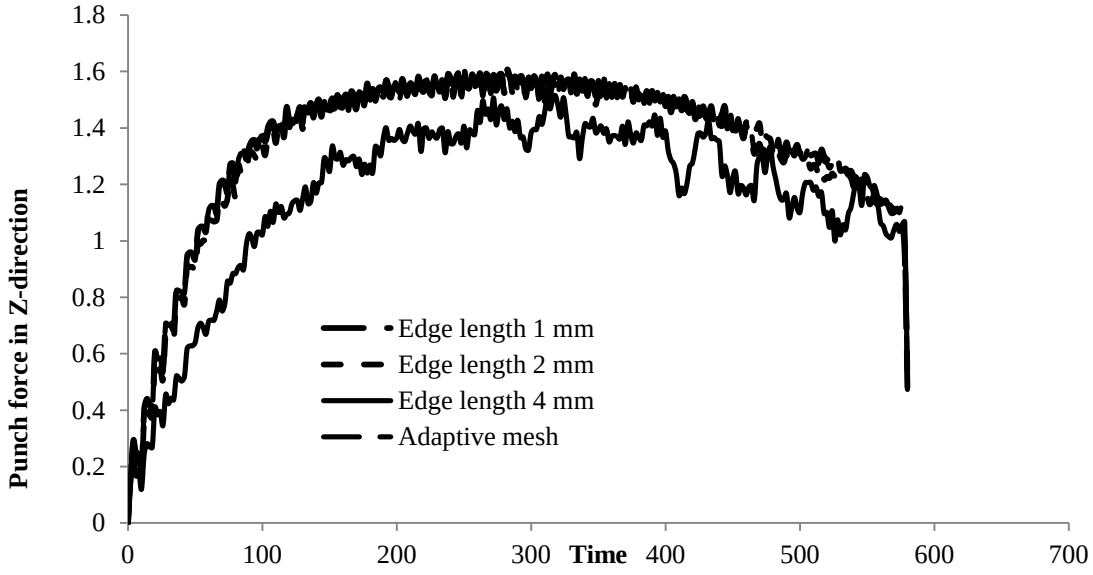

Fig. 3.23 Distribution of punch force in z-direction with different mesh topologies

3.6.4 Effect on final shape of geometry

The Fig. 3.24 shows the cross-section of deformed geometry with different meshes. The deformed cross-section with element edge length 1 mm and adaptive mesh is very close to the designed cross-section in the wall region. However, there is some deviation at the entrance and the bottom of the cup. The deviation at the entrance of the cup is due to bending of the blank over the radius provided on the backing plate. The deviation at the bottom of the cup is due to pillowing effect during forming the sheet. In case of coarse mesh, the deformed cross-section was deviated more from the goal shape. This deviation is more towards the bottom of the cup compared to the wall region. This could be due to the severe distortion of the elements towards the bottom of the cup.

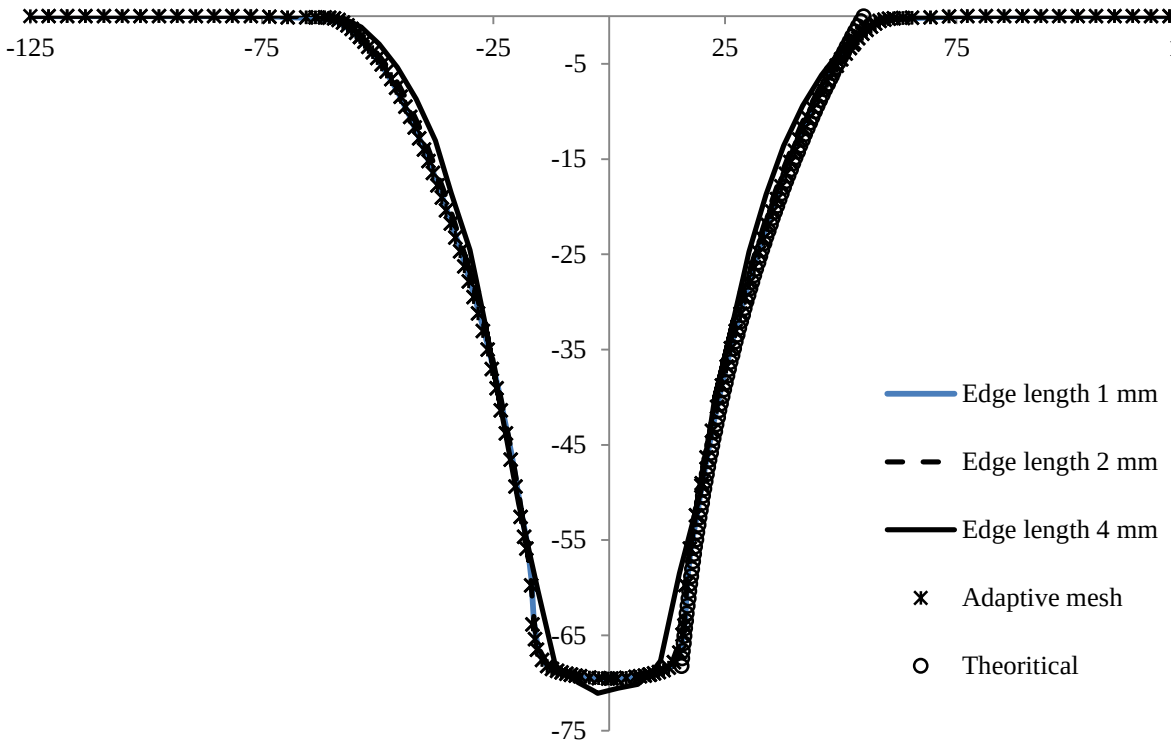

Fig. 3.24 Deformed cross-section with different mesh topologies

The study reveals that the results obtained with adaptive mesh are as good as fine mesh. At the same time the computational time with adaptive mesh is less compared to the fine mesh. The computation time with element edge length of 1 mm was found to be 752 min, while the simulation with adaptive mesh took only 314 min. It shows nearly 50% saving in computational time with adaptive mesh. The coarse mesh with element edge length 4 mm took only 11 min, but the results are not satisfactory. The adaptive mesh is highly efficient for numerical simulation of ISF process as the deformation is very much localized in this process.

In summary, this section presented the effect of adaptive re-meshing technique in numerical simulation of ISF process. The results obtained with this technique are as good as the results obtained with fine mesh. Additionally, the computational time is reduced by 50% with adaptive re-meshing technique. Thus this technique can be used to overcome the problem of long computational time due to long tool paths associated with ISF process.

3.7 Effect of mass scaling and time scaling

Another technique to minimize the long computational time associated with the ISF process is by using mass scaling and time scaling techniques. In this section the effect of time scaling and mass scaling on forming forces, plastic strain, internal energy, kinetic energy, thickness distribution and computational time is studied. A continuously varying wall angle conical frustum is simulated for this study.

To study the effect of mass scaling and time scaling, the punch velocity is varied over three levels and the mass scaling factor is varied over three levels. Full factorial design is used to plan the number of simulations in order to study the effect of input parameters on various response variables. The experimental plan for numerical simulations is shown in Table 3.10.

In order to study the effect of mass scaling and time scaling, numerical simulations are performed in the explicit finite element code LS-Dyna. The forming tool and the backing plate are treated as rigid. Blank material is extra deep drawing steel and is modeled using rate-independent power law plasticity model (MAT 18). For this model, strength coefficient is defined as 570 MPa and strain hardening exponent is taken as 0.23.

Incremental forming process generally takes several minutes due to longer tool path. This duration is very long for explicit simulations. In general, explicit simulations are performed for simulating the processes which happens over a short duration of time. In explicit finite element simulation the time step should be smaller than the critical time step size calculated using Courant criterion for numerical stability. Due to long processing time in ISF and small time step size restriction in explicit simulations, increases the computational time. To overcome this large computational time, the punch velocities are artificially increased. In general the punch velocities in ISF will be in the range of 10 mm/s to 30 mm/s. In the current simulations punch velocities are increased to 10 m/s, 25 m/s and 40 m/s. If punch velocities are increased artificially, it produces dynamic effects in the solution. Therefore, it is important to observe the kinetic energy of the system to get proper results. The kinetic energy of the system should be below 10% of the internal energy for the system to be quasi-static in nature.

Another technique to save computation cost in explicit simulations is mass scaling. For a simple shell element the time step size is calculated using Eq. 3.12. From this relation it is clear that the time step size can be changed by changing element length (L), Youngs modulus (E) and density (ρ). But changing L will change the mesh density, and it deteriorates the results, changing E is not recommended as it greatly effects the material stiffness. Last option is changing the density which may not have significant effect on analysis results. This process of changing density to increase the time step and to minimize the computational time is called as mass scaling.

$$\Delta t_c = \frac{L}{c} \qquad where \quad c = \sqrt{\frac{E}{\rho(1-\nu^2)}} \tag{3.12}$$

Mass scaling is done manually or automatically in commercial software packages. In manual mass scaling, the density of material is changed in the material card. In automatic mass scaling minimum time step size is defined under DT2MS with negative sign in *CONTROL_TIMESTEP card of LS-Dyna. By doing this, the density of those elements with time step size less than the absolute value of DT2MS is increased. In this section the effect of mass scaling has been studied using the simulations without mass scaling and with mass scaling factors of 5, 10. The excess mass scaling also induces dynamic effects thus it is important to monitor the kinetic energy of the system to understand the effect of mass scaling on the results.

Table 3.10 Experimental plan for numerical simulation

Exp.No	Punch Velocity	Mass scaling factor
S1	10	0
S2	10	5
S3	10	10
S4	25	0
S5	25	5
S6	25	10
S7	40	0
S8	40	5
S9	40	10

3.7.1 Kinetic energy and Internal energy

A series of simulations are performed as per the experimental plan suggested in Table 3.10. Time scaling and mass scaling are used to minimize the computational time for numerical simulations. But, this approach produces the inertial effects in the simulation. To check the inertial effects due to mass scaling and time scaling in incremental forming simulation, the kinetic energy and internal energy are monitored continuously as shown in Fig. 3.25. From the Fig. 3.26 it is evident that the kinetic energy is negligible compared to the internal energy in all the nine simulations. With increase in the mass scaling factor the internal energy of the system is decreasing. But the variation in internal energy, between the simulations with mass scaling and without mass scaling is not very significant.

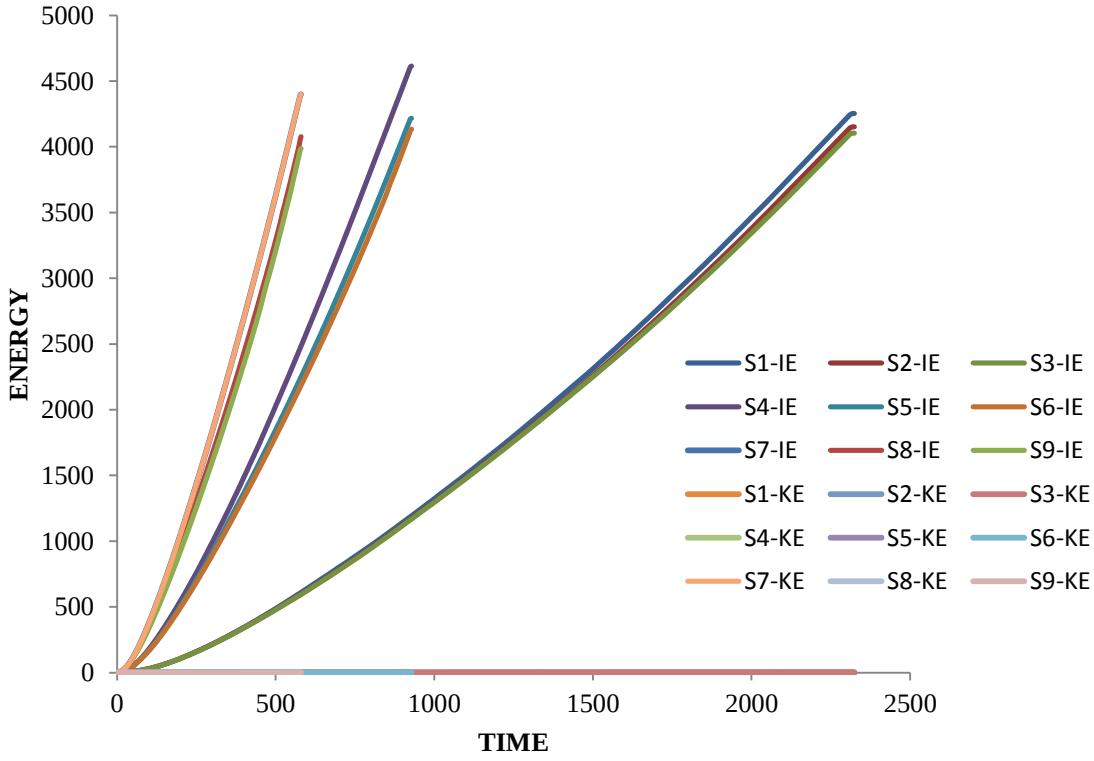

Fig. 3.25 Distribution of internal energy and kinetic energy

3.7.2 Plastic strain

The increase in velocity of the punch increases the strain rate of material by the same factor, if the material model is rate sensitive. In the present work, the rate independent material model has been used to for simulation of ISF with different time and mass scaling factors. The maximum plastic strain obtained in various simulations are plotted and shown in Fig. 3.26. It can be observed from the results that the distribution of plastic strain is not getting effected with punch velocity. The plastic strain is increasing with increase in mass scaling factor. But this increase is not very significant compared to the plastic strain obtained without mass scaling.

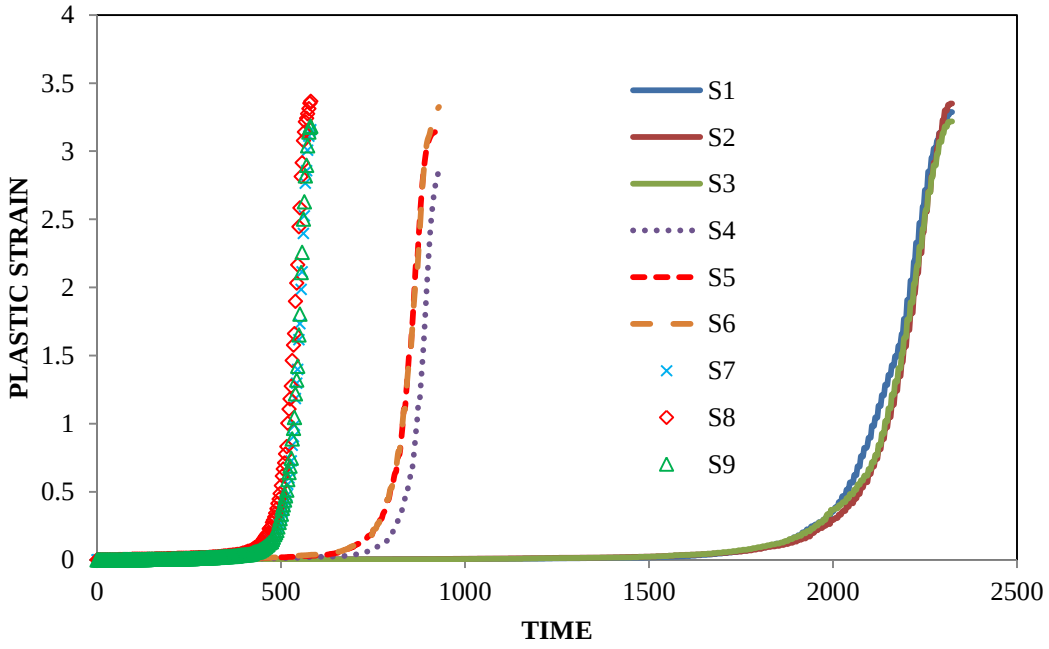

Fig. 3.26 Distribution of maximum plastic strain

3.7.3 Punch force

The distribution of forming force on the punch in the vertical direction is shown in Fig. 3.27. The results revels that the forming force is not getting affected by the punch velocities. The force seems to be increasing with mass scaling factor. However, in the selected range of mass scaling factors the variation in force distribution is very less.

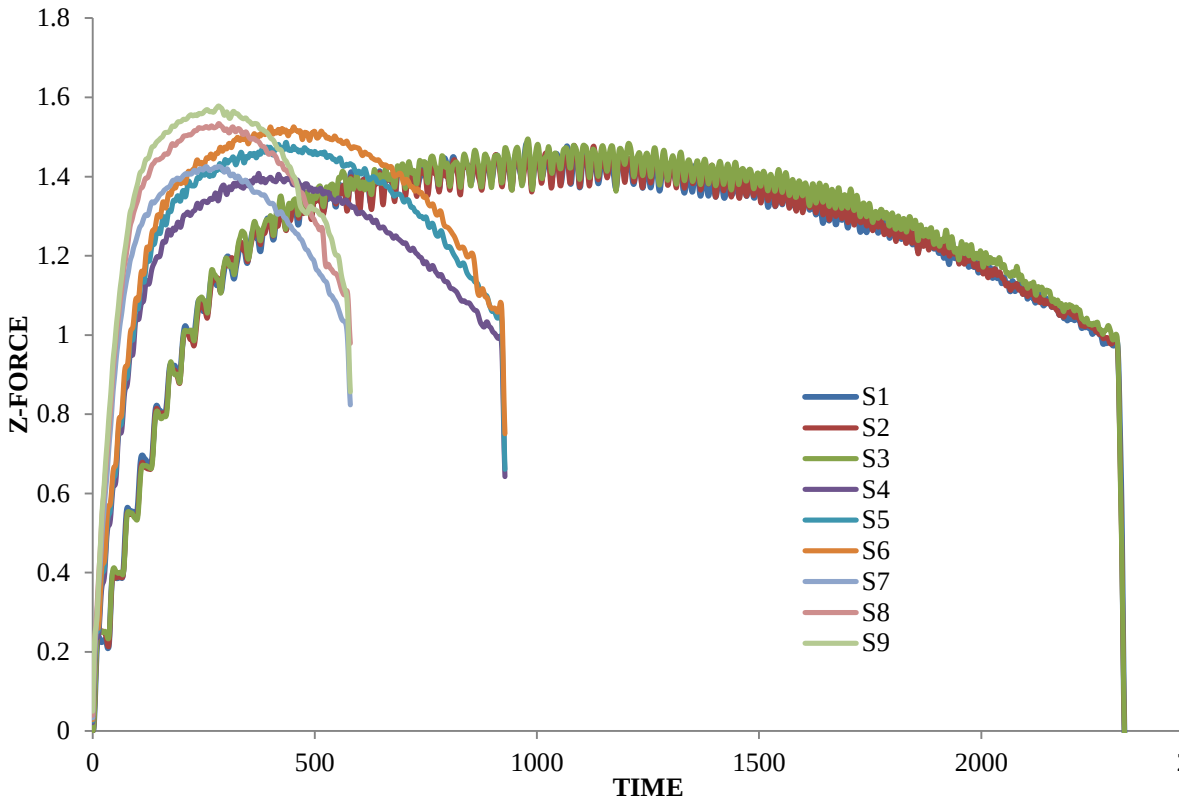

Fig. 3.27 Distribution of punch force

3.7.4 Computational time

The computational time for different combinations of time and mass scaling factors is shown in Table 3.11. The simulation with punch velocity of 10 m/s without mass scaling took nearly 155 hours, while the simulation with punch velocity of 40 m/s and mass scaling factor of 10 took 12.5 hours without sacrificing the accuracy of results. Nearly 50% reduction in computational time is observed with mass scaling factor compared to the simulations without mass scaling. Time scaling also has significant effect on computational time. The computational time is reduced by 60% when the punch velocity is increased from 10 m/s to 25 m/s, while from 25 m/s to 40 m/s the computational time is reduced by 40%.

Table 3.11 Computational time with different time and mass scaling factors

Exp.No	Punch Velocity	Mass scaling factor	Computational time (in MIN.)
S1	10	0	9297
S2	10	5	4117
S3	10	10	2913
S4	25	0	3727
S5	25	5	1696
S6	25	10	1203
S7	40	0	2352
S8	40	5	1068
S9	40	10	752

In this section, the effect of mass scaling and time scaling on numerical simulation results of ISF process has been studied. From the results, it can be concluded that the punch velocity can be increased up to 40 m/s and mass scaling factor can be increased up to 10 without having any significant effect on the results. At the same time, a huge saving has been observed in terms of computational time.

3.8 Summary

This chapter provides a platform to understand the ISF process mechanics through finite element simulations. The methodology to input a simple 2-D tool path and complex 3-D tool path for FE simulations has been discussed. Wherever possible the simulation results have been validated with available results in the literature. The guidelines established in this chapter for finite element simulation of ISF process have been used in all the simulations in the subsequent chapters. The preliminary simulations in this chapter also provide a base to understand the effect of process parameters on material forming behavior in the ISF process.

Chapter 4 Formability

This chapter presents the experimental and numerical studies related to the formability of EDD steel in ISF. The formability of the material has been quantified in terms of maximum formable wall angle using varying wall angle conical and pyramidal frustums. The deformation behavior of the material has been analyzed using experimental works and finite element simulations. The effect of process parameters on formability and thickness distribution has also been studied.

4.1 Formability of EDD in ISF

This section focuses on the formability and thickness distribution in ISF of EDD steel. In ISF, the formability of the material is primarily measured by the maximum formable wall angle and maximum allowable thinning. The maximum wall angle is generally obtained by forming frustum of cones and square pyramids having different wall angles till fracture, which requires large number of experiments. Therefore in the present study, a continuously varying wall angle conical frustum (VWACF) is used to predict the maximum wall angle to minimize the number of experiments. VWACF is generated using circular, parabolic, elliptical and exponential generatrices. In order to get the maximum allowable thinning, the thickness of the formed geometry has been measured at various points along the depth. In addition, the thickness distribution has been computed theoretically based on the sine law and also using finite element code LS-Dyna. Theoretical and simulated thickness values have been compared with measured thickness values. It was found from the results that the finite element model is more accurate than theoretical model in predicting thickness distribution.

In ISF, the wall thickness of the part varies as per sine law. If t_i and t_f are initial and final thickness of the part with wall angle α with horizontal then the final thickness can be predicted by using the following relation [Jeswiet et al. (2005)]. The schematic representation of thickness variation in constant wall angle part is shown in Fig. 4.1.

$$t_f = t_i \cos\alpha \tag{4.1}$$

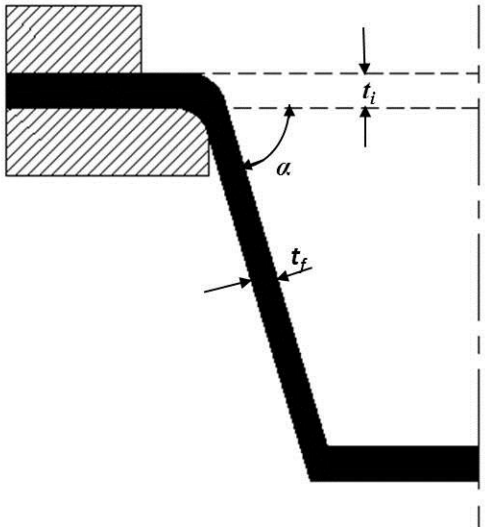

Fig. 4.1 Thickness variation in ISF

From Eq. 4.1, it is clear that with the increase in wall angle, the thickness tends to reach to zero, which leads to fracture. Thus, the maximum wall angle and minimum allowable thickness to which the part can be formed without fracture can be used as the parameters for assessing the formability in ISF. Also, the maximum formable wall angle of the part varies linearly with thickness and is given by the following relation [Jeswiet (2005)]:

$$\psi_{\max} = kt_0 + \beta \tag{4.2}$$

where, k is the slope of the line in deg/mm, t_o is the initial thickness of the blank and β is the y-intercept of the line.

4.1.1 Methodology

The varying wall angle conical frustums with circular, elliptical, parabolic and exponential generatrices are used to assess the formability of EDD steel in ISF. The geometry of the generatrices are shown in the Appendix. These curve segments are represented in parametric form due to their inherent advantages over explicit and implicit representation. The parametric equations simplify mathematical formulations for predicting wall angle and thickness at any point p on the generatrix. In all the geometries, the top diameter is kept as 110 mm and the wall angle is varied from 40^0 to 80^0. The variation of wall angle along the depth is shown in Fig. 4.2 for all the four generatrices.

In case of circular, elliptical and exponential generatrices, the wall angle variation is uniform along the depth, while in parabolic generatrix the wall angle is 73^0 for a depth of 50 mm and 7^0 for the remaining depth from 50 mm to 157.5 mm.

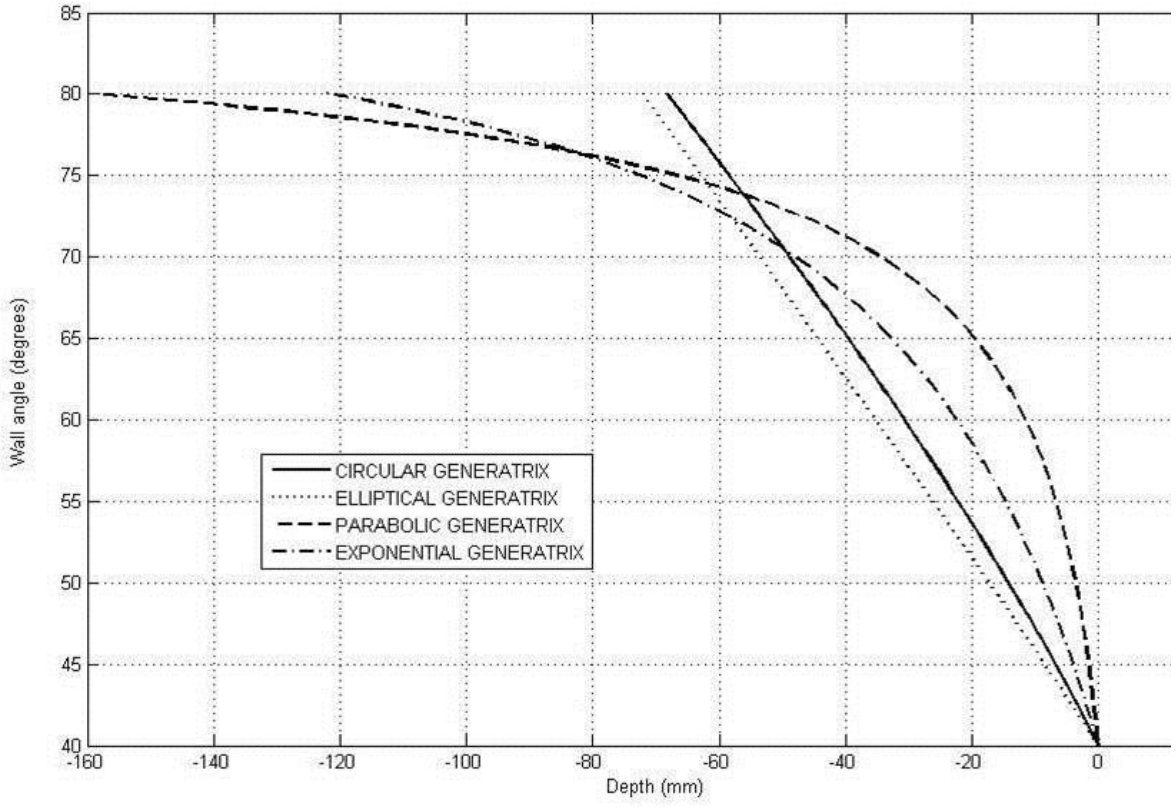

Fig. 4.2 Variation of wall angle with depth for different geometries

4.1.2 Experimental study

All the ISF experiments are performed on Bridgeport Hardinge 3-axis CNC milling machine with a fixture to hold the blank and a cylindrical tool with hemispherical head. The tool is made of EN36 and is heat treated to 60 HRC. The tool is polished with fine grade abrasive paper and lapping paste to improve the surface finish and to minimize the friction between the blank and sheet. A backing plate has been provided below the blank to prevent the bending of the sheet and to improve the form accuracy of the part. The backing plate is of 250 mm X 250 mm X 12 mm in size with 110 mm diameter hole in the center. The edge of the circular hole is provided with 5 mm radius to prevent the tearing of sheet due to sharp corners. EDD steel sheet of 250 mm X 250 mm X 1 mm size

is used as a blank material to make different parts. SAE-40 lubricating oil is applied to minimize the friction and temperature between the blank and tool. All the experiments are performed with 10 mm diameter tool at 750 mm/min feed rate and 0.5 mm step depth. The schematic diagram of the process and complete experimental setup are shown in Fig. 4.3.

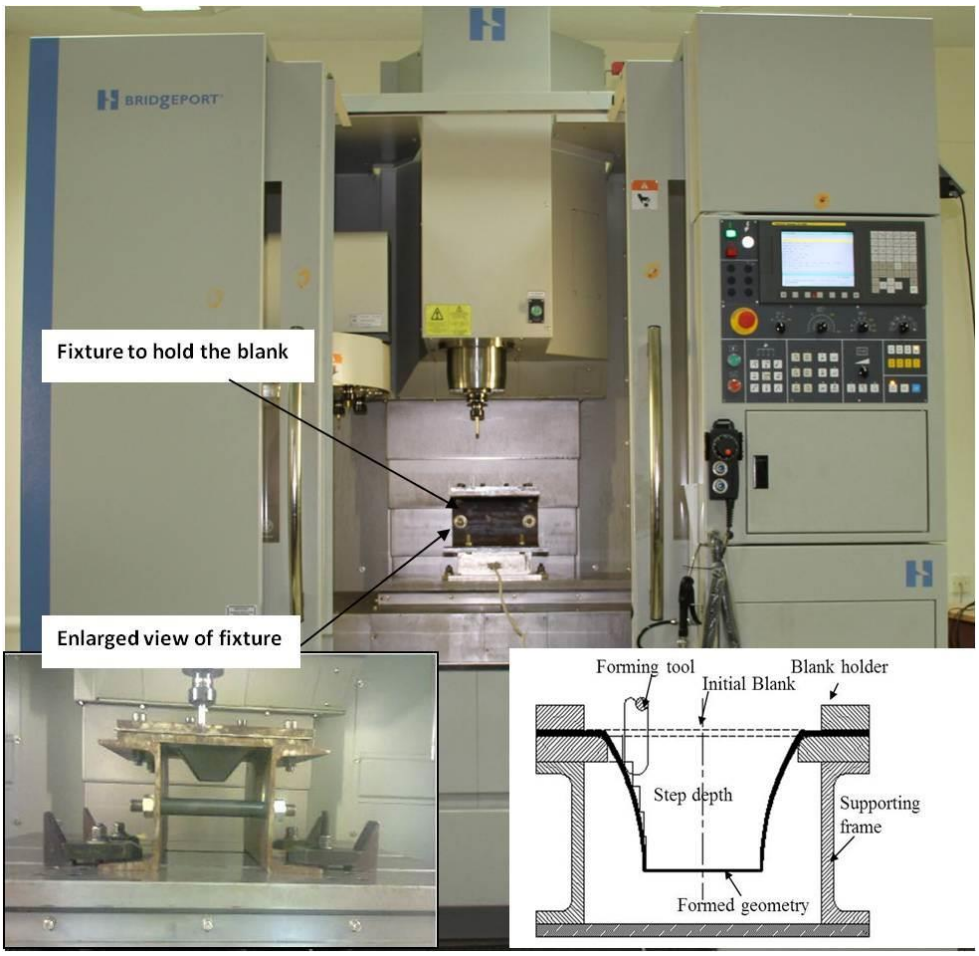

Fig. 4.3 Experimental setup with schematic diagram of process

To generate the tool path for the part geometries, the curve segments are designed in Pro-E software using the parametric equations given in Table 4.1. These curves are rotated about an axis to get the final part geometry with top base diameter of 110 mm. The formed parts are shown in Fig. 4.4.

Table 4.1 Parametric equations of generatrices

(a)	(b)
$x(u) = 115\cos 2\pi(0.3611 + 0.1111u) + 128.94$ $z(u) = 115\sin 2\pi(0.3611 + 0.1111u) - 88.08$ $0 \le u \le 1$	$x(u) = 160\cos 2\pi(0.3776 + 0.0968u) + 170$ $z(u) = 130\sin 2\pi(0.3776 + 0.0968u) - 90.38$ $0 \le u \le 1$
(c)	(d)
$x(u) = 48.348u - 54.998$ $z(u) = -5(0.8402 + 4.8348u)^2 + 3.53$ $0 \le u \le 1$	$x(u) = 48u - 55$ $z(u) = 4e^{0.04(41.5+48u)} - 21$ $0 \le u \le 1$

4.1.3 Finite element modeling

A 3-D finite element model is developed in explicit finite element code LS-Dyna for numerical simulation of ISF process. The blank, die and forming tool are modeled with shell elements of type-2. Fine mesh is used for blank with element edge length of 1 mm. Total five integration points are defined in thickness direction. The blank of EDD sheet is modeled using power law plasticity (MAT 18). The die and punch are modeled using the rigid material model (MAT 20). The strength coefficient and strain hardening exponent of blank are specified as 560 MPa and 0.23 respectively. The contact pairs, the tool and the blank, the blank and the die are modeled using forming one way surface to surface algorithm. Coulomb's friction law is used to model the friction between different contact surfaces. Due to the application of sufficient lubricating oil at tool sheet interface, very small friction efficient of 0.01 is used for simulations as recommended by Elford et al. (2013). The tool path for finite element simulations has been generated as per the methodology described in section 3.5. The mass scaling and time scaling factors have been chosen based on the guidelines established in section 3.8.

Fig. 4.4 Varying wall angle conical frustums formed in ISF

4.1.4 Results and discussion

The maximum wall angle is the primary parameter to assess the formability in ISF. To obtain the maximum wall angle, the varying wall angle conical frustums are formed on the CNC milling machine till the fracture. Two parts are formed for each generatrix design to improve the accuracy of results. After the occurrence of fracture the machine tool is stopped manually and the part is removed from the fixture. The depth of the part upto the fracture is measured using Vernier Height Gauge. Angle corresponding to this depth is called as the maximum formable angle, which is calculated using Eq. 4.3. The maximum wall angle is calculated for all eight parts and the average value is taken as a liming wall angle for EDD steel in ISF.

$$\theta_p = \tan^{-1}\left(\frac{dz/du}{dx/du}\right) \tag{4.3}$$

In the above equation *((dz/du)/(dx/du))* gives the slope at any point *p* on the generatrix with co-ordinates *x(u)* and *z(u)* and θp represents wall angle at *p*.

In order to get the thickness distribution along the depth, the parts are sectioned from the middle for ease of thickness measurement. For measuring the thickness, the points are marked for every 5 mm from the top to the bottom of the part using Vernier Height Gauge. For better clarity of thickness distribution in the bending region, the points are marked for every 2.5 mm. Thickness at every point is measured using Digital Pointed Anvil Micrometer having least count of 0.01 mm. In case of VWACF the wall angle and hence the thickness changes continuously with the depth. Hence, the wall angle (θ_p) and theoretical thickness (t_p) corresponding to each marked point (p) is calculated using Eqs. 4.3 and 4.4 respectively. Measured, theoretical and simulated thickness distribution for different geometries is shown in Fig. 4.5. Fig. 4.5 shows that the analytical model is poor in predicting thickness in the bending region, whereas numerical simulations are good in both bending and stretching region. From Table 4.2, it is clear that a very good correlation was observed between measured and simulation results, when compared to the correlation between measured and analytical thickness distribution for all the geometries. Based on the statistical parameters, it can be concluded that the simulation model is more accurate than analytical model in thickness prediction. Contour plots of thickness distribution from numerical simulations are shown in Fig. 4.6.

$$t_p = t_i \cos\theta_p \tag{4.4}$$

Table 4.2 Correlation coefficients

	R^2 values	
Part with	Measured Vs Theoretical	Measured Vs Simulated
Circular generatrix	0.9436	0.9944
Elliptical generatrix	0.9345	0.9933
Parabolic generatrix	0.9693	0.9827
Exponential generatrix	0.9659	0.9900

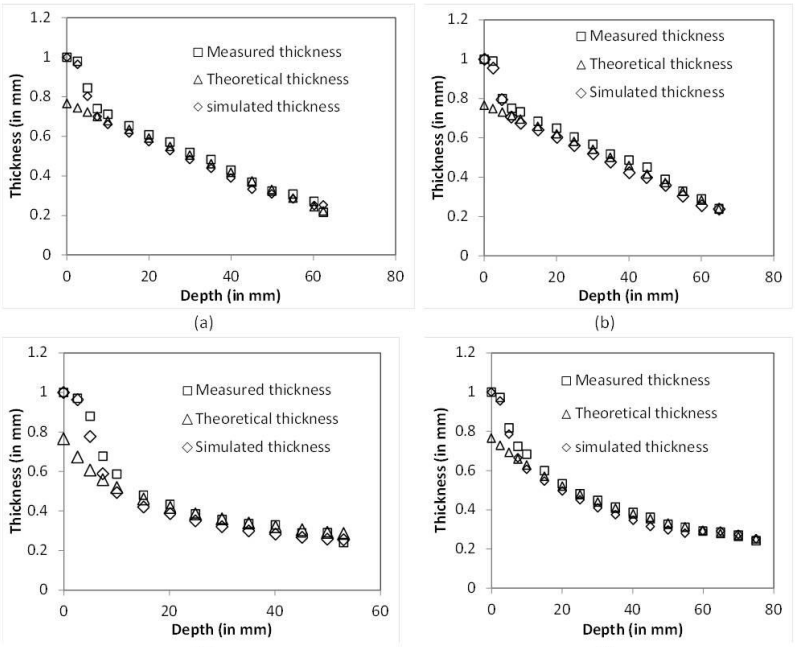

Fig. 4.5 Thickness distribution along the depth

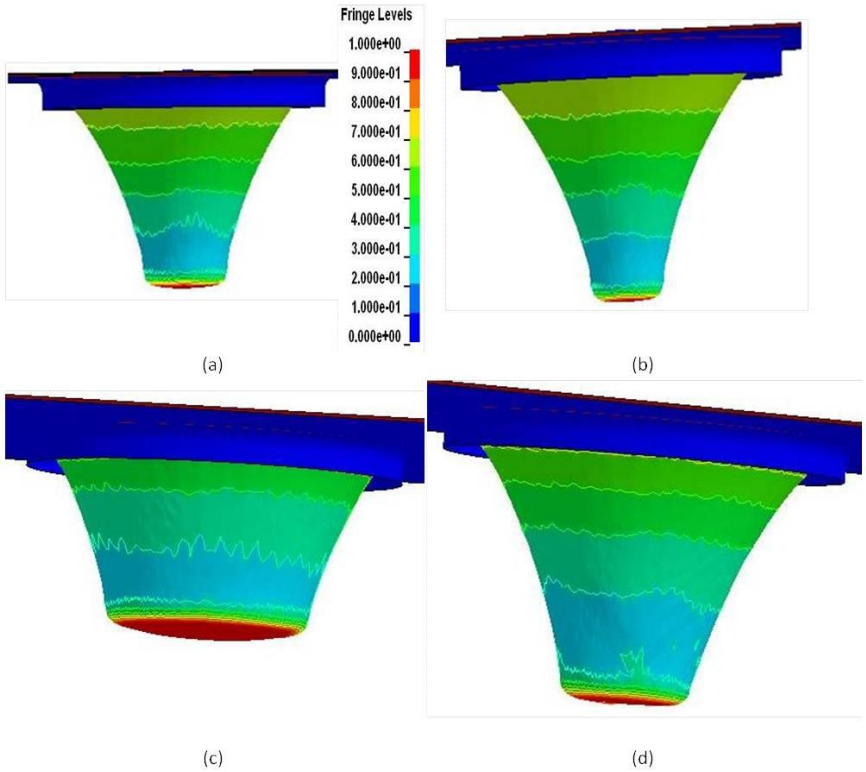

Fig. 4.6 Contour plots of thickness distribution

Table 4.3 Maximum wall angle and thinning limit with different geometries

Part Description	Part Number	Depth at fracture (mm)	Wall angle (deg)	Maximum thinning (mm)
Circular generatrix	1	62.5	77.15	
	2	63.5	77.66	0.236
Elliptical generatrix	1	62.0	74.60	
	2	65.0	76.23	0.241
Parabolic generatrix	1	50.0	73.00	
	2	53.0	73.43	0.290
Exponential generatrix	1	70.5	74.71	
	2	75.0	75.40	0.242

Depth, wall angle and maximum allowable thinning corresponding to the fracture point of various parts formed in ISF are summarized in Table 4.3. The values of maximum wall angles obtained with different geometries are close to each other. The average value of maximum formable wall angle with EDD steel is computed as 75.27^0. The maximum allowable thinning is 0.252 mm. The maximum variation in wall angle with different geometries is 4.6^0. Lesser wall angle was obtained in part with parabolic generatrix, this could be due to steep variation in wall angle with this particular geometry. The variation in wall angle with different part geometries could be due to variation in slope distribution and curvature. Hussain and Gao (2007) reported that the thickness of the sheet deviates from the sine law thickness at some point along its depth. They called this point as transition point and is used to measure the maximum allowable thinning. But, in this work, there is no such major deviation from the sine law thickness, therefore the minimum thinning in the part is considered as the allowable thinning. Parts with circular, elliptical and exponential generatrices are good choices to consider as benchmark parts for maximum wall angle prediction in ISF. In case of parabolic generatrix, the variation in wall angle is very less after reaching certain depth. The wall angle computed using parts with varying wall angle conical frustums are generally more than the parts with constant wall angle. This is due to the larger force in case of constant wall angle parts compared to varying wall angle parts.

The fracture surface of the incrementally formed part is analyzed using SEM photographs. The fractured specimen is cut to the required size for fractography study. The low magnification fractured surface is shown in Fig. 4.7(a). The scanning electron microscope (SEM) photographs of fractured surface at higher magnifications are shown in Fig. 4.7 (b-d), it indicates that the fracture is predominantly ductile in nature. In ductile fracture, damage accumulates due to nucleation, growth and coalescence of voids. Continuous nucleation of small voids takes place at the second phase particles and non metallic inclusions (Fig. 4.7c) over a wide range of plastic strains. Continuous nucleation of small voids at second phase particles leads to material failure. It is clearly evident from Energy-dispersive X-ray spectroscopy (EDS) analysis shown in Fig. 4.8 that this inclusion could be aluminum oxide. The composition of inclusion from EDS study was presented in Fig. 4.8. The cleavage cracks could be due to inhomogeneous plastic deformation in fracture zone or the aluminum oxide inclusions. From SEM studies it can be concluded that the ductile fracture models such as Gurson, J-C and Lamatire models can be used to model the fracture and for constructing the fracture forming limit diagram in ISF.

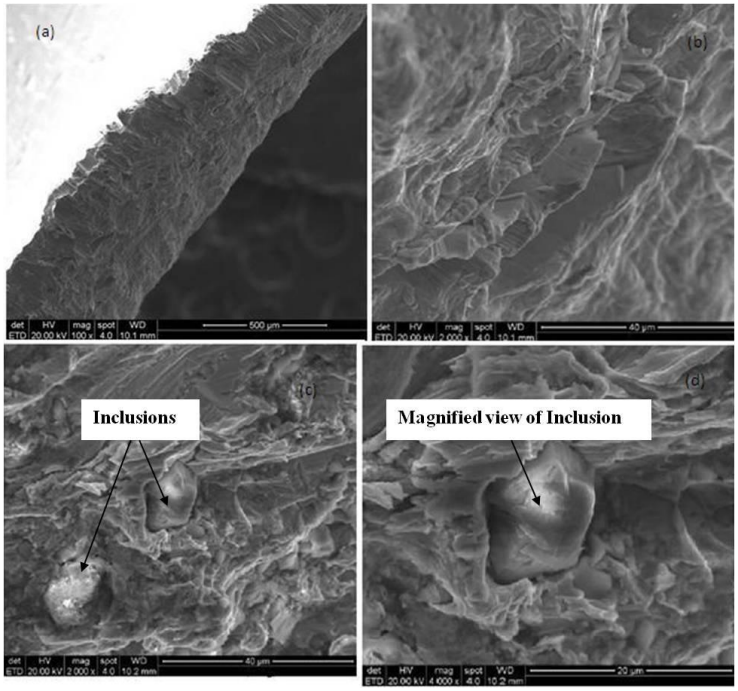

Fig. 4.7 SEM photographs of fractured surface

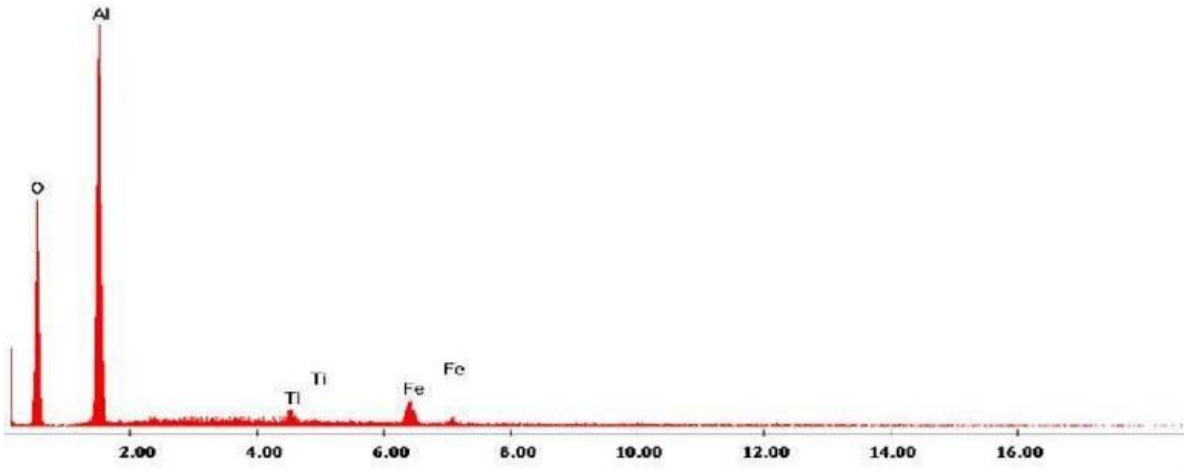

Fig. 4.8 EDS analysis of inclusion

In this section, the maximum wall angle and the thinning limit of EDD steel sheet in single pass single point negative incremental forming has been investigated. For this purpose, parts with varying wall angle along the depth were formed till the fracture. Numerical simulations are performed following the experimental phase to get the thickness distribution using LS-Dyna. Thickness distribution obtained from numerical simulations was found to be more accurate than the values obtained from theoretical model. Theoretical model was found to be poor in predicting thickness in bending region, whereas the finite element model is good in predicting thickness both in bending and stretching regions. A correlation coefficient of above 0.99 was observed between measured and simulated thickness with different part geometries. Limiting wall angle and allowable thinning were found to be 75.27^0 and 0.252 mm respectively. Maximum variation in wall angle with different generatrix curves was found to be 4.60. This variation could be due to variation in the curvature and slope distribution of different parts.

4.2 Deformation behavior of EDD

This section focuses on investigation of formability, thickness distribution, strain distribution and microstructural changes of EDD steel in SPIF process using varying wall angle pyramidal frustums. The parts were designed by rotating circular, elliptic, parabolic and exponential curve segments. The Varying Wall Angle Pyramidal Frustums

(VWAPF) can minimize the number of experiments required to find the maximum wall angle compared to conventional constant wall angle pyramidal frustum. The maximum wall angle corresponding to fracture depth and thickness distribution along the depth has been measured for parts with different generatrices. The maximum formable wall angle has been found to be 73 ± 2^0. Experimental thickness distribution has been compared with the thickness distribution obtained from numerical simulations using LS-Dyna software. A good correlation has been found between experimental and numerical results. Further, the distribution of strains from numerical simulations revealed that the faces of the pyramid are under plane strain condition, while the corners are towards bi-axial stretching. The microstructural study showed that there is a grain refinement after incremental forming of the sheet.

4.2.1 Maximum wall angle

To evaluate the maximum wall angle, the parts are formed till the occurrence of the fracture. The formed parts are shown in Fig 4.9. In all the parts, the fracture has occurred at the corners. Similar kind of phenomena was observed in the constant wall angle pyramidal frustums [Minutolo et al. (2007)]. To measure the wall angles, the part was removed from the fixture after the occurrence of the fracture. The depth of the fracture has been measured with vernier height gauge. The wall angle corresponds to fracture depth *(z(u))* has been evaluated using the Eq. 4.3. Three parts are formed for each generatrix to improve the accuracy of wall angle measurements. The average of the three values is reported as the limiting wall angle of the material. The maximum wall angle with different generatrices was varied from 71.47^0 to 74.6^0. Lowest maximum wall angle was observed with parabolic generatrix and highest maximum wall angle was observed in parts with elliptical generatrix. The variation in wall angle could be due to the variations in radius of curvature and steepness of wall angle.

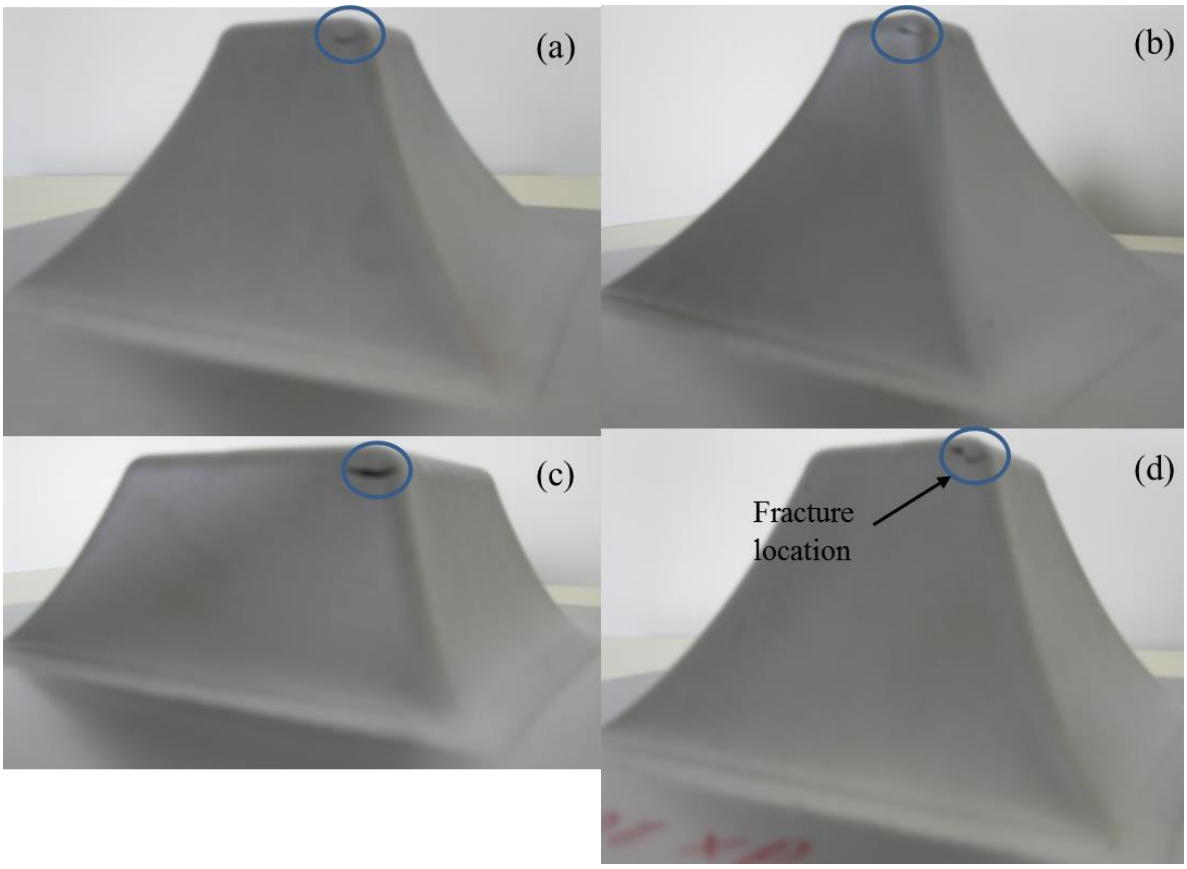

Fig. 4.9 Varying wall angle pyramidal frustums formed in ISF

The fracture depth and corresponding wall angle with different generatrices are given in Table 4.4. The wall angle with VWAPF was found to be lesser than the wall angle obtained with varying wall angle conical frustums. This is due to the increase of hoop strains at the corners of VWAPF due to larger contact area. However, in VWACF owing to large curvature radius of the part, the forming tool does not make significant contact in the hoop direction and thus the hoop strain is negligible. The limiting wall angles obtained with different generatrices of varying wall angle conical and pyramidal frustums are shown in Fig. 4.10. The maximum wall angle difference of 4.6^0 between two geometries (VWACF and VWAPF) was observed in parts with circular generatrix.

Table 4.4 Fracture depth and limiting wall angle with different generatrices

Generatrix type	Fracture depth	Limiting wall angle
Circular	54	72.76^0
Elliptic	62	74.6^0
Parabolic	41	71.47^0
Exponential	59.16	72.67^0

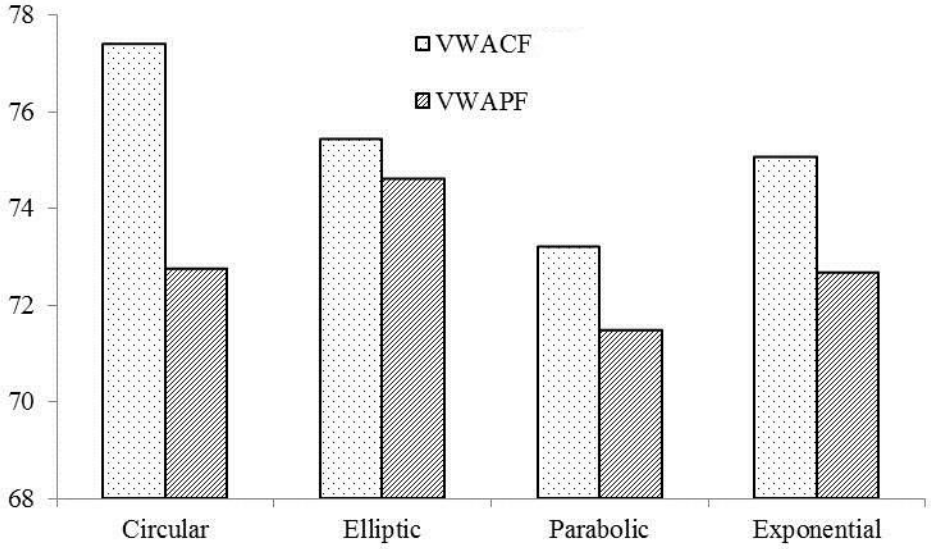

Fig. 4.10 Maximum obtainable wall angle with VWACF and VWAPF

4.2.2 Thickness distribution

Thinning is an important phenomenon in sheet metal forming to assess the quality of formed parts. The excessive thinning of the part leads to fracture. Thus, the allowable thinning of the material must be available to production engineer to deform the sheet without fracture. To get the thickness distribution in VWAPF, the formed parts are sectioned to the middle for the ease of thickness measurement. The thickness was measured for every 5 mm interval along the depth direction with a digital pointed anvil micrometer. In the bending region, the thickness was measured for every 2.5 mm to obtain better quality of thickness distribution.

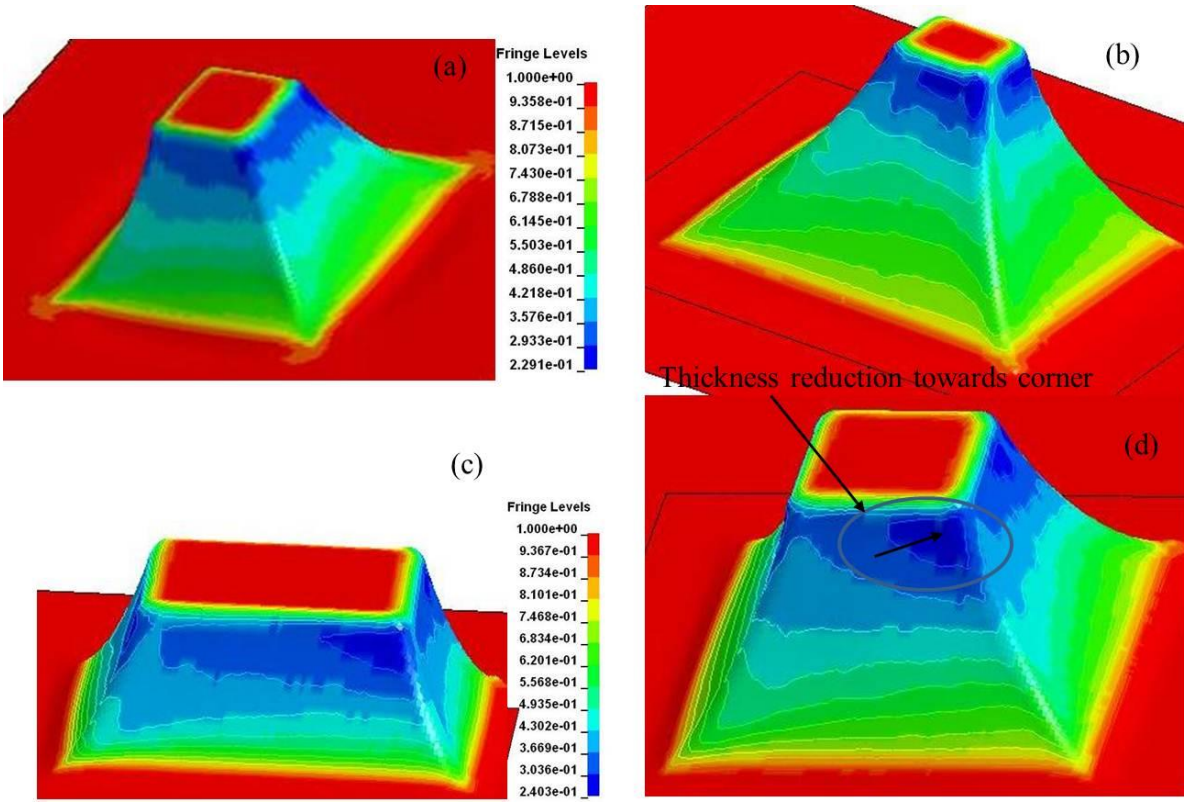

Fig. 4.11 Contour plots of thickness distribution

Fig. 4.11 shows the contour plots of thickness distribution obtained with different part geometries from finite element simulations. In all the geometries, the thickness is getting reduced towards the corners (as indicated in Fig. 4.11) and subsequently leading to the fracture. From the simulations it was found that the sheet can be formed without fracture up to 75% of thickness reduction. The measured and simulated thickness distribution with different part geometries are shown in Fig. 4.12. During the forming, the material near the corner of backing plate is subjected to bending and wall region is subjected to pure shear [Young et al. (2004)]. The results in Fig. 4.12 show that finite element simulations are capable to capture the thickness distribution both in bending as well as in shear deformation zones. The thickness distribution in wall region is found to be more uniform over the bending region. In all the part geometries the simulated thickness distribution is found to be lower than the experimental thickness distribution. A good correlation coefficient of 0.997 is observed between the measured and simulated

thickness distribution of part with elliptical generatrix. The lowest correlation coefficient of 0.968 was observed with the part having parabolic generatrix.

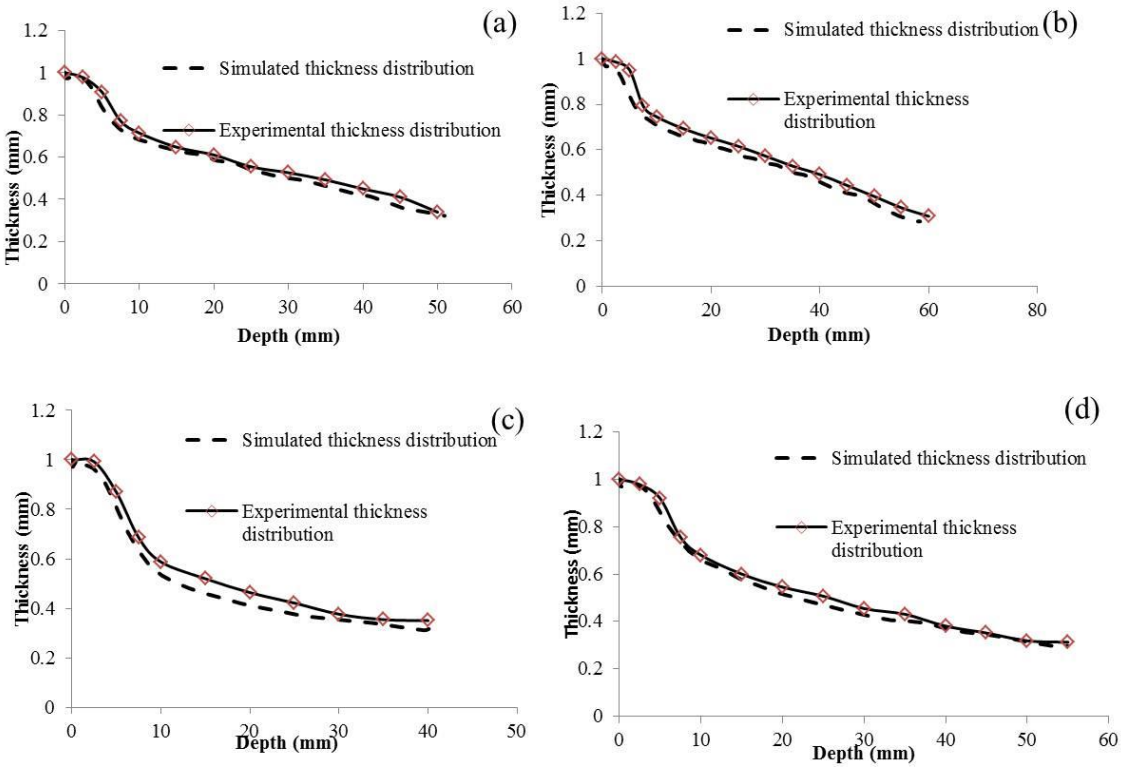

Fig. 4.12 Thickness distribution along the part depth

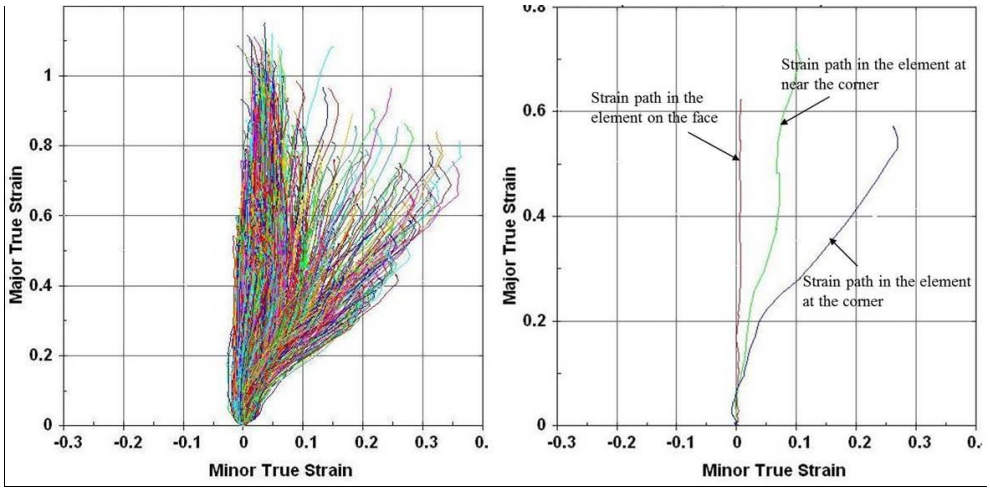

Fig. 4.13 Strain paths of different elements in VWAPF

4.2.3 Strain distribution

Silva et al. (2008) studied the possible deformation modes associated with SPIF and developed the analytical models. The strain distribution in ISF of VWAPF has been studied through finite element simulations. The simulation results reveal that the material is undergoing different strain paths in between plane strain and bi-axial stretching (Fig. 4.13). To understand this in a better way, three different elements are selected on the deformed geometry. The element on the face has been subjected to plane strain conditions and element at the corner was subjected to bi-axial stretching. While the element nearer to the corner has a strain path in between plain strain and bi-axial stretching (Fig. 4.13). The evolution of principal strains has been studied considering two elements, one on the face (F1) and another on the corner (C1). The maximum and minimum strains are zero up to sometime in the beginning (region A) as the element F1 is not yet deformed by the tool, when tool comes in contact with the element it undergoes continuous plastic deformation and reaches to maximum value (region B), with time the tool moves away from the element F1 thus the plastic strain remains constant (region C) (Fig. 4.14a). Similar kind of strain distribution was observed in the element C1 with respect to maximum and minimum principal strains (Fig. 4.14b). However, it is worth to note the variations in the intermediate principal strains of element F1 and C1. In the element F1, the intermediate principal strain is almost zero, thus it is in the plane strain state. The non-zero intermediate principal strain in the element C1 reveals that it is towards bi-axial stretching. The tri-axiality ratio in bi-axial stretching is more compared to plane strain conditions, thus the fracture has occurred at the corners of the pyramidal parts.

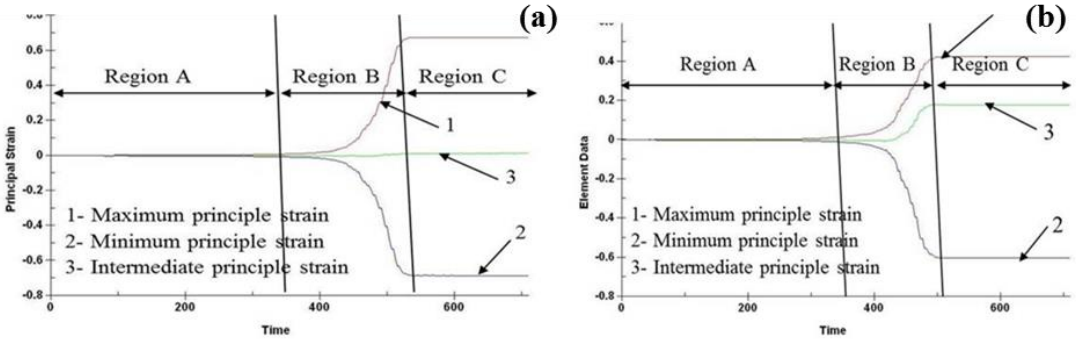

Fig. 4.14 Distribution of principal strains

4.2.4 Microstructure and hardness

The microstructure of as-received material and deformed pyramidal frustum has been analyzed using optical microscope. To analyze the microstructure of incrementally formed pyramidal part, three different samples have been taken from different locations of the formed geometry. The samples are prepared and etched with 2% Nital. The ASTM E 407 and ASTM E112 standards have been followed for etching and grain size measurement. The microstructure of base material and bending region of the formed cup consists of elongated ferrite grains in the matrix with ASTM grain size number 6. The microstructure study (Fig. 4.15) indicates that the ferritic grains, which have excellent ductility have undergone large amount of elongation. Further, due to excellent adhesion between the ferritic and pearlitic grains, the ferritic grains in turn forced the pearlitic grains also to elongate. The resistance to deformation is mainly offered by pealitic grains which are tougher. The grains are heavily deformed in the middle and bottom of the wall region and the grain size number was found to be ASTM-5. The present microstructural study shows that the steel sheet undergoes appreciable grain refinement in ISF unlike aluminum alloys [Radu et al. (2013)]. This could be due to the excessive forming forces required for forming the steel sheets and presence of alloying elements.

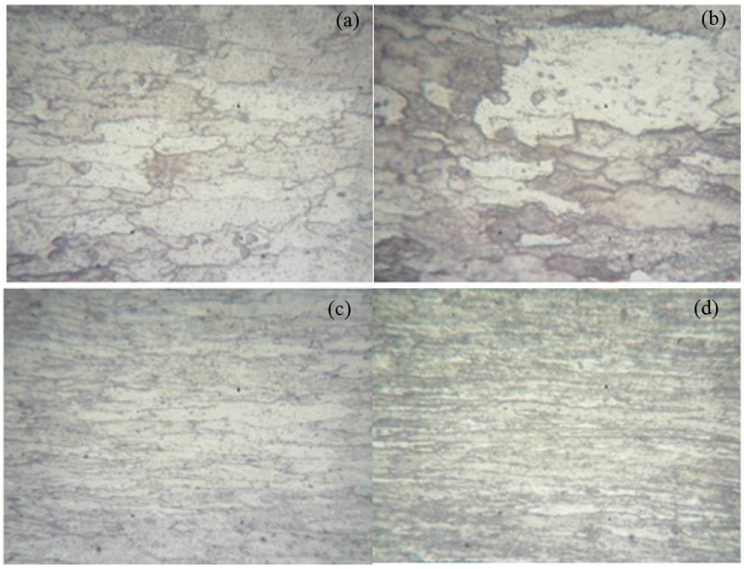

Fig. 4.15 Optical micro structure of EDD steel

The variation in the hardness along the cross section of the VWAPF due to microstructural changes has been studied using Vickers micro hardness test. Tests have

been conducted with 300 gf and dwell time of 15 sec. The hardness value in the bending region is almost equal to the base material and is equal to 134 HV. The hardness values in the wall region and tail end of the part was found to be 185 HV and 208 HV respectively. The increase in hardness towards the bottom of the cup is mainly due to the grain elongation and strain hardening of the material. Further studies are required to understand the effect of grain elongation on other mechanical properties. The optical micrographs of different samples are shown in Fig. 4.15.

The formability, thickness distribution, strain paths and microstructure of EDD steel in SPIF have been analyzed using VWAPF. The results of the study can be summarized as follows:

- The limiting wall angle in incremental forming of EDD steel under bi-axial stretching was found to be 73 ± 2^0. Further, the material can be formed without any fracture up to 75% reduction in thickness.
- Finite element studies using LS-Dyna revealed that the VWAPF have been undergoing different strain paths during incremental forming. The material on the face of the pyramid is under plane strain condition, while the material at the corners is towards bi-axial stretching.
- The microstructure study shows that the grain size has decreased from ASTM grain size number 6 to 5 in the deformed pyramidal geometry.

4.3 Analysis of formability with FE simulations

Maximum wall angle is a primary parameter to assess the formability of material in incremental forming. However, the forming limit diagram or forming limit curve is generally used for predicting the forming behavior of the sheet metal. The conventional forming limit curve can not be used to assess the formability of material in ISF due to better formability of material in this process. Instead, the fracture forming limit curve (FFLC) is used to analyze the material formability in ISF. Many empirical equations have been proposed to get the FFLC of a given material. In this section the empirical equation proposed by Fratini et al. (2004) has been used to define the FFLC for EDD steel. They proposed the following equation to find the FLD_0 as a function of strength coefficient

(*K*), strain hardening exponent (*n*), percentage reduction in area (*A*) and normal anisotropy (R_n).

$$FLD_0 = 8.64 – 36.2n – 0.00798K + 0.373R_n – 0.104A\% + 0.0301K*n + 0.607n*A\% \quad (4.5)$$

The FFLC of EDD steel sheet in incremental forming was calculated using Eq. 4.5. The *y*-intercept of forming limit curve (FLD_0) for EDD steel was found to be 1.59. 20% of FLD_0 is considered as a safety margin. This safety margin can take care of experimental uncertainties and effect of process parameters on FFLC. The FFLC has been given as a input to finite element simulations to measure the formability of VWACF and VWAPF parts formed in the section 4.2 and 4.3.

The principal strain history of varying wall angle conical frustums with different generatrices is shown in Fig. 4.16. The strain history in the figure revels that the material is undergoing plane strain conditions. The depth of the fracture and corresponding wall angle with conical frustums is found from forming limit diagram. The fracture depth calculated from numerical simulations is found to be very close to experimental values. The maximum error has occurred with part having exponential generatrix and is equal to 3.62%.

The principal strain history in pyramidal frustums with different generatrices is shown in Fig. 4.17. The strain history of these parts reveals that the faces of frustums are under plane strain condition, while the corners of the parts are undergoing bi-axial stretching. In all the pyramidal parts, the fracture has occurred at the corners. The maximum error has occurred with part having exponential generatrix and is equal to 2.65%.

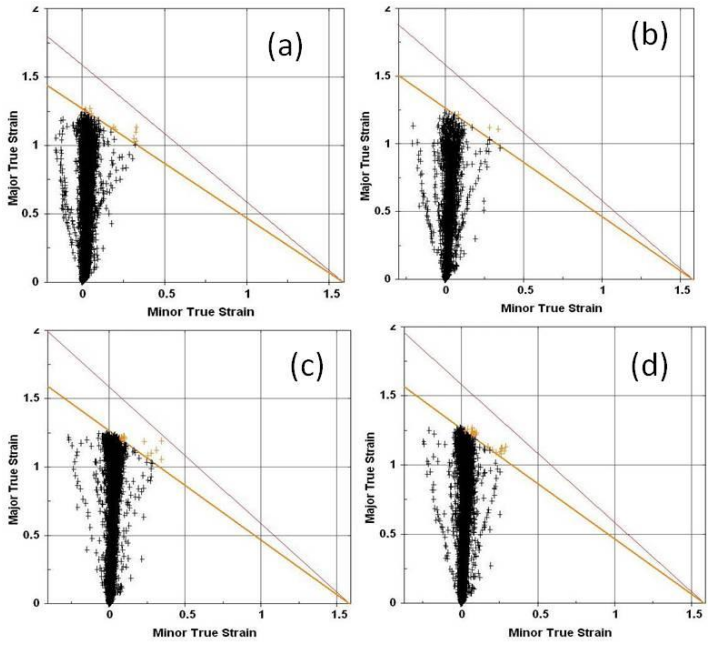

Fig. 4.16 Distribution of major and minor principal strains in VWACF

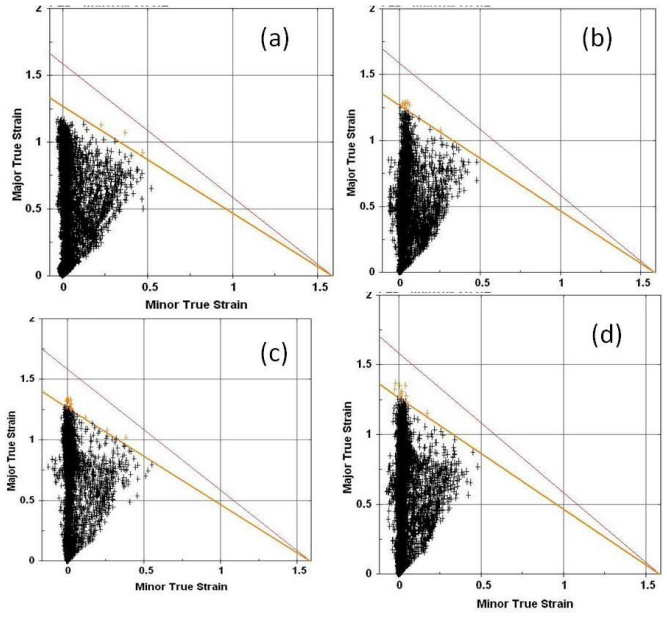

Fig. 4.17 Distribution of major and minor principal strains in VWAPF

The experimental and simulated values of fracture depth with different conical and pyramidal frustums are shown in Fig. 4.18.

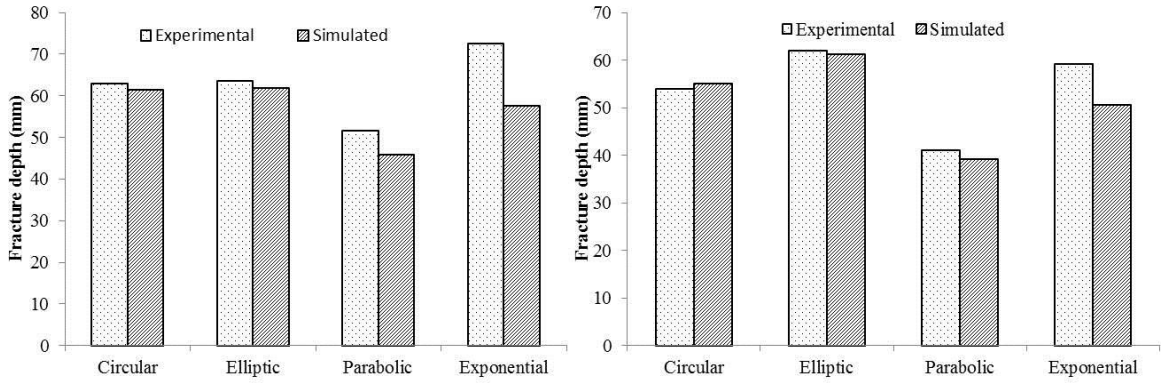

Fig. 4.18 Experimental and simulated fracture depth of VWACF and VWAPF

4.4 Effect of process parameters

The main objectives of the studies in this section are to investigate the effect of process parameters on maximum wall angle in incremental forming of EDD steel. For this purpose, four important process parameters namely, tool diameter, feed rate, shape of the part geometry and step depth have been correlated with maximum wall angle. Experiments have been conducted on CNC milling machine in accordance with Taguchi L_9 orthogonal array. The statistical methods, signal to noise (S/N) ratio and Pareto ANOVA have been used to find out the optimum process settings and percentage of contribution of different process parameters on maximum wall angle. A linear regression model was also proposed to predict the wall angle as a function of process parameters. Based on the studies, the optimum conditions were found to be A1B2C1D1. It was also found that the tool diameter has significant effect on maximum wall angle followed by feed rate, shape and step depth. Furthermore, wall thickness distribution of formed parts under different process conditions has been studied through experiments and finite element simulations using LS-Dyna. A good correlation was found between experimental results and numerical simulations.

4.4.1 Experimental study

Taguchi based experimental designs have been used extensively to study the effect of process parameters and optimization of various manufacturing processes. Therefore, the present study uses the Taguchi method to determine the optimum process

settings in SPIF. The method has been used to plan the experiments, analyze the effect of process parameters on response variable and to select the optimum combination of process settings. A standard L_9 (3^4) Taguchi orthogonal array has been used to design the experimental matrix. The maximum wall angle was considered as a response variable and four factors – tool diameter, feed rate, shape of the part and step depth have been considered as important process parameters. Each of these factors are varied over three levels. The factor levels and process conditions are given in Table 4.5.

Table 4.5 Factor levels and process conditions

Symbol	Process parameters	Level-1	Level-2	Level-3
A	Tool diameter (mm)	6	10	14
B	Feed rate (mm/min)	750	1500	2250
C	Shape of the part	-1	0	1
D	Step depth (mm)	0.7	1.1	1.5

In this study, EDD steel sheet of dimensions 250 mm X 250 mm with 0.5 mm thickness has been used as a blank material. The experiments and simulations have been performed as described in section 4.2. The shape of the part is one of the process parameters among the four. Three different shapes namely, frustum of cone, frustum of pyramid and combination of cone and pyramid (D-shape) have been used for maximum wall angle prediction. The cone has a top base diameter of 110 mm, pyramid has top side length of 110 mm and D-shape has a top side length of 120 mm. The wall angle of all these parts have been varied from 40^0 to 80^0 from top base to bottom base by using circular arc segment as a generatrix. Different part shapes have been formed on CNC milling machine as per process settings shown in till the occurrence of the fracture. After the fracture, the part is removed from the fixture and fracture depth has been measured with the vernier height gauge. The angle correspond to fracture depth has been calculated using the Eq. 4.6 and given in Table 4.6.

.

Table 4.6 Measured and predicted wall angle under different process conditions

Ex. No	Control factors and their levels				$\varphi_{max\text{-}Exp}$	η	$\varphi_{max\text{-}pre}$	% error
	A	B	C	D				
1	1	1	1	1	73.44	37.31865	74.122	0.928649
2	1	2	2	2	72.24	37.17555	71.197	1.443798
3	1	3	3	3	67.59	36.59765	68.272	1.009025
4	2	1	2	3	69.45	36.83345	69.204	0.354212
5	2	2	3	1	69.66	36.85967	69.039	0.891473
6	2	3	1	2	68.8	36.75177	69.039	0.347384
7	3	1	3	2	66.49	36.45513	67.046	0.836216
8	3	2	1	3	67.35	36.56675	67.046	0.451373
9	3	3	2	1	66.81	36.49683	66.881	0.106272

4.4.2 Results and discussion

Taguchi method uses Signal to Noise (S/N) ratio to determine the optimum process settings for process response. Mainly, there are three S/N ratios that are used for calculations based on the objective function for the response: the lower the better, the nominal the better and the larger the better. For the present study, higher φ_{max} indicates the better performance. Therefore, the larger-the-better was used to calculate the S/N ratio. The larger-the-better S/N ratio can be calculated using Eq. 4.6.

$$\eta = S/N = -10\log\left(\frac{1}{m}\sum_{k=1}^{m}\frac{1}{y_k^2}\right) \tag{4.6}$$

where y_k is the response variable (φ_{max}) and m is the number of replications. The S/N ratios (η) calculated for each experimental setting is given in Table 4.7.The average S/N ratio values for every level of the process parameters is calculated based on the values given in Table 4.6 and shown in Table 4.7. In Taguchi method, the level of the process parameter corresponds to highest S/N ratio gives the optimum combination. Thus, the optimum process settings for maximum wall angle should be the first level of A factor (tool diameter), the first level of B factor (feed rate), the first level of C factor (part shape) and the first level of D factor (step depth). The difference between the maximum and minimum S/N ratios of each parameter is calculated and shown in Table 4.7. The

maximum difference of 0.52 was found with tool diameter. Based on the Taguchi analysis, the larger difference between values of S/N ratio will have a more significant effect on maximum wall angle. Thus, it can be concluded that the tool diameter has major influence on φ_{max} followed be feed rate, shape of the part and step depth.

Table 4.7 Mean S/N ratios

Level	S/N values			
	A_i	B_i	C_i	D_i
1	**37.03**	**36.87**	**36.88**	**36.89**
2	36.81	**36.87**	36.84	36.79
3	36.51	36.62	36.64	36.67
Delta	0.52	0.25	0.24	0.23
Rank	1	2	3	4

The percentage contribution of different process parameters on maximum wall angle of EDD steel in ISF has been analyzed using Pareto ANOVA. Pareto ANOVA is a simple method that uses the Pareto principle to analyze the results [Pa et al. (2012)]. Computational scheme of Pareto ANOVA for four factor three level design is shown in Table 4.8. The contribution of different process parameters on maximum wall angle and cumulative contribution is shown in Pareto diagram (Fig. 4.19).

Table 4.8 Computational scheme of Pareto ANOVA

Level	Factors - Mean S/N values			
	A_i	B_i	C_i	D_i
1	η_{A1}	η_{B1}	η_{C1}	η_{D1}
2	η_{A2}	η_{B2}	η_{C2}	η_{D2}
3	η_{A3}	η_{B3}	η_{C3}	η_{D3}
Sum of squares (S)	η_A	η_B	η_C	η_D
Total summation of squares of difference (S_t)		η_T		
Contribution ratio (S/S_t)	η_A/η_T	η_B/η_T	η_C/η_T	η_D/η_T
$\eta_A = (\eta_{A1}-\eta_{A2})^2 + (\eta_{A1}-\eta_{A3})^2+(\eta_{A2}-\eta_{A3})^2$; $\eta_B = (\eta_{B1}-\eta_{B2})^2 + (\eta_{B1}-\eta_{B3})^2+(\eta_{B2}-\eta_{B3})^2$;				
$\eta_C = (\eta_{C1}-\eta_{C2})^2 + (\eta_{C1}-\eta_{C3})^2+(\eta_{C2}-\eta_{C3})^2$; $\eta_D = (\eta_{D1}-\eta_{D2})^2 + (\eta_{D1}-\eta_{D3})^2+(\eta_{D2}-\eta_{D3})^2$				

The Pareto analysis for maximum wall angle shows that the tool diameter effects the φ_{max} at about 58% followed by feed rate, part shape and step depth at about 17.7%, 14% and 10.3% respectively. This result is similar to the results obtained from S/N response analysis.

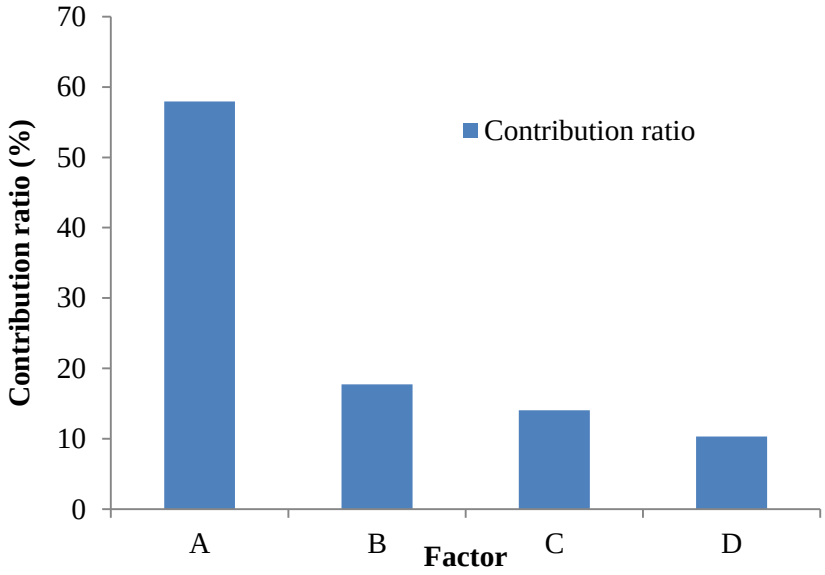

Fig. 4.19 Pareto plot

The main effect plot of mean wall angle is shown in Fig. 4.20. It can be observed from the figure that the wall angle has decreased with the increase in tool diameter. As the tool diameter increases, the deformation zone size is also increased due to large contact area, and deformation is no more localized in nature thus the formability decreases with the increase in tool diameter. The feed rate has no effect on the wall angle in the range of 750 mm/min to 1500 mm/min. However, with the increase of feed rate beyond this value has decreased the wall angle. Higher wall angle was observed with variable wall angle conical frustum over other part geometries. This could be due to the plain strain condition that prevails in the conical geometry. In other part geometries, the strains are towards bi-axial stretching at the corner which leads to pre-mature fracture. The increase in step depth has a negative effect on the wall angle. This is due to the increase of strains due to the increase of step depth.

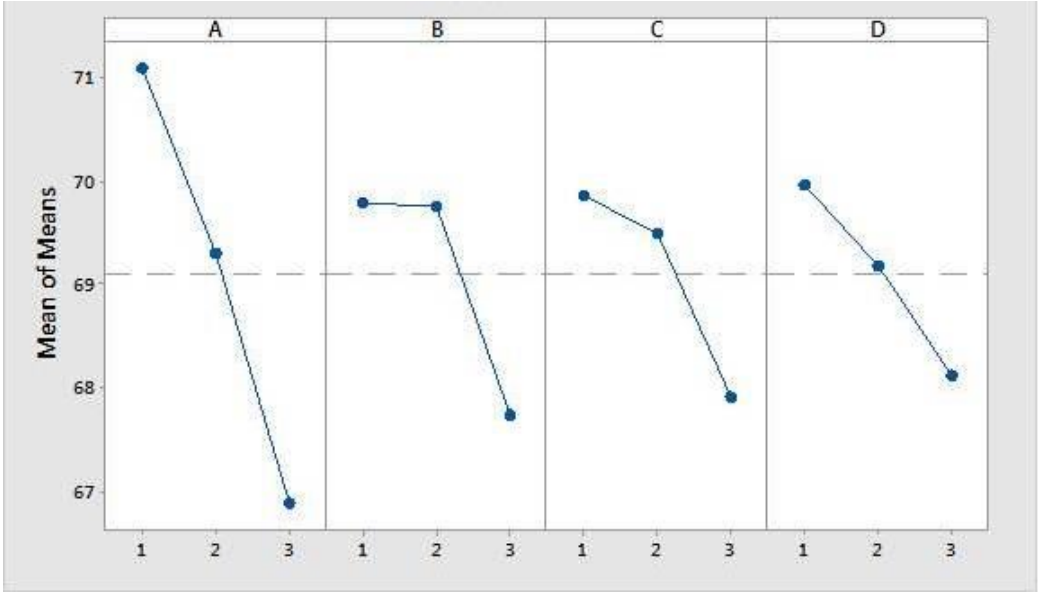

Fig. 4.20 Main effects plot of means

The fracture location under different forming conditions is shown in Fig. 4.21. At small tool diameter and low feed rates, the fracture is localized in the small area. With increase in feed rate the fracture has spread along the tool path. The increase in feed rate and tool diameter has spread the fracture over large area along the tool path. This is due to the large contact area between the tool and sheet, and also the large inertia force of the forming tool.

The regression analysis establishes the relationship between the process parameters and response variables. In the present study, a linear first order model was developed to predict the maximum wall angle as a function of process parameters. The general form of the first order linear model is given by the Eq. 4.7. The linear regression model for predicting the maximum wall angle is given by the Eq. 4.8.

$$y = \beta_0 + \sum_{j=1}^{p} \beta_j x_j + \varepsilon \tag{4.7}$$

where y is the response variable, β is the coefficient of each parameter, p is the number of parameters and ε is the error.

$$\varphi_{\max} = 79.15 - 2.103A - 1.030B - 0.975C - 0.920D \tag{4.8}$$

$R^2 = 93.72\%$ R^2 (adj) = 87.44%

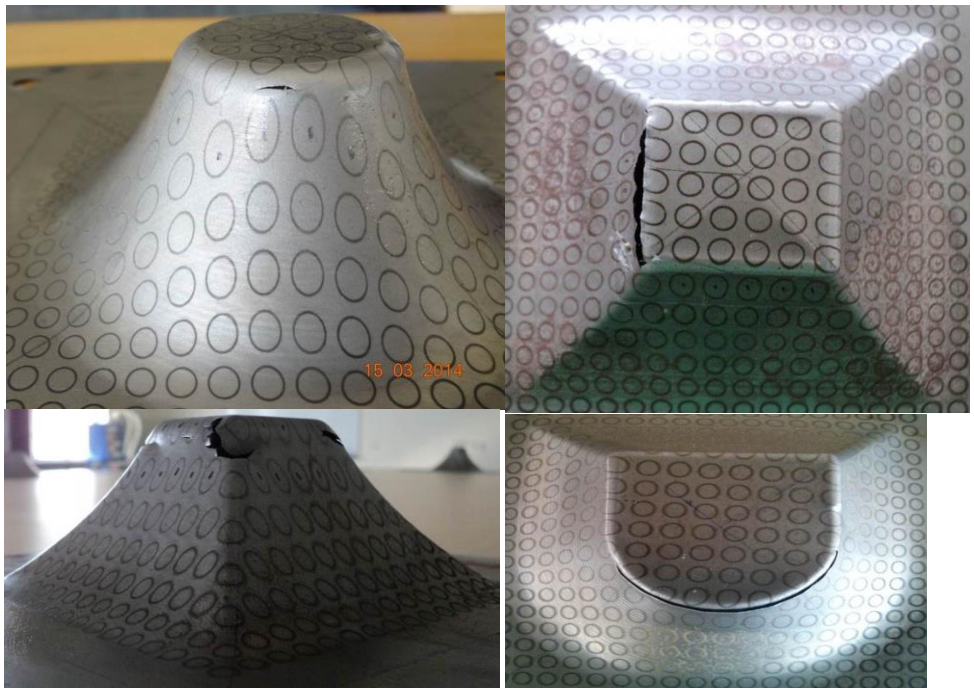

Fig. 4.21 Formed part geometries with fracture

To justify the validity of the first order model, R^2 and $R^2_{(adj)}$ values are calculated using Eqs. 4.9 and 4.10 respectively. In the regression analysis R^2 value should be in the range of 0.8 to 1. In this study, the regression equation was found to be consistent with experimental value (R^2>90%) and the first order model has been used to predict the maximum wall angle in incremental forming of EDD steel.

$$R^2 = 1 - \frac{\sum_{i=1}^{n}(y_i - f_i)^2}{\sum_{i=1}^{n}(y_i - \bar{y})^2} \tag{4.9}$$

Where y_i is the measured response variable in i^{th} experiment, f_i is the predicted value of the response variable in i^{th} experiment, $\bar{y}$ is the mean value of measured response variable and n is the total number of experimental runs.

$$R^2(adj) = 1 - \left(1 - R^2\right)\left(\frac{n-1}{n-p-1}\right) \tag{4.10}$$

The predicted values obtained from the first order model have been compared with experimental results and was plotted as shown in Fig. 4.22. The Fig. 4.22 shows that there is a good correlation between experimental and predicted values.

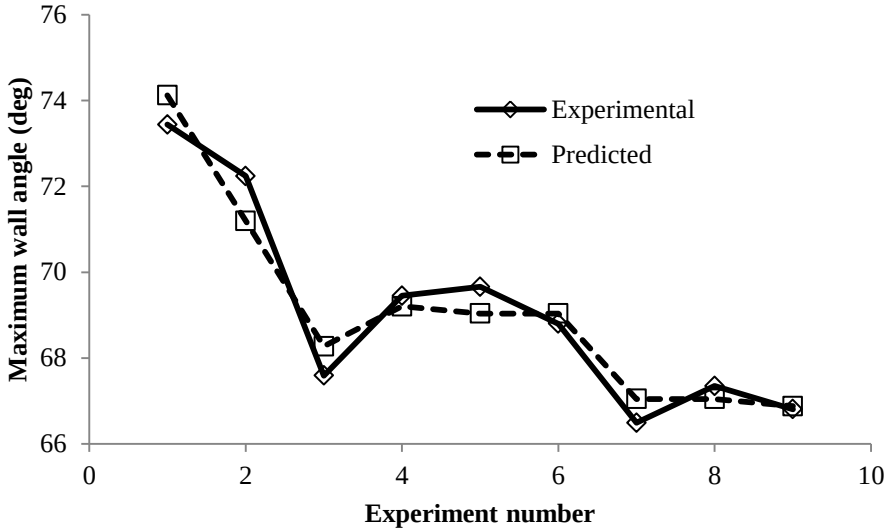

Fig. 4.22 Measured and predicted wall angle under different process conditions

The relative percentage error between the predicted values by the first order linear model and experimental values of maximum wall angle are computed. The relative percentage of error is computed using the following formula:

$$\text{Relative error}\,(\%) = \frac{\left|\text{Predicted value} - \text{Experimental value}\right|}{\text{Experimental value}} \times 100 \qquad (4.11)$$

The relative percentage error in maximum wall angle prediction is shown in Table 4.6. The error statistics reveal that the maximum and minimum percentage of error in maximum wall angle prediction with first order linear model was found to be 1.443% and 0.106% respectively. The mean percentage of error was found to be 0.707%.

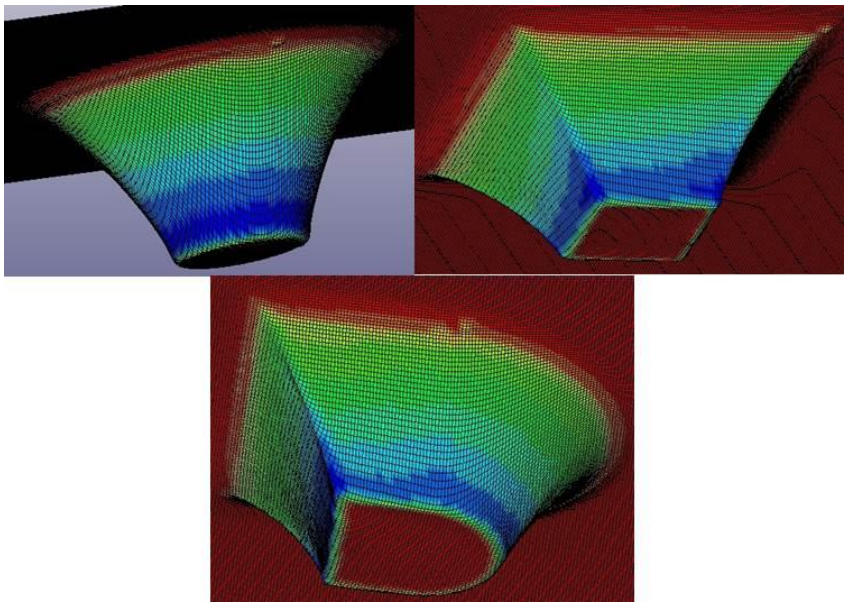

Fig. 4.23 Contours plots of thickness distribution

Table 4.9 Experimental thickness distribution of formed parts

Depth	Ex.No. 1	Ex. No. 2	Ex.No. 3	Ex.No. 4	Ex.No. 5	Ex.No. 6	Ex.No. 7	Ex.No. 8	Ex.No. 9
0	0.5000	0.5000	0.5000	0.5000	0.5000	0.5000	0.5000	0.5000	0.5000
2.5	0.4810	0.4490	0.4907	0.4947	0.4947	0.4690	0.4920	0.4670	0.4800
5	0.4217	0.4033	0.4330	0.4583	0.4060	0.4140	0.4827	0.4187	0.4023
7.5	0.3830	0.3517	0.3690	0.3857	0.3557	0.3603	0.4060	0.3750	0.3583
10	0.3617	0.3327	0.3517	0.3640	0.3350	0.3407	0.3657	0.3253	0.3383
15	0.3450	0.3033	0.3273	0.3293	0.3133	0.3137	0.3350	0.2980	0.3097
20	0.3140	0.2883	0.2903	0.3097	0.3000	0.2970	0.2997	0.2763	0.2853
25	0.2907	0.2730	0.2660	0.2873	0.2733	0.2730	0.2820	0.2587	0.2650
30	0.2673	0.2507	0.2343	0.2597	0.2543	0.2553	0.2627	0.2407	0.2487
35	0.2370	0.2273	0.2237	0.2370	0.2297	0.2320	0.2500	0.2133	0.2147
40	0.2240	0.1917	0.2077	0.2177	0.2063	0.2100	0.2333	0.1820	0.2110
45	0.1973	0.1833		0.2093	0.1757	0.1970	0.2143		0.1933
50	0.1773								
55	0.1513								

The formed parts under different forming conditions have been sectioned in the middle to measure the thickness. The thickness has been measured for every 5 mm depth from the top surface using pointed anvil micrometer. The measured thickness values are given in Table 4.9.

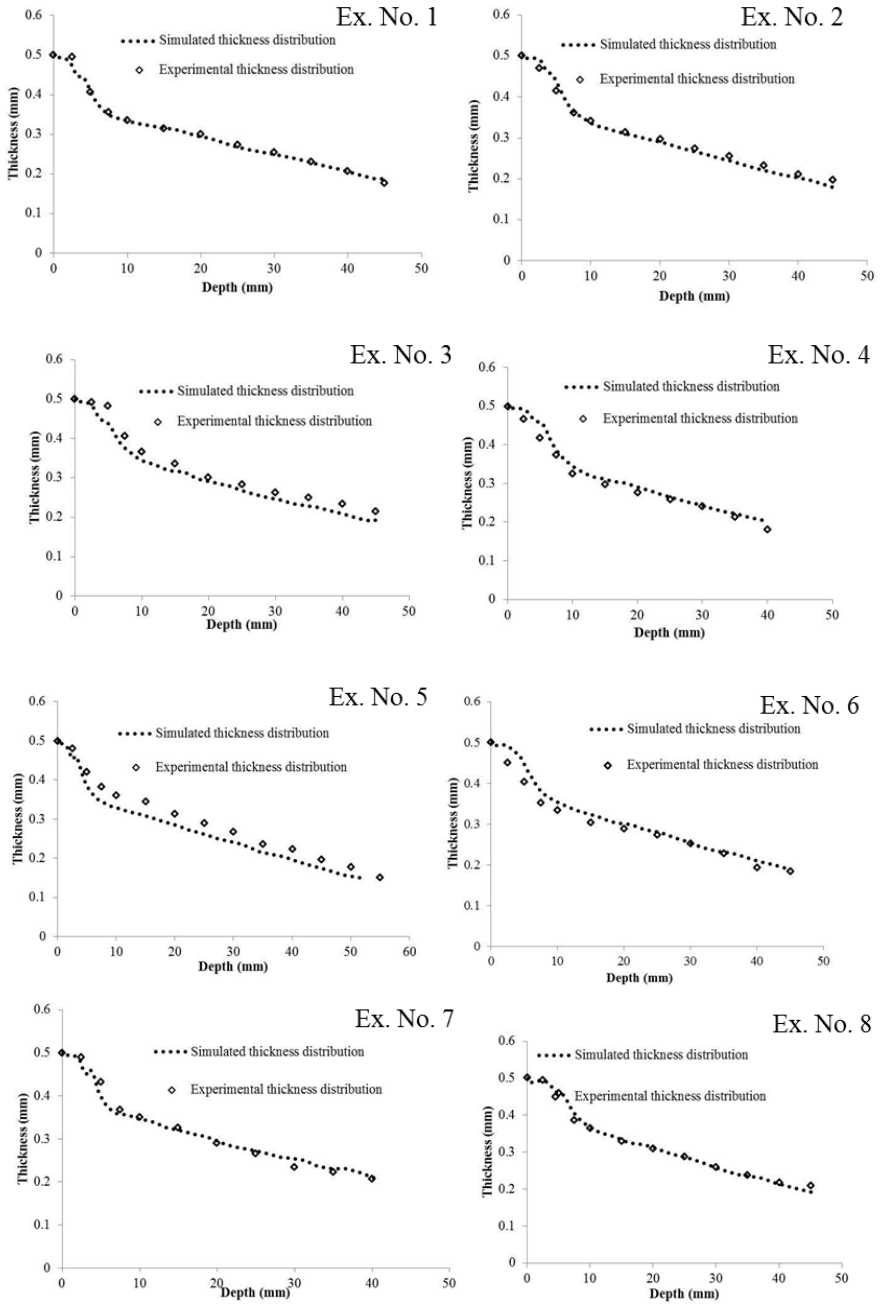

Fig. 4.24 Comparision of thickness distribution between experiments and FE simulations

In order to verify the effectiveness of finite element simulations in thickness prediction, the parts have been simulated using LS-Dyna software. The contour plots of thickness distribution in experiment numbers 1 – 3 are shown in Fig. 4.23. The thickness distribution of parts from finite element simulations has been compared with the

experimental results (Fig. 4.24). The results of finite element simulations match well with the experimental results.

The Taguchi experimental design has been used to study the effect of process parameters on maximum wall angle in incremental forming of 0.5 mm thick EDD steel sheets. The results obtained from the study are summarized below.

- Tool diameter, feed rate and step depth have negative effect on maximum wall angle. The tool diameter has maximum influence on the wall angle followed by feed rate and step depth.
- The optimum process parameters for maximum wall angle was found to be A1B2C1D1 (A = 6 mm, B = 1500 mm/min, C = VWACF, and D = 0.7 mm).
- Good correlation was found between the measured thickness distribution and finite element simulation results using LS-Dyna under different forming conditions.

The present study explained how to use the Taguchi experimental design and Pareto ANOVA to plan the experiments, to obtain optimum process settings and to find the percentage of contribution of different process parameters on response variable in SPIF process. It also demonstrated the capability of finite element method to simulate the SPIF process.

4.5 Summary

This chapter described the experimental setup used for SPIF process to study the formability of EDD steel. The formability of material has been analyzed in terms of maximum wall angle using VWACF and VWAPF with different generatrices. The fracture depth of these parts has been predicted with finite element simulations using analytical fracture forming limit curve. Distribution stresses and strains in the formed parts have simulated and validated with experimental results. The fracture and micro structural changes of formed parts have been studied using SEM and optical microscope. Further, the effect process parameters on maximum wall angle and thickness distribution have been studied through systematic experimental plan using Taguchi orthogonal arrays.

Chapter 5 Surface Roughness

In this chapter, the effects of process parameters on surface roughness of formed parts have been studied through systematic experimental design. Empirical models have been developed using response surface methodology and different soft computing techniques. The developed models have been used for single and multi-objective optimization.

5.1 Parametric Study and Multi-objective Optimization

. The surface finish of the parts produced in SPIF process gets affected by various process parameters. To get the proper quality of parts for functional applications it is important to understand the effect of various process parameters on part quality. Another drawback with this process is long processing time which also gets effected by different process parameters. Thus, the first objective of this section is to study the effect of various process parameters on surface roughness and manufacturing time. Second objective is to carry out the multi-objective optimization to get optimum process parameters. For this, detailed experiments are conducted using Box-Behnken design. The effects of step depth, tool diameter, wall angle, feed rate and lubricant type on surface roughness and processing time have been investigated. Based on experimental data, mathematical models have been developed for both the response variables *viz.* surface roughness and manufacturing time. Since the response variables are mutually exclusive in nature, multi-objective optimization algorithm NSGA-II has been used to get optimum process parameters. The Pareto front obtained from this algorithm helps the manufacturing engineer to select optimum process parameters in SPIF process.

5.1.1 Experimental study

Design of experiment (DOE) is an effective and efficient tool to understand the effect of process parameters and to optimize the manufacturing processes with minimum number of experiments. Factorial designs, Taguchi orthogonal arrays and response surface methodology are widely used DOE techniques in literature to study the performance of various machining operations. In the present study, Box-behnken design

has been used to plan the experiments. This is one of the most widely used response surface designs when factors are 4 or more. In this design, each factor is varied over three levels and can fit a quadratic model. The five factor box behnken design involves ten blocks and in each block two factors are varied through the four possible combinations of high and low, while the other factors are kept at the central values. This gives total 40 experiments, in addition to this, six repetitive experiments are performed, with settings corresponding to the center of the process space. The repetitive experiments are useful in estimating the variance (standard deviation) in the responses. The process parameters along with their limits are shown in Table 5.1.

Table 5.1 Process parameters and their levels used in experimentation

			Levels					
			Original			Coded		
Parameter	Notation	Unit	Low	Middle	High	Low	Middle	High
Tool diameter	A	mm	6	10	14	-1	0	1
Step depth	B	mm	0.15	0.3	0.45	-1	0	1
Wall angle	C	degree	35	45	55	-1	0	1
Feed rate	D	mm/min	700	900	1100	-1	0	1
Lubricant	E		MOS_2+Canola	Canola oil	SAE	-1	0	1

The incremental forming experiments have been carried out on Hardinge 3-axis CNC milling machine. The machine has a spindle speed range of 1 - 8000 rpm and maximum feed rate of 12000 mm/min. In the present work, Extra Deep Drawing (EDD) steel sheet of 250 mm X 250 mm X 1mm was used as a blank material. This material has good formability and dent resistance and widely used in automotive industry. The geometry of the part used for analyzing the surface roughness and manufacturing time is shown in Fig. 5.1. The blank was formed into the required shape using hemispherical headed tools made of EN-36 material. The tools are heat treated to 60 HRC to reduce the wear and abrasion. The forming tools are polished with fine grade abrasive paper and lapping paste to minimize the friction and ploughing action between the tool and blank interface. Further, three different lubricants are used to minimize the friction and to improve the surface finish of the part. These three are (i) canola oil, which is derived from natural canola seeds (ii) mixture of 5% (w/v) of molybdenum disulphide (MoS_2) powder of particle size 100 μm or less in canola oil and (iii) commercially available SAE-

40 oil. The required tool trajectories to deform the sheet into the desired shape are generated using pro-manufacturing software. The roughness of formed parts was measured by Surtronic 25 instrument of Taylor Hobson make shown in Fig. 5.1b. The surface roughness was measured at five different locations on the formed geometry to improve the accuracy of measurement. The average value was reported as the surface roughness of the formed component. For all the measurements, the evaluation length is taken as 4 mm and cutoff length as 0.8 mm. The manufacturing time of all the formed geometries was measured using stop watch.

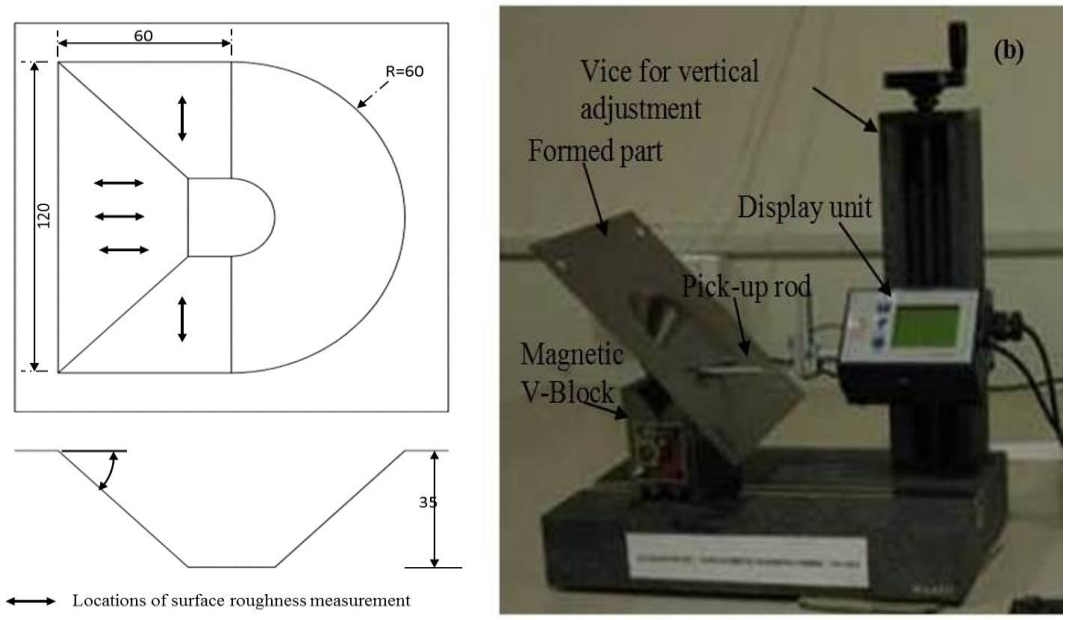

Fig. 5.1 Experimental setup for surface roughness measurement

5.1.2 Results and discussion

The surface roughness and manufacturing time data obtained from incremental forming experiments using Box-Benkhen design (Table 5.2) has been analysed using Design Expert software.The summary of model statistics reveal that the quadratic model is the most appropriate to analyze the surface roughness as well as the manufacturing time in ISF. The analysis of variance (ANOVA) table for quadratic model of R_a is shown in Table 5.3. The value of p in the ANOVA table is less than 0.05, this indicates that the regression model is statistically significant with a confidence intervel of 95%. In the quadratic model, linear, quadratic and interaction terms are significant as their p-value is

less than 0.05. Estimated coefficients of regression equation for R_a is given in Table 5 in coded and un-coded units. From this table, the most significant factors that influence the surface roughness are found to be *A*, *B*, *AB*, and A^2 . The ANOVA results reveal that there are more number insignificant factors in the model. Reducing the number of insignificant factors from the model can improve the acuuracy of prediction. Thus, the model has been reduced using backward elimination algorithm. The response surface equation of R_a after model reduction is given by the Eq. 5.1. The high correlation coefficient value (R^2=0.9337) of the developed model indicates that the developed regression equation provides a very good relationship between the input parameters and response (R_a). Further, the adequacy of model has been tested with normal probability plot of the residuals. The normal probability plot shown in Fig. 5.2(a) reveals that the calculated residuals (difference between the experimental and predicted values of response variable) are falling along a straight line. This indicates that the errors are following normal distribution and the developed model is reasonablly acceptable.

$$R_a = 0.76 - 0.56 * \mathrm{A} + 0.2 * \mathrm{B} - 0.21 * \mathrm{A} * \mathrm{B} + 0.64 * \mathrm{A}^2 \qquad (5.1)$$

The ANOVA results for quadratic model of manufacturing time are given in Table 5.4. The results indicate that the developed model is suitable for predicting the manufacturing time (p<0.05) and lack of fit is insignificant (p>0.5). However, the normal probability plot of the residuals shown in Fig. 5.2b indicates that the residuals are deviating more from the straightline. This shows that the residuals are not following the normal distribution. It is also a fact that the processes involving time metrics (cycle time, waiting time in queue, calls per hour etc) may not follow normal distribution. The most common method to deal with the non-normal data is transforming the data. Thus, the manufacturing data has been tranformed using Box-Cox power tranformation. In Box-Cox power tranformation an appropriate exponent lambda is used to transform the data to normal distribution. The labmda value indicates the power to which all data has to be raised and its value varies from -5 to 5. The Box-Cox plot of manufacturing time (Fig. 5.3) suggested the lambda value of 0.5 (square root transformation). The normal probability plot of residuals after square root transformation is shown in Fig. 5.2c. All the data points are falling along the straightline indicating that the residuals are following

normal distribution and the model is acceptable for predicting the manufacturing time in ISF.

Table 5.2 Experimental results

S.no	A	B	C	D	E	Ra	Time	S.no	A	B	C	D	E	Ra	Time
1	6	0.15	45	900	0	1.312	79	24	10	0.45	55	900	0	0.8304	24
2	14	0.15	45	900	0	0.697	75	25	6	0.3	45	700	0	2.2584	51
3	6	0.45	45	900	0	2.3151	25	26	14	0.3	45	700	0	0.7931	49
4	14	0.45	45	900	0	0.8622	24	27	6	0.3	45	1100	0	1.9998	33
5	10	0.3	35	700	0	0.677	43	28	14	0.3	45	1100	0	0.9464	32
6	10	0.3	55	700	0	0.6452	51	29	10	0.3	35	900	-1	0.829	33
7	10	0.3	35	1100	0	0.7399	27	30	10	0.3	55	900	-1	0.6329	40
8	10	0.3	55	1100	0	0.75	33	31	10	0.3	35	900	1	0.8356	33
9	10	0.15	45	900	-1	0.534	77	32	10	0.3	55	900	1	0.9821	40
10	10	0.45	45	900	-1	0.8383	24	33	6	0.3	45	900	-1	2.1073	40
11	10	0.15	45	900	1	0.5647	77	34	14	0.3	45	900	-1	0.6589	39
12	10	0.45	45	900	1	0.9329	24	35	6	0.3	45	900	1	1.8854	40
13	6	0.3	35	900	0	1.9934	34	36	14	0.3	45	900	1	0.746	40
14	14	0.3	35	900	0	1.0262	33	37	10	0.15	45	700	0	0.6745	95
15	6	0.3	55	900	0	1.8069	42	38	10	0.45	45	700	0	1.416	30
16	14	0.3	55	900	0	0.9209	39	39	10	0.15	45	1100	0	0.5376	64
17	10	0.3	45	700	-1	0.7262	50	40	10	0.45	45	1100	0	0.884	20
18	10	0.3	45	1100	-1	0.5704	33	41	10	0.3	45	900	0	0.892	39
19	10	0.3	45	700	1	0.7439	50	42	10	0.3	45	900	0	0.6746	40
20	10	0.3	45	1100	1	0.5656	33	43	10	0.3	45	900	0	0.701	40
21	10	0.15	35	900	0	0.7838	65	44	10	0.3	45	900	0	0.7217	40
22	10	0.45	35	900	0	1.0503	21	45	10	0.3	45	900	0	0.7148	40
23	10	0.15	55	900	0	0.6277	79	46	10	0.3	45	900	0	0.8777	40

Table 5.3 ANOVA for surface roughness

Source	Sum of Squares	Degrees of freedom	Mean Square	F	P	Coefficients of factors	
						Actual	Coded
Model	10.14	4	2.54	144.37	0.0001		
A	5.09	1	5.09	289.97	0.0001	-0.8327	-0.56
B	0.64	1	0.64	36.39	0.0001	4.8236	0.2
AB	0.18	1	0.18	9.99	0.003	-0.3491	-0.21
A^2	4.24	1	4.24	241.11	0.0001	0.0398	0.64
Residual	0.72	41	0.018				
Lack of Fit	0.67	36	0.019	2.06	0.215		
Pure Error	0.045	5	0.009				
Total	10.86	45					

Table 5.4 ANOVA for manufacturing time

Source	Sum of Squares	Degrees of freedom	Mean Square	F	P	Coefficients of factors	
						Actual	Coded
Model	72.2	10	7.22	4784.51	0.0001		
A	0.058	1	0.058	38.15	0.0001	0.027	-0.06
B	58.98	1	58.98	39080.7	0.0001	-29.412	-1.92
C	1.31	1	1.31	870.6	0.0001	0.284	0.29
D	7.5	1	7.5	4969.51	0.0001	-0.009	-0.68
AC	0.005	1	0.005	3.7	0.0627	-0.0009	-0.037
BC	0.065	1	0.065	43.01	0.0001	-0.084	-0.13
BD	0.16	1	0.16	104.14	0.0001	0.006	0.2
B^2	2.92	1	2.92	1932.76	0.0001	24.145	0.54
C^2	0.59	1	0.59	394.19	0.0001	-0.002	-0.25
D^2	0.084	1	0.084	55.6	0.0001	0	0.092
Residual	0.053	35	0.001				
Lack of Fit	0.048	30	0.001	1.5	0.3476		
Pure Error	0.005	5	0.001				
Total	72.26	45					

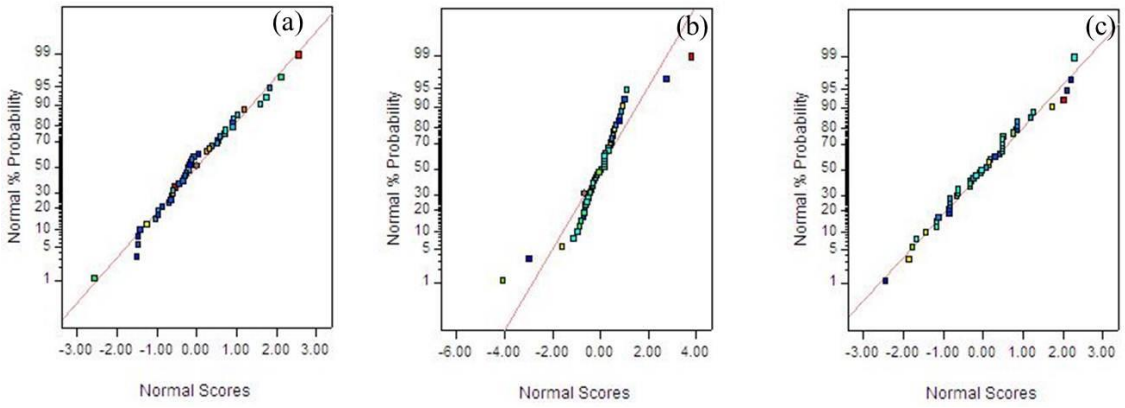

Fig. 5.2 Normal probability plot of residuals

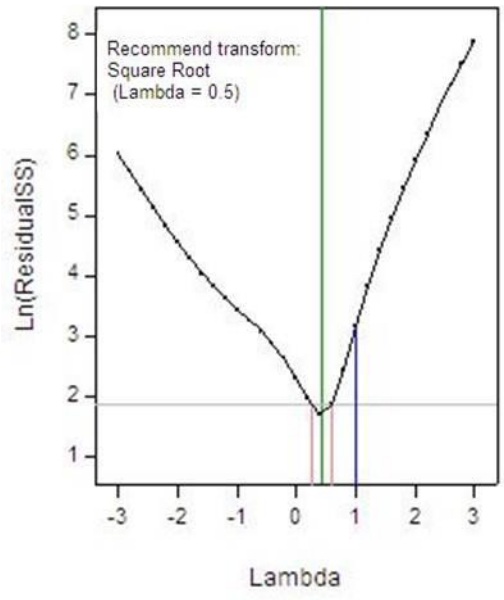

Fig. 5.3 Box–Cox plot for manufacturing time

The claculated values of regression equation coefficients for square root of manufacturing time (T) are given in Table 5.4. The values in the table reveal that the parameters A,B,C,D,BC,BD,B^2,C^2 and D^2 (parameters with $p<0.05$) are having significant effect on manufacturing time. To improve the model accuracy, the model has been reduced using backward elimination approach. The response surface model of manufacturing time for reduced quadratic model is given by the Eq. 5.2. The high R^2 value of the model indicates that the developed model establishes a good relation between the input and output parameters. Further,

$$\sqrt{T} = 6.31 - 0.061 * \mathrm{A} - 1.92 * \mathrm{B} + 0.29 * \mathrm{C} - 0.68 * \mathrm{D} - 0.037 * \mathrm{AC} - 0.13 * \mathrm{BC} + 0.2 * \mathrm{BD} + 0.54 * \mathrm{B}^2 - 0.25 * C^2 + 0.092 * D^2 \quad (5.2)$$

The equations (2) and (3) are subjected to following constraints

$$-1 \le A \le 1$$
$$-1 \le B \le 1$$
$$-1 \le C \le 1$$
$$-1 \le D \le 1$$

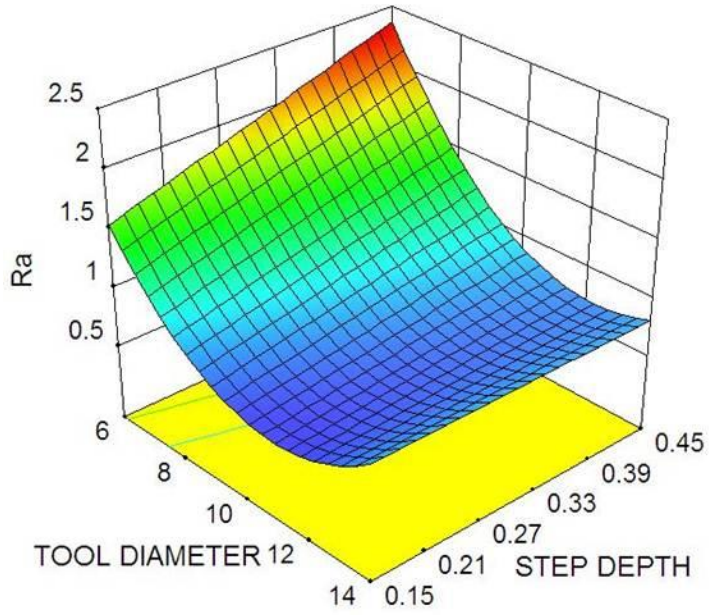

Fig. 5.4 Response surface plot of surface roughness

The response surface plot (Fig. 5.4) shows the variation of surface roughness with tool diameter varying from 6 mm to 14 mm. From this figure, it can be noted that the surface roughness increases and then decreases with increase in tool diameter. The highest roughness was observed with 6 mm diameter tool and it is decreased to a minimum value of 0.633 µm (Fig 5.5a) and again increased with increase in tool diameter. While forming with 6 mm diameter tool, small wear particles are observed in the forming zone. When the diameter is increased the overlap between the successive tool path contours is more due to larger contact area and thus surface roughness is decreasing. However, with increase in diameter beyond a certain value, the larger surface strains are causing the increase in surface roughness.

In ISF, the tool moves in successive contours to deform the sheet into the required shape. The distance between successive contours is called as step depth. The effect of step depth on surface roughness is shown in Fig. 5.4 and 5.5b. From the response surface plots shown in Fig. 5.4, it can be observed that the surface roughness is continuously increasing with the increase in step depth. At smaller step depths, there is more overlap between the successive contours which leads to better surface finish. With increase in

step depth, the metal is partially undeformed by the forming tool between successive contours which leads to increase in surface roughness. The surface roughness increased from 0.558 μm to 0.956 μm over a step depth range of 0.15 mm to 0.45 mm keeping other factors at their medium level (Figure. 5.5b). Similar observations were made during forming aluminum sheets [Hagan and Jeswiet (2004); Cavaler et al. (2010)]. However, Cavaler et al. (2010) observed a decrease in roughness with increase in step depth.

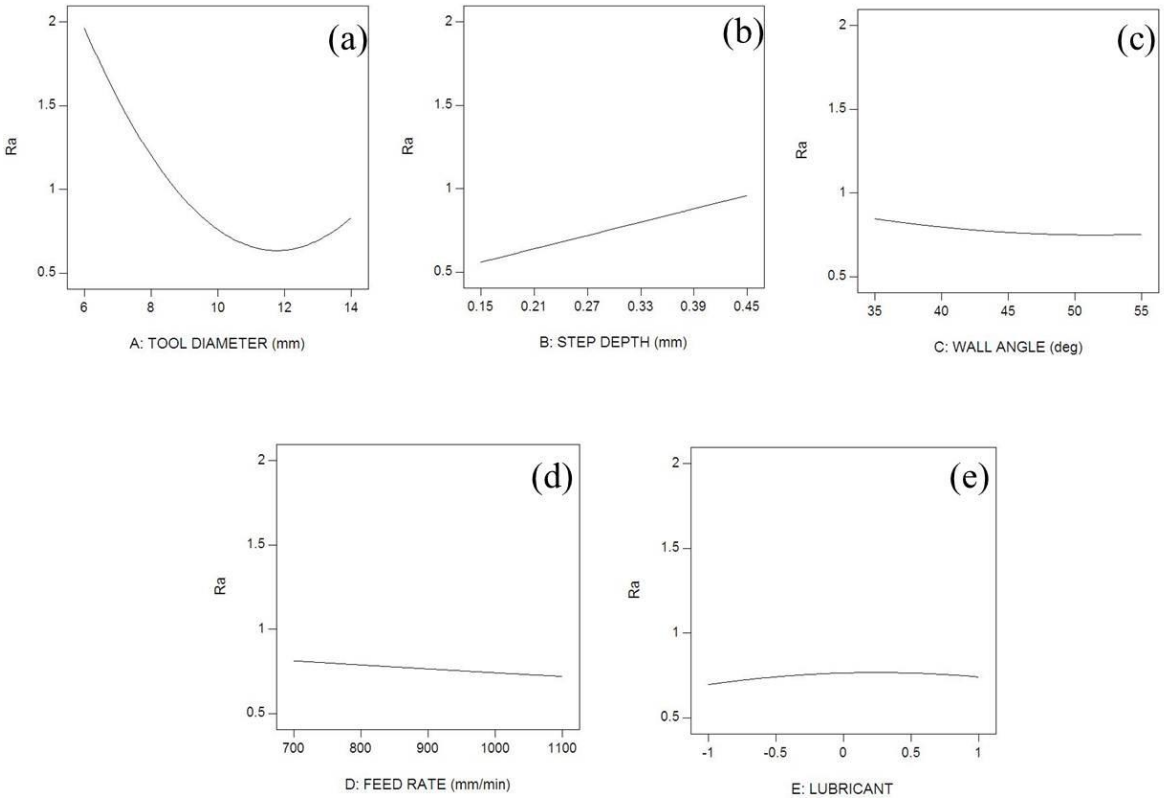

Fig. 5.5 Single-parameter effects on surface roughness

To study the effect of wall angle, the angle of the formed part is varied from 30^0 to 55^0. Fig. 5.5c shows the effect wall angle on surface roughness. The increase in wall angle can increase the height of scallop and consequently surface roughness. However, the experimental results reveal that, within the selected range of wall angle, it does not have a significant effect on surface roughness of the part formed with EDD steel sheets. This could be due to the more predominant effect of tool diameter and step depth on

scallop height than the wall angle. This can be observed clearly in the Fig. 5.5a showing the maximum roughness of 2.452 μm at tool diameter of 14 mm and step depth 0.45 mm.

The increase in feed rate generally causes an increase in temperature at tool-sheet interface that leads to an increase in wear rate and surface roughness due to breakage of lubricant film. However, Fig. 5.5d indicates that the feed rate in the selected range has insignificant effect on the surface roughness of EDD steel sheets in ISF. When the parts are formed with constant tool diameter, step depth and wall angle of 10 mm, 0.3 mm and 45^0 respectively the surface roughness changed from 0.85 μm to 0.732 μm for a feed rate range of 700 mm/min to 1100 mm/min.

The lubricant is very essential to minimize the friction between tool-sheet interface and the tool wear in ISF, which consequently deteriorates the surface quality of the formed parts. The effect of lubricant type has been studied with three different lubricants. The results show that the type of lubricant has not having significant effect on surface roughness, the maximum variation in surface roughness with different lubricants was found to be 0.045 μm (Fig. 5.5e). However, in case of forming high strength material the type of lubricant plays a very vital role on surface quality of parts [Hussain et al. (2007); De Bruyn et al. (2012)]. In high strength materials the lubricant film could break due to high forming forces and high temperatures. This leads to variations in surface roughness with different lubricants. However, in case of EDD steel sheets such type of problems were not observed due to low forming forces and less chance of heat accumulation due to high thermal conductivity of material. Even though the lubricant type does not have major effect on surface roughness, some kind of lubricant is very essential in deformation zone to reduce the friction at tool sheet interface and consequently to improve the surface finish and formability.

After surface roughness, another major limitation with ISF process is the long manufacturing time. Very few studies were done on the effect of process parameters on processing time. Sarraji et al. (2012) studied the effect of process parameters on manufacturing time using L_{18} Taguchi orthogonal array. The effect of process parameters on manufacturing time while forming the part shown in Fig. 5.1 has been studied. The variation of manufacturing time with different process parameters is shown in the Fig.

5.6. A large reduction in manufacturing time is observed with high step depths. This is due to the great reduction in number of contours and consequently total length of the tool path. The manufacturing time varied from 76.89 min to 24.34 min for a step depth range of 0.15 mm to 0.45 mm (Fig. 5.7b). Even though the increase in step depth decreases the manufacturing time, it has negative effect on surface roughness and formability of material. After step depth, feed rate has significant effect on reducing the manufacturing time. Due to high speed of the tool the manufacturing time is reduced from 50.16 min to 32.66 min (Fig. 5.7d) for feed rate variation from 700 mm/min to 1100 mm/min. The increase in wall angle has increased the forming time due to long tool paths. The length of the tool path was varied from 3 m to 4 m for a wall angle change of 35^0 to 55^0 of the selected geometry. The manufacturing time increased from 34.33 min to 40.29 min in the selected range of wall angle keeping all other parameters at their medium level (Fig. 5.7c). The increase in diameter of the tool decreased the processing time, but the change is small (Fig. 5.7a). The lubricant type has no effect on processing time of the part in ISF.

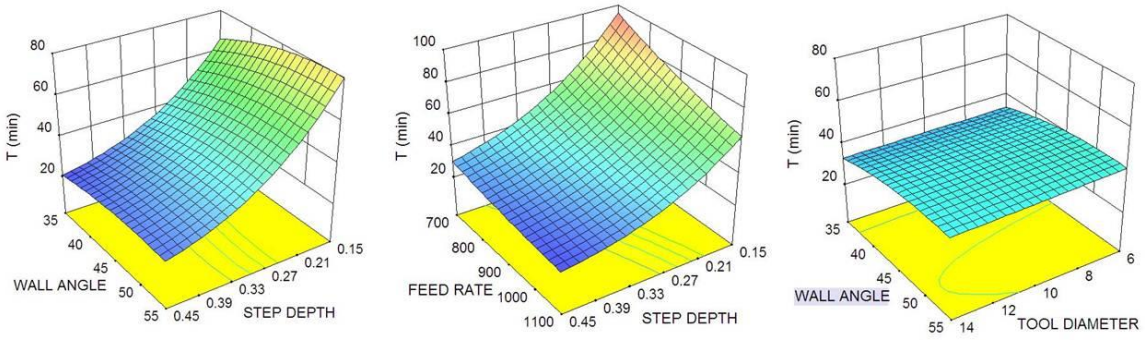

Fig. 5.6 Response surface plots of manufacturing time

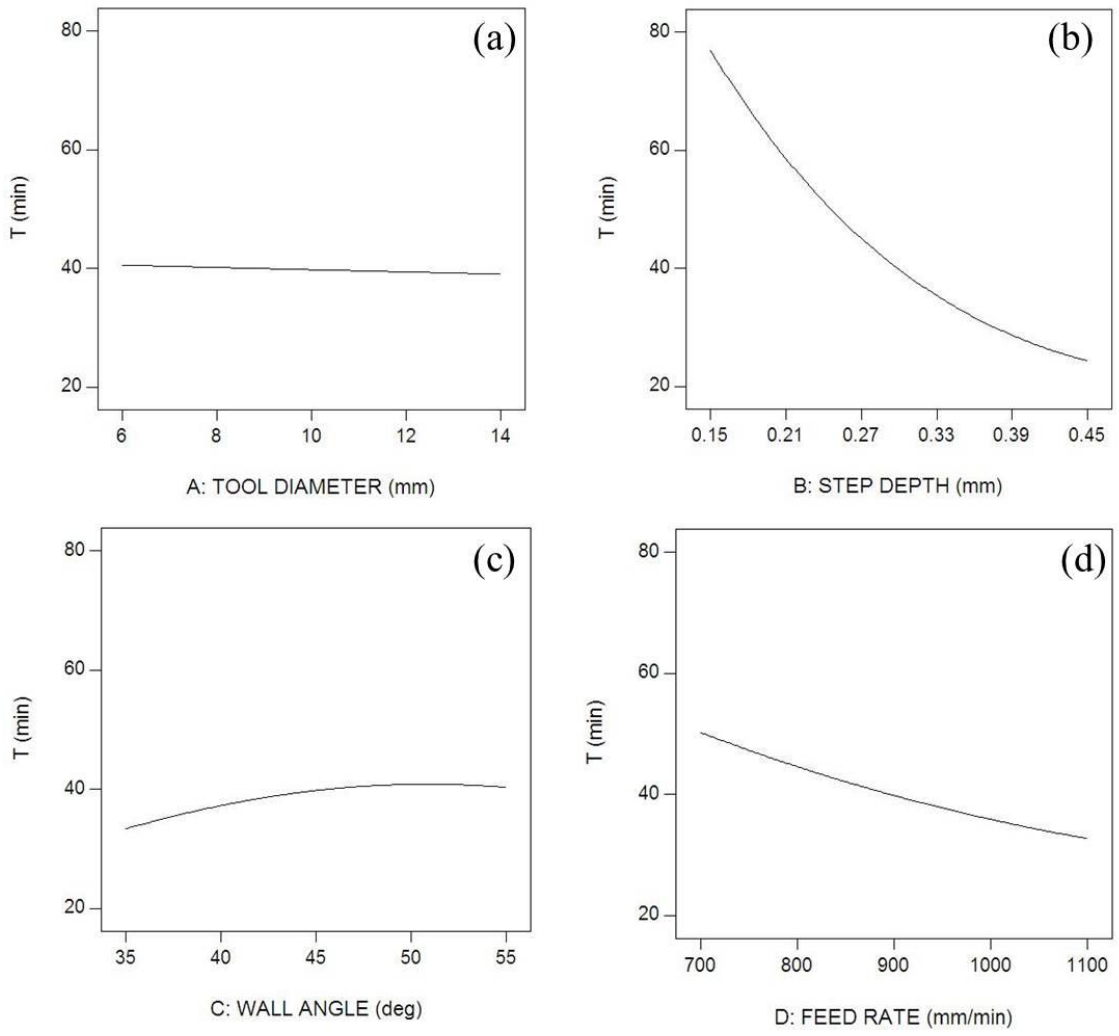

Fig. 5.7 Single-parameter effects on manufacturing time

In the present study, the multi objective optimization problem is formulated to minimize the surface roughness and to minimize the manufacturing time in ISF process. For this, tool diameter, step depth, wall angle, feed rate and lubricant type are considered as decision variables. The objective functions and constraints for optimization are given by the equations 5.1 and 5.2. The two objective functions are optimized simultaneously using NSGA-II algorithm in MATLAB. The values of various parameters used in NSGA-II are shown in Table 5.5. The NSGA-II generally gives a set of trade-off solutions between the two objective functions. The trade-off solution set obtained from the optimization is shown in Fig. 5.8, in this *x*-axis represents surface roughness and *y*-axis represents manufacturing time.

Table 5.5 Control parameters for NSGA-II

Parameters for NSGA-II	
Population size	300
Crossover probability	90%
Mutation probability	10%
Generations	500

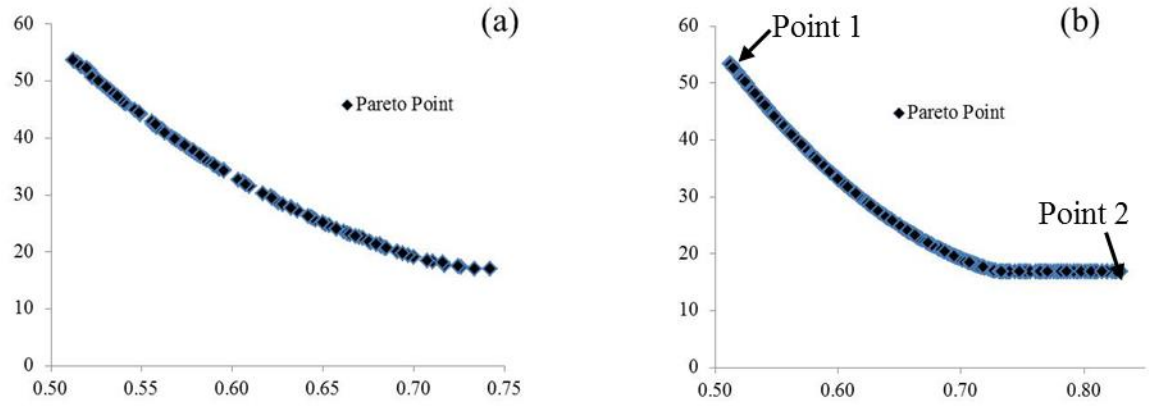

Fig. 5.8 Solution sets at different generations

The point 1 in the Fig. 5.8 represents the optimum process parameters for minimum surface roughness and point 2 corresponds to optimum process parameters for minimum manufacturing time. Among the 300 non-dominated optimal solutions at the end of 500 generations, 100 optimal solutions along with the decision variables and objective function values are given in Appendix. All the solutions in the non-dominated set are acceptable solutions. However, the production engineer has to select appropriate process parameters based on the process requirements. A very low surface roughness of 0.5122 µm is possible with process parameters A= 11.04 mm B=0.15 mm, C=35.260 and D=1100 mm/min and corresponding manufacturing time is found to be 53.70 min. The minimum manufacturing time of 17 min is possible with process parameters of A= 13 mm B=0.289 mm, C=350 and D=1100 mm/min and corresponding surface roughness is found to be 0.742 µm.

To verify the accuracy of results obtained from NSGA-II, two confirmation experiments have been performed. The process parameters for confirmation experiments have been chosen from table in Appendix corresponding to S.no 60 and 88. The experimental and predicted values of surface roughness and manufacturing time are given in Table 5.6. The results in Table 5.6 reveal that the error percentage is within the permissible limits and the process parameters provided by NSGA-II can be used to enhance the performance of ISF process.

Table 5.6 Results of confirmation experiments

						Experimental value		Prediction by NSGA	
S.no	A	B	C	D	E	RA	T	RA	T
1	11.00	0.15	35.00	1100.00	1.00	0.5312	54	0.5122	53.70
2	12.00	0.27	35.00	1097.00	1.00	0.7102	20	0.6970	19.47

In this section, the surface roughness and manufacturing time in incremental sheet metal forming have been analyzed by systematic experimental plan using Box-Behnken design. The process has been further optimized using multi-objective optimization algorithm NSGA-II. The results of this study are as follows

- The quadratic model is found to be more appropriate to relate the surface roughness and manufacturing time with process parameters in ISF process of EDD steel sheets.
- Step depth and tool diameter are having a significant effect on surface roughness, while step depth, feed rate, wall angle and tool diameter are having predominant effect on manufacturing time. In case of interaction effects, AB and A^2 have major influence on surface roughness, while BC,BD,B^2,C^2 and D^2 are having significant effect on manufacturing time.
- The increase in step depth increases the surface roughness. The surface roughness value is decreasing with increase in tool diameter up to some value and again increasing with increase in diameter. The manufacturing time is decreased with increase in step depth, feed rate and tool diameter.
- Pareto front obtained from optimization can be used to select appropriate set of process parameters for better surface finish and minimum

manufacturing time depending upon the requirement of process engineer. The confirmation experiments show that the results obtained from NSGA-II algorithm can be used to improve the performance of ISF process effectively.

5.2 Modeling using soft computing techniques

Surface roughness in SPIF has been modeled using three different soft computing techniques namely, Artificial Neural Networks (ANN), Support Vector Regression (SVR) and Genetic Programming (GP). In the development of these predictive models, tool diameter, step depth, wall angle, feed rate and lubricant type have been considered as model variables. Arithmetic mean surface roughness (R_a) and maximum peak to valley height (R_z) are used as response variables to assess the surface roughness of incrementally formed parts. The developed models are having satisfactory goodness of fit in predicting the surface roughness. Further, the GP model has been used for optimization of R_a and R_z using genetic algorithm. The optimum process parameters for minimum surface roughness in SPIF have been obtained and validated with the experiments and found highly satisfactory results within 10% error.

5.2.1 Soft computing techniques

ANN became more popular in the recent past for development of predictive models. This network will have three layers namely input layer, output layer and hidden layer. Hidden layer performs non linear mapping between input and output through a suitable basis function. In this section feed forward back propagation algorithm is used to model the surface roughness in incremental forming. During training phase this method uses gradient search technique to adjust the weights and to minimize the mean square error of the output. The proposed network is having five neurons in the input layer namely, tool diameter, step depth, wall angle, feed rate and lubricant. There are ten neurons in the hidden layer and two neurons in the output layer namely R_a and R_z. The architecture of this 5-10-2 network is shown in Fig. 5.9.

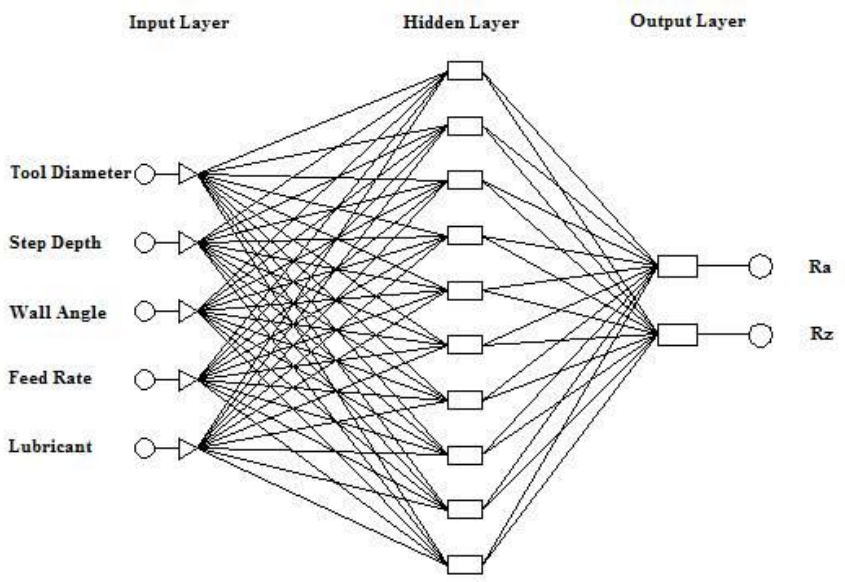

Fig. 5.9 ANN architecture for surface roughness modeling in SPIF

Hyperbolic tangent sigmoid basis function and linear basis functions are used at hidden layer and output layer respectively to map the output parameters. MATLAB ANN toolbox has been used for training, testing and validation. Based on the recommendations of Zhang et al. (1998), 90% data has been used for training, 5% data has been used for testing and 5% data has been used for validation. The network has been trained using Levenberg–Marquardt function. The error between the ANN output and experimental output is calculated using mean square error performance function (MSE). Other parameters related to the network are summarized in Table 5.7.

Table 5.7 ANN control parameters

Parameters for ANN	
No of Hidden Layers	1
Size of Hidden Layer	10
Training Function	Levenberg-Marquardt
Performance Function	SSE
Training Samples	90%
Testing Samples	5%
Validation Samples	5%

The concept of Support Vector Machines (SVM) was developed in early sixties by Vapnik and his co-workers [Vapnik (1995)]. The SVM framework was rooted in statistical learning theory and got successful results in optical character recognition and object recognition tasks. In the recent past this concept has been extended to regression and time series prediction and got good results [Çaydaş et al. (2012); Gupta AK (2010)]. Training set of SVR will have input vector (x_i) and output vector (y_i) and the relationship between input and output is constructed using a non linear function. The resultant regression model is given by the following equation.

$$f(x) = w^T \phi(x) + b \tag{5.3}$$

Where *w* is the weight vector and *b* is the bias term. *f(x)* varies at most ε from the target and is as flat as possible. If the deviation is more than ε the function is proportionately penalized with constant λ. The flattest of *f(x)* is obtained by searching the smallest *w*. For this ε-SVR is formulated as the following equation.

$$\min \frac{1}{2} w^T.w + \lambda \sum_i^l \left(\xi_i + \xi_i^*\right) \tag{5.4}$$

Subjected to

$$\begin{aligned} & y_i - \left(w^T \phi(x) + b\right) \le \varepsilon + \xi_i \\ & \left(w^T \phi(x) + b\right) - y_i \le \varepsilon + \xi_i^* \\ & \xi_i, \xi_i^* \ge 0 \end{aligned} \tag{5.5}$$

ξi, ξi*are slack variables, everything above ε is captured in ξi and everything below ε is captured in ξi*. This ε-insensitive loss function is defined as follows

$$\begin{aligned} |\xi|_\varepsilon &= 0 \quad ; if \ |f(x) - y| < \varepsilon \\ & |f(x) - y| - \varepsilon \quad ; otherwise \end{aligned} \tag{5.6}$$

SVR model with an allowable error ε is shown in Fig. 5.10. In this figure, the data points which are falling on the margin lines are called support vectors, the points within the tube are called remaining set and outside the tube are called error set. Increasing the insensitive region ε, increases the error percentage in the model.

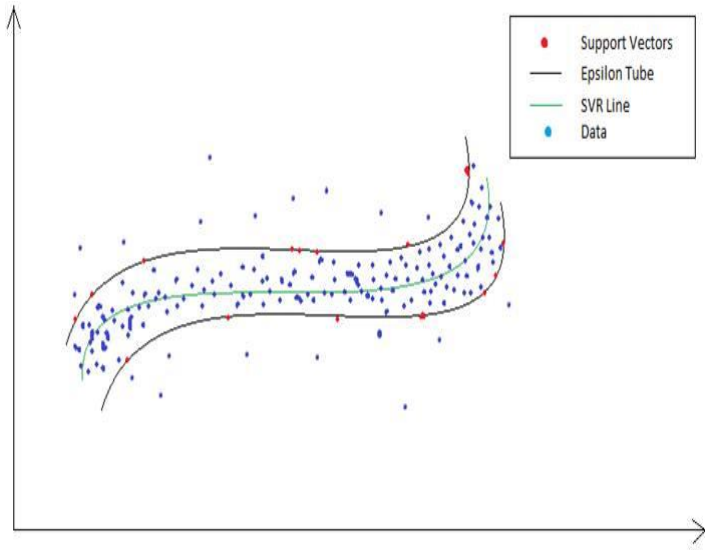

Fig. 5.10 Non linear regression with ε-insensitive function

Table 5.8 SVR control parameters

Parameters for SVR	
Cost Function	100
Epsilon	0.0001
Kernel type	RBF
Kernel Parameter	30

Table 5.9 GP control parameters

Parameters for GP	
Population Size	300
No of Generations	50
Maximum Genes	3
Maximum Tree Depth	6
Selection Method	Tournament
Crossover Probability	85%
Reproduction Probability	10%
Mutation Probability	5%
Fitness Function	R-squared
Functions Used	+, -, *, /

Online SVR toolbox developed by Parrella (2007) has been used to model the surface roughness in incremental forming. The training set X is the combined vector of all five input parameters (step depth, tool diameter, feed rate, wall angle and lubricant) and the training set Y is the response parameters (mean surface roughness and peak to valley height). Forty six input-output pairs are used for training SVR. Kernel type, cost function, ε value and other constants used for training are given in Table 5.8. SVR trains the data one by one by adding each sample to the function if and only if the Karush–Kuhn–Tucker (KKT) conditions are verified. If the KKT conditions are verified the sample is added, or else the sample is stabilized using the stabilization technique. The stabilization technique changes the SVR parameters such as cost function and ε to optimize the values.

The terminology and principles of genetic programming is formulated by Koza et al. (1999). It is an extension of Genetic Algorithms and proved to be an effective tool for modeling and regression [Kök et al. (2011); Salman et al. (2008)]. In GP, the solution is represented in tree structure with terminal nodes and functional nodes. Terminal nodes represent input parameters or constants and functional nodes represent arithmetic operators and/or non linear functions. In surface roughness modeling the terminal set includes five input process parameters and function set consists of +, -, *, /. In the first step, GP generates initial population by randomly combining the terminal set and functional set for a given population size. Each generation is tested with appropriate performance measure, and subsequent generations are improved using genetic operators such as selection, crossover and mutation. The tournament selection method has been chosen and this method keeps only good individuals in the subsequent population. In the crossover operation, two of the fittest individuals are selected to be parents and selected parts of the parents are swapped. Mutation maintains the diversity of the population and prevents the solution from being trapped in a local minimum. In modeling the surface roughness, probabilities of mutation and cross over are set as 5% and 85% respectively. Number of generations is used as a criterion for termination. Various parameters defined for GP are shown in Table 5.9. GP is stochastic in nature, thus the operator has to make multiple runs with the given number of generation. Among all the runs the model with the best performance measure (highest R^2value) is given by the following relations.

$$R_a = \frac{0.03002 + 0.002x_5}{x_2} - \frac{0.03002x_3 + 13.5}{x_1} + \frac{1708x_2(x_2 + 1)}{x_1^{\,3}} - \frac{1314x_2^{\,5}(x_1 + 449.6)(x_4 - 691.6)}{x_1^{\,4}x_4} + 1.531 \quad (5.7)$$

$$R_z = 0.2623x_1 - \frac{0.2623x_3}{x_1} + \frac{1251(x_2 + 0.001x_5)}{x_1^{\,2}} - \frac{0.009966\left(x_2x_4 - \frac{x_4}{x_1}\right)\left(x_2x_4 - \frac{2x_4}{x_1}\right)}{x_1^{\,3}x_2} - 0.1457 \quad (5.8)$$

Subjected to constraints

$$6 \le x_1 \le 14$$
$$0.15 \le x_2 \le 0.45$$
$$35 \le x_3 \le 55$$
$$700 \le x_4 \le 1100$$
$$-1 \le x_5 \le 1$$

Genetic Algorithm (GA) is the most robust search algorithm with its concepts rooted in evolutionary theory. This technique was applied successfully in many fields and different variants of genetic algorithms have been developed subsequently. In this section, the mathematical function generated using genetic programming for surface roughness prediction in SPIF has been used as an objective function for optimization using GA. The lower and upper limits of process are represented as two binary string functions called chromosomes. Initially, population of chromosomes is generated randomly between the upper and lower limits of the process parameters. In the present problem, population size is taken as 100. The binary data of the chromosomes is decoded using the Eq. 5.9, and fitness of the individual is calculated using the fitness function (Eq. 5.10). Based on the fitness value, parents are selected for generating the new population. The new population of the offspring was generated with a crossover probability of 80% and constraint dependent mutation function. This new population becomes the parents for the next generation. This process is continued till the specified termination criterion is satisfied.

$$x_i = x_i(L) + \frac{x_i(U) - x_i(L)}{2n-1} \tag{5.9}$$

where x_i is the decoded decimal value of process parameter, $x_i(L)$ and $x_i(U)$ are lower and upper limits of process parameters, n is the sub-string length.

$$f(x) = \frac{1}{1+R_a} \tag{5.10}$$

where $f(x)$ is the fitness function and R_a is the objective function.

5.2.2 Results and discussion

The predictive models for arithmetic mean surface roughness and peak to valley height in SPIF have been developed as a function of tool diameter, step depth, wall angle, feed rate and lubricant type. Three different techniques, ANN, SVR and GP have been used to develop these models for the estimation of surface roughness. The validity of the models have been tested with correlation coefficient R^2 and adj R^2 values calculated using Eq. 5.11 and Eq. 5.12. The R^2 values for R_a model with ANN, SVR and GP were found to be 0.954, 0.994 and 0.946 respectively. For the adequacy of model, R^2 value should be in between 0.8 to 1. The high R^2 (>0.94) values indicates that the developed models can be used to predict the surface roughness well. Among these three models, SVR model has better capability to predict the surface roughness followed by ANN and GP. Similar results were found for the predictive models developed for the estimation R_z. The estimated R^2 values for the responses R_a and R_z are summarized in Table 5.10. The predicted and experimental values of R_a and R_z with ANN, SVR and GP have been plotted as shown in Fig. 5.11. This figure shows a minimum variation between the experimental and predicted values with the three selected techniques for surface roughness modeling in SPIF.

$$R^2 = 1 - \frac{\sum_i (y_i - f_i)^2}{\sum (y_i - \bar{y})^2} \tag{5.11}$$

$$R^2_{adj} = 1 - \frac{(1-R^2)(n-1)}{n-p-1} \tag{5.12}$$

where y_i, f_i and are experimental, predicted and mean values of the surface roughness respectively. n and p are sample size and number of predictors respectively.

Table 5.10 Descriptive statistics of R^2 values

	R^2		*Adj.* R^2	
Model	R_a	R_z	R_a	R_z
ANN	0.95494	0.976858	0.944699	0.971599
SVR	0.994896	0.993676	0.993736	0.992238
GP	0.946345	0.921008	0.934151	0.903056

Table 5.11 Error statistics with ANN, SVR and GP

Response	Model	Count	Mean	SE Mean	Std Dev	Median	Minimum	Maximum
	ANN	46	0.066	0.0119	0.0809	0.0465	0.0026	0.4949
R_a	SVR	46	0.0088	0.00504	0.0341	0.0001	0.0001	0.1703
	GP	46	0.0944	0.0092	0.0630	0.0900	0.0013	0.2274
	ANN	46	0.1366	0.0522	0.3541	0	0	1.3576
R_z	SVR	46	0.0501	0.0283	0.1921	0.0001	0.0001	1.1436
	GP	46	0.5351	0.0660	0.4476	0.4315	0.0303	2.3015

Table 5.12 Descriptive statistics of hypothesis tests

95% CI	*P*-value					
	R_a			R_z		
	ANN	SVR	GP	ANN	SVR	GP
Mean paired t-test	0.479	0.296	0.930	0.753	0.93	0.994
Variane F-test	0.678	0.984	0.850	0.86	0.984	0.783
Levene's test	0.76	0.958	0.676	0.944	0.991	0.604

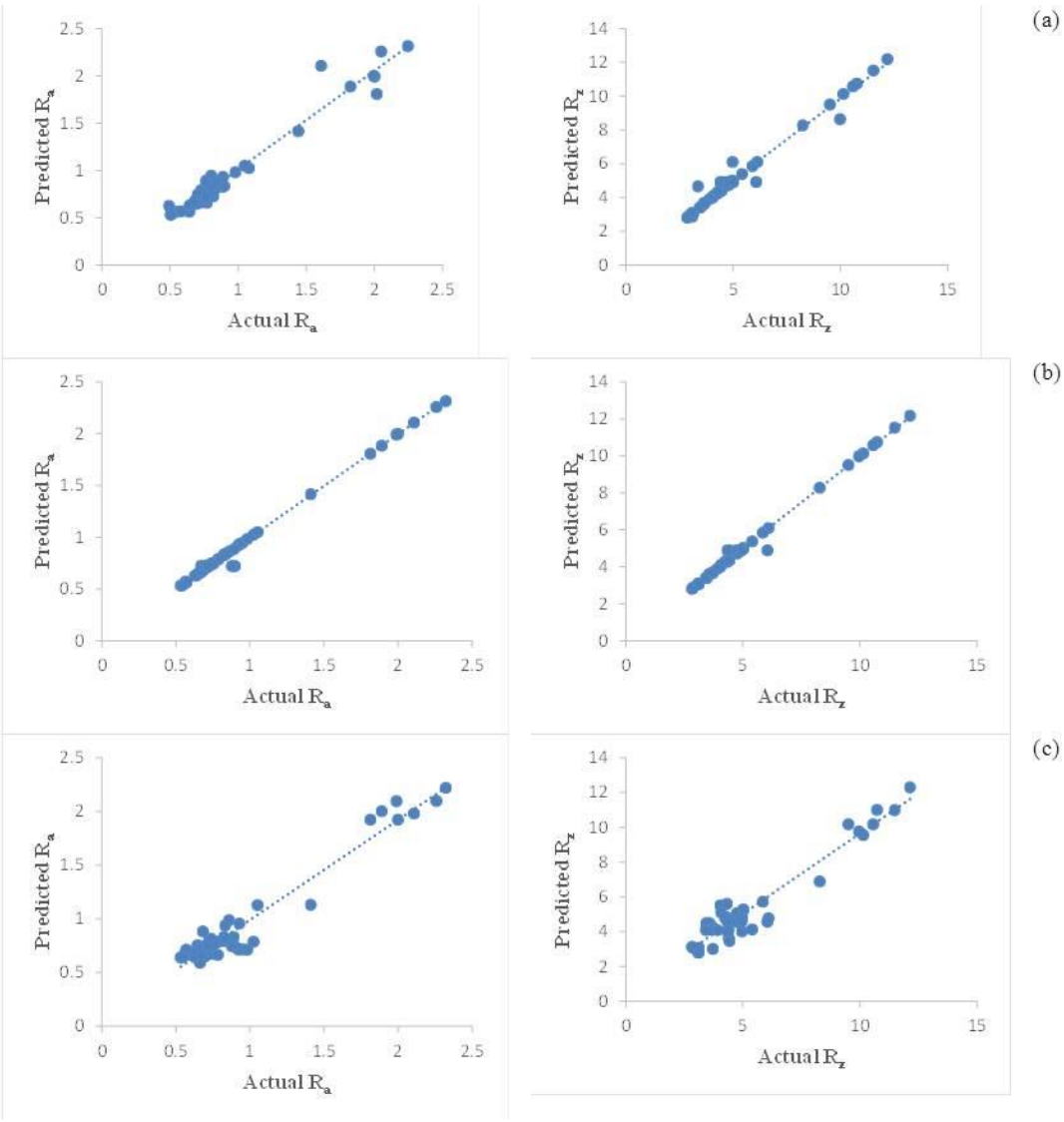

Fig. 5.11 Predicted and actual values of Ra and Rz

Performances of these techniques have been evaluated by calculating the percentage of error between predicted and experimental values. The error in surface roughness parameters prediction with different techniques is shown in Fig. 5.12. The statistics of the errors with different modeling techniques have been summarized in Table 5.11. The error statistics reveals that the ANN and SVR techniques are having better performance over GP. Among ANN and SVR, the maximum error has occurred in ANN model. Further, the mean error in SVR was found to be less compared to ANN. Even

though, the error statistics reveal that ANN and SVR have better performance than GP, the performance of GP cannot be underestimated. The positive aspect of GP is that it produces an explicit relationship between input and output parameters, whereas, ANN and SVR both are black box methods.

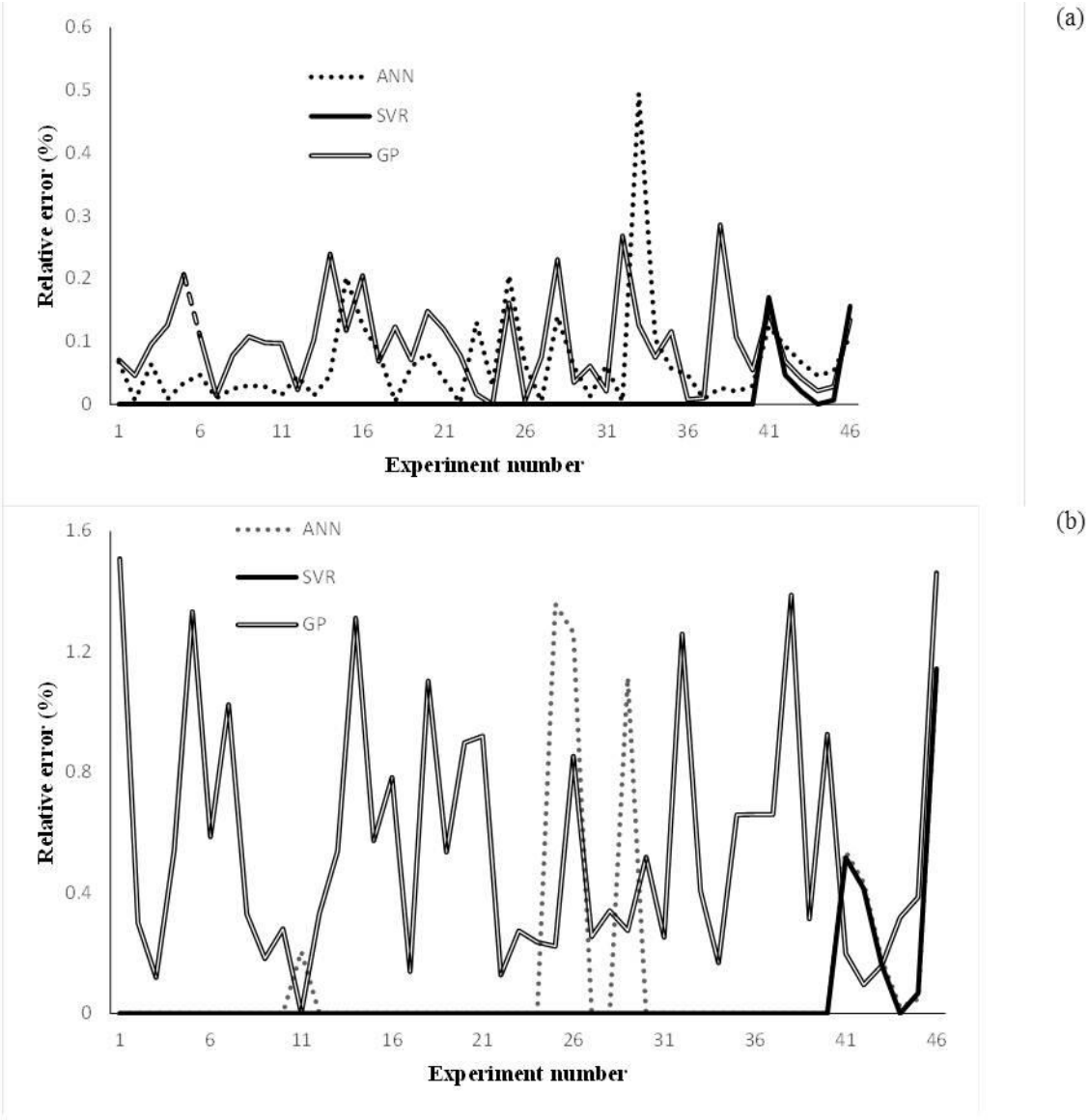

Fig. 5.12 Relative percentage of error with different predictive modeling techniques

To test the goodness of fit with different modeling techniques, t-test, F-test and Levene's test are conducted. Results of hypothesis tests are given in Table 5.12. In all

three modeling techniques (ANN, SVR and GP), the calculated *p*-value with three hypothesis tests are greater than 0.05. This indicates that there is no significant difference between experimental and predicted values using ANN, SVR and GP.

Table 5.13 Optimum process parameters

Process parameter	Optimum process parameters for minimum	
	Ra	*Rz*
Tool diameter	10	10
Step depth	0.15	0.15
Wall angle	55	55
Feed rate	1100	1100
Lubricant type	-1	-1

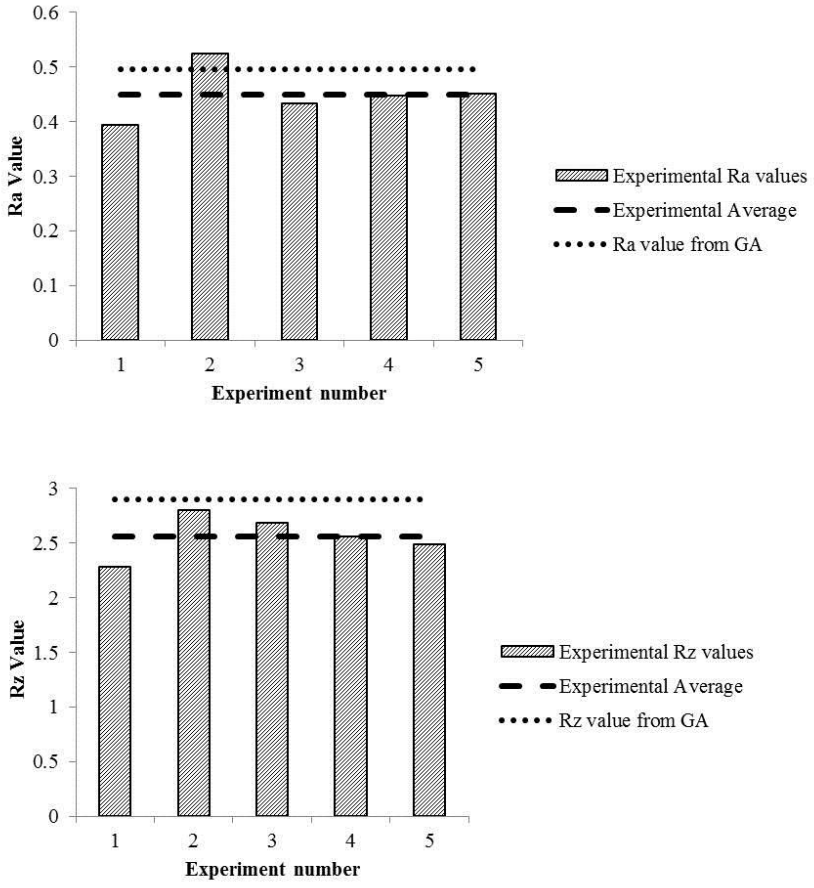

Fig. 5.13 Experimental Ra and Rz values at optimum process settings

Following the development of predictive models, the process parameters in SPIF have been optimized for minimum surface roughness using GA toolbox in MATLAB. The objective function and constraints for the optimization problem has been given by the Eq. 5.7. In GA modeling, the lubricant was treated as a discrete variable with limits -1, 0 and 1. For the manufacturing simplicity the diameter of tool was also treated as a discrete variable with limits 6, 10 and 14. The optimum process parameters and minimum surface roughness values obtained from the model are given in Table 5.13. To verify the results obtained from the GA, the experiments have been performed with the optimum settings. The measured and estimated values of surface roughness parameters are shown in Fig. 5.13. The measured *Ra* and *Rz* values with these settings were found to be 0.4502 μm and 2.564 μm respectively. The results shows that the optimum process parameters obtained from GA can be used to enhance the surface quality of parts produced in SPIF process.

In summary, this section presents the predictive models developed by using ANN, SVR and GP. Adequacy of model is tested using hypothesis tests and performance is evaluated using R^2 value. The models developed using ANN and SVR are performing better than GP. However, GP produces explicit relationship between input and output variables. GP model is stochastic in nature, thus this model can be improved further by changing different parameters. Among ANN and SVR, SVR exhibited better performance in predicting R_a and R_z. The developed models using GP has been used for optimization using genetic algorithm with the objective of minimum surface roughness. The R_a and R_z values corresponding to optimum process parameters are found to be be 0.4956 μm and 2.9 μm respectively. For validation, experiments have been conducted with optimum settings and the results were found to be in very good agreement with the predicted values by GA. The reported results are applicable only for EDD steel sheets within the specified range of process parameters.

5.3 Multi-objective optimization using grey relational analysis

This section presents the application of Taguchi based grey relational analysis for optimization of multiple performance characteristics in SPIF process. In this study, tool diameter, feed rate, shape of the geometry and step depth have been considered as the

process parameters with the objective of optimizing the maximum wall angle (φ_{max}) and arithmetic mean surface roughness (R_a) simultaneously. The incremental forming experiments have been performed on CNC milling machine as per Taguchi $L_9(3^4)$ orthogonal array. The analysis of variance (ANOVA) has been used to understand the effect of process parameters on individual response variables. Further, the grey relational grade has been calculated using the grey relational approach for simultaneous optimization maximum wall angle and surface roughness. The ANOVA analysis indicated that the step depth is most influential factor on grey relational grade followed by feed rate, tool diameter and shape of the geometry.

Taguchi experimental designs are very popular in manufacturing to study the effect of process parameters with minimum number of experiments. This approach uses the tables called as *orthogonal arrays to* design the experiments. In this investigation, tool diameter, feed rate, shape of the geometry and step depth has been considered as important process parameters. Each of these parameters has been varied over three levels as shown in Table 5.14. This four factor three level design possess eight degrees of freedom (Dof). A suitable orthogonal array which satisfies the required Dof is $L_9(3^4)$. Thus, the experiments are conducted as per L_9 orthogonal array shown in Table 5.15.

Table 5.14 Factors and levels of three level Taguchi design

Code	Variable	Level 1	Level 2	Level 3
A	Tool diameter (mm)	6	10	14
B	Feed rate (mm/min)	750	1500	2250
C	Shape	Conical	Pyramidal	D-Shape
D	Step depth (mm)	0.7	1.1	1.5

During the experimental work, three different shapes namely, cone, pyramid and combination of cone and pyramid (D-shape) have been formed as per the experimental plan to measure the maximum wall angle and surface roughness. The parts are having same directrices for both maximum wall angle and surface roughness but different generatrix. The part geometries used for maximum wall angle has varying wall angle along the depth. The varying wall angle along the depth has been obtained by using

circular arc segment as a generatrix. The part geometries used for surface roughness has constant wall angle of 50^0 and a depth of 40 mm.

Table 5.15 Experimental plan for L_9 (3^4) orthogonal array with responses

	Control factors and their levels				Response variables	
Ex. No	A	B	C	D	Wall angle	Surface roughness
1	1	1	1	1	76.64	1.607
2	1	2	2	2	76.59	2.230
3	1	3	3	3	75.49	2.620
4	2	1	2	3	73.09	1.787
5	2	2	3	1	73.80	0.882
6	2	3	1	2	73.49	1.524
7	3	1	3	2	73.80	0.990
8	3	2	1	3	70.66	1.084
9	3	3	2	1	73.09	0.976

In Taguchi methods different Signal to Noise (S/N) ratios are used to analyze the results. S/N ratio represents both average and variation of the experimental results. In ISF, the larger wall angle and smaller surface roughness are the indication of better performance. Therefore, the larger-the-better for the maximum wall angle and smaller-the-better for the surface roughness have been selected for obtaining optimum performance characteristics in ISF. The formulas used for calculating the S/N ratios for larger-the-better and smaller-the-better are given by the Eqs. 5.13 and 5.14 respectively.

$$S/N = -10\log_{10}\left[\frac{1}{n}\left(\sum_{k=1}^{n}\frac{1}{y_{ijk}^2}\right)\right] \tag{5.13}$$

$$S/N = -10\log_{10}\left[\frac{1}{n}\left(\sum_{k=1}^{n} y_{ijk}^2\right)\right] \tag{5.14}$$

Where y_{ijk} is measured i^{th} response variable in j^{th} experiment of k^{th} trial and n is the number of experimental trials at each experimental setting. The mean S/N ratio values for each factor level of maximum wall angle and surface roughness are shown in Table 5.16 and Table 5.17 respectively. The main effect plots of S/N ratio are plotted in Fig. 5.14 and 5.15. In Taguchi method, the factor levels with highest S/N ratio corresponds to

optimum settings. The optimal parameters are highlighted by circles in Fig. 5.14 and 5.15.

Table 5.16 S/N response table for maximum wall angle

Level	Diameter	Feed rate	Shape	Step depth
1	**37.64**	**37.44**	37.33	37.44
2	37.32	37.34	37.41	**37.46**
3	37.21	37.39	**37.43**	37.27
Delta	0.44	0.1	0.09	0.18
Rank	1	3	4	2

Table 5.17 S/N response table for surface roughness

Level	Diameter	Feed rate	Shape	Step depth
1	-6.4841	-3.0252	-2.8269	**-0.9396**
2	-2.5372	**-2.1920**	-3.9325	-3.5128
3	**-0.1341**	-3.9382	**-2.3960**	-4.7030
Delta	6.3501	1.7462	1.5365	3.7635
Rank	1	3	4	2

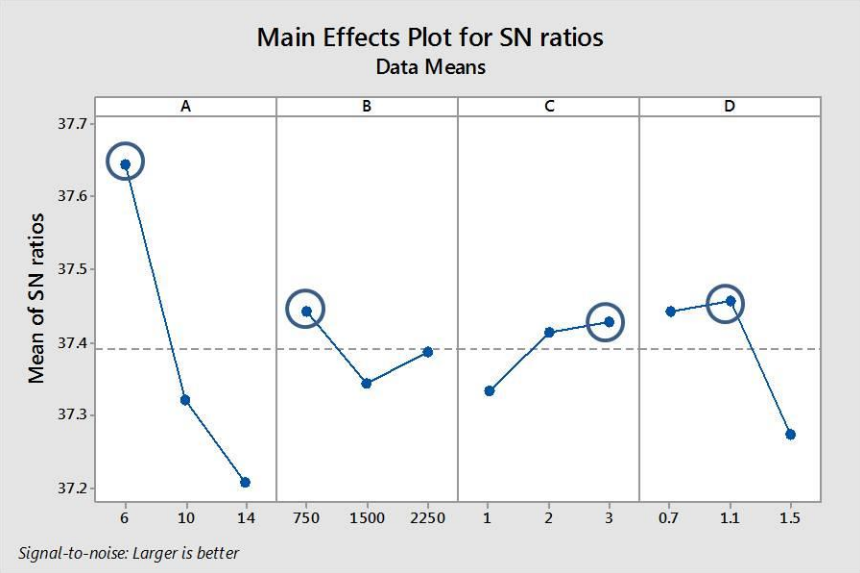

Fig. 5.14 Main effects plot of S/N ratio for maximum wall angle

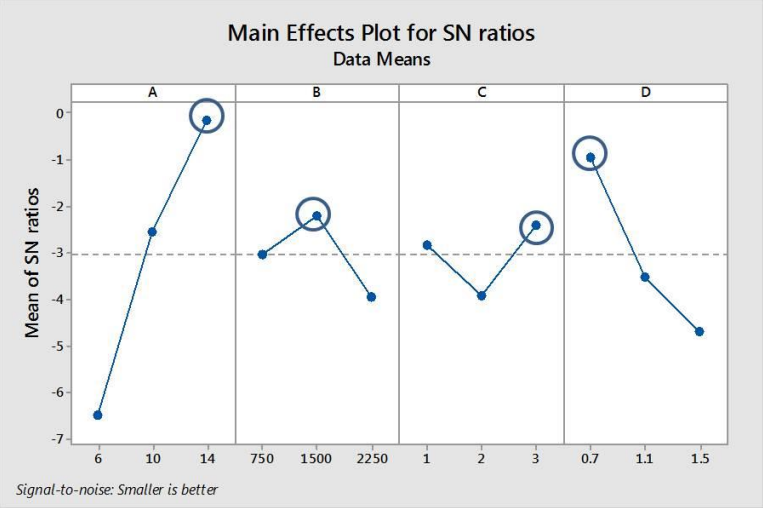

Fig. 5.15 Main effects plot of S/N ratio for surface roughness

Table 5.16 and Fig. 5.14 show the influence of process parameters on maximum wall angle. The optimum process parameters for maximum wall angle are found to be tool diameter at level 1 (6 mm), feed rate at level 1 (750 mm/min), shape of the geometry at level 3 (D-shape) and step depth at level 2 (1.1 mm). Table 5.17 and Figure 8 show the influence of process parameters on surface roughness. The optimum process parameters for minimum surface roughness are found to be tool diameter at level 3 (14 mm), feed rate at level 3 (1550 mm/min), shape of the geometry at level 3 (combination of cone and pyramid shape) and step depth at level 1 (0.7 mm). In short, the optimum settings for maximum wall angle and minimum surface roughness are A1B1C3D2 and A3B2C3D1 respectively.

Analysis of variance (ANOVA) is used to determine the percentage of contribution of process parameters on response variables. In this section, Pareto ANOVA [Pa et al. (2012)] has been used to study the importance of selected process parameters on maximum wall angle and surface roughness. Pareto ANOVA is a simplified ANOVA method, which is based on Pareto principle. The Pareto ANOVA technique is a quick and easy method to analyze results of the parametric design. The Pareto ANOVA technique does not need F-test. In this method the contribution of each parameter is calculated using Eq. 5.15.

$$\%Contribution = \frac{Sum\ of\ squares of\ differences\ (SS)}{Total\ summation of\ squares of\ differences (SS_T)} \quad (5.15)$$

The degree of importance of each process parameter on response variables namely, maximum wall angle and surface roughness are summarized in Table 5.18. The Table 5.18 shows that, except tool diameter and step depth other parameters are having insignificant impact on the maximum wall angle. This table also reveals that the tool diameter, feed rate, shape of the geometry and step depth affect the maximum wall angle by 75.5%, 3.8%, 4.2% and 16.5% respectively. Similar investigations have been performed for surface roughness. The results given in Table 5.18 indicate that the tool diameter and step depth are having significant effect on surface roughness. Moreover, the tool diameter, feed rate, shape of the geometry and step depth affect the surface roughness value by 66.9%, 5%, 4.1% and 24% respectively.

Table 5.18 Contribution of process parameters on wall angle and roughness

Process Parameter	Maximum wall angle		Surface roughness	
	SS	% Contribution	SS	% Contribution
Tool diameter	0.2994	75.5	61.675	66.9
Feed rate	0.015	3.8	4.577	5
Shape	0.0168	4.2	3.768	4.1
Step depth	0.0654	16.5	22.201	24

Table 5.19 Calculated grey relational grades

Ex.No	Experimental results		Normalization		Grey relational coeff.		Grade
	φ_{max}	R_a	φ_{max}	R_a	φ_{max}	R_a	
1	76.64	1.607	1.0000	0.5829	1.0000	0.5452	0.7726
2	76.59	2.230	0.9916	0.2244	0.9836	0.3920	0.6878
3	75.49	2.620	0.8077	0.0000	0.7222	0.3333	0.5278
4	73.09	1.787	0.4064	0.4793	0.4572	0.4899	0.4735
5	73.80	0.882	0.5251	1.0000	0.5129	1.0000	0.7564
6	73.49	1.524	0.4732	0.6306	0.4870	0.5751	0.5310
7	73.80	0.990	0.5251	0.9379	0.5129	0.8895	0.7012
8	70.66	1.084	0.0000	0.8838	0.3333	0.8114	0.5724
9	73.09	0.976	0.4064	0.9459	0.4572	0.9024	0.6798

Taguchi method is an effective method for mono-objective optimization. However, this method can't be used to optimize the multiple performance characteristics simultaneously. To overcome this problem, in the present study, grey relational analysis has been used for multi-objective optimization. This method involves three steps namely, normalization, calculation of grey relational coefficient and calculation of grey relational grade.

The process of normalization converts the response variables on 0-1 scale irrespective of their units and range. Different relations are used for normalization based on the type of performance characteristics. In the present study, the maximum wall angle has to be maximized and surface roughness has to be minimized. The relations for normalizing the larger-the-better and smaller-the-better performance characteristics are given by the Eqs. 5.13 and 5.14.

Normalization formula for larger-the-better performance characteristics:

$$x_{ij} = \frac{y_{ij} - \min_j y_{ij}}{\max_j y_{ij} - \min_j y_{ij}} \tag{5.16}$$

Normalization formula for smaller-the-better performance characteristics:

$$x_{ij} = \frac{\max_j y_{ij} - y_{ij}}{\max_j y_{ij} - \min_j y_{ij}} \tag{5.17}$$

where x_{ij} is the normalized i^{th} response variable in j^{th} experiment, y_{ij} is the measured i^{th} response variable in j^{th} experiment. The normalized data of maximum wall angle and surface roughness is shown in Table 5.19. . The normalized values are ranged between zero and one. The normalized value one indicates the best performance and zero indicates the poor performance.

Grey relational coefficient establishes the relationship between ideal and normalized values. The grey relational coefficient ξ_{ij} for i^{th} response variable in j^{th} experiment is expressed as follows.

$$\xi_{ij} = \frac{\Delta_{\min} + \zeta\Delta_{\max}}{\Delta_{ij} + \zeta\Delta_{\max}} \tag{5.18}$$

Where

$$\Delta_{\min} = \min_i \min_j \left| x_i^0 - x_{ij} \right|$$

$$\Delta_{\max} = \max_i \max_j \left| x_i^0 - x_{ij} \right|$$

$$\Delta_{ij} = \left| x_i^0 - x_{ij} \right|$$

In the above equations x_i^0 is the reference value or ideal value of the i^{th} response variable. ζ is the distinguishing coefficient ($\zeta \in [0, 1]$) and is used to adjust the difference of the relational coefficient [Kuram et al. (2013)]. The purpose of ζ is to expand or compress the range of the grey relational coefficient. Different distinguishing coefficients may lead to different solution results. Decision makers should try several different distinguishing coefficients and analyze the impact on the results [Venkata Rao (2011)]. In this study ζ was taken as 0.5 and the grey relational coefficient calculated using Eq. 5.18 is given in Table 5.19.

Grey relational grade represents the level of correlation between the reference and the comparability sequence. The grey relational grade is calculated as follows

$$\alpha_j = \frac{1}{m} \sum_{i=1}^{m} w_i \xi_{ij} \tag{5.19}$$

where m is the number of response variables (in this study m is 2), w_i is the weight factor for each response variable (in this study w_i is considered as 1). The weight factor can also calculated using standard methods such as principal component analysis [Khan et al. (2012)] and entropy method [Wen et al. (1998)]. The grey relational grades calculated using Eq. 5.19 is given in Table 5.19.

The experimental parameters corresponds to higher grey relational grade is closer to the optimal. Finally, the calculated grey relational grades are considered for optimization of multiple performance characteristics (response variables). Since higher multiple performance is required, larger-the-better S/N quality characteristic given by the Eq. 5.13 has been adopted for grey relational grade. The calculated S/N ratio values for

the grey relational grade are shown in Fig. 5.16. The level of parameters corresponds to highest S/N ratio gives the optimum settings. Thus, the optimum settings for simultaneous maximization of wall angle and minimization of surface roughness are found to be A1B2C3D1. Further, Pareto ANOVA revels that the step depth (54.1%) has major effect on grey relational grade followed by feed rate (20.9%), tool diameter (19%) and shape of the part (6%) (Table 5.20). The optimum process settings for single objective optimization and multi-objective optimization are summarized in Table 5.21.

The grey relational grade corresponds to the optimum settings have been calculated using the following relation.

$$\hat{\alpha} = \alpha_m + \sum_{i=1}^{q} \left(\overline{\alpha}_i - \alpha_m \right) \tag{5.20}$$

where α_m is the total mean of the grey relational grade, $\overline{\alpha}_i$ mean of the grey relational grade at the optimum level, and q is the number of process parameters that significantly affect the grey relational grade. Using the Eq. 5.20, it is possible to calculate the grey relational grade for the settings of process parameters that are not available in the orthogonal array.

Table 5.20 Contribution of process parameters on grey relational grade

Process Parameter	SS	% Contribution
Tool diameter	2.359	19.0
Feed rate	2.600	20.9
Shape	0.750	6.0
Step depth	6.746	54.1

Table 5.21 Optimum process settings from grey relational analysis

Process parameters	Optimum process settings		
	Single objective optimization		Multi-objective optimization
	Maximum wall angle	Surface roughness	
Tool diameter	A1	A3	A1
Feed rate	B1	B2	B2
Shape	C3	C3	C3
Step depth	D2	D1	D1

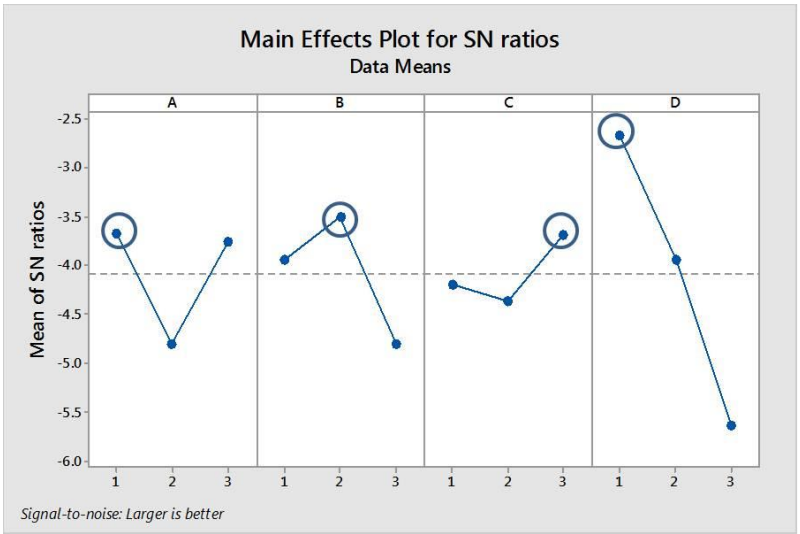

Fig. 5.16 Main effects plot of S/N ratio for grey relational grade

The confirmation experiment is conducted at optimum settings to verify the quality characteristics of the incremental forming process. The values of response variables at optimum settings are φ_{max} = 76.92^0 and R_a = 1.432 μm. The grey relational grade corresponding to optimum settings has been calculated using Eq. 5.20 and is found to be 0.8322.The grey relational grade of the confirmation experiment has been improved by 31.34% from the mean grade value. Hence the Taguchi based grey analysis is a very useful tool for optimization of multiple performance characteristics in incremental forming process.

The multi-objective optimization of single point incremental forming of extra deep drawing steel by grey relational analysis has been presented in this section. The grey relational analysis converts the multiple performance characteristics (i.e maximum wall angle and surface roughness in this study) in to the optimization of single performance characteristic called grey relational grade. The effectiveness of the proposed method has been verified by experiment and Pareto ANOVA. The Pareto ANOVA reveals that the step depth, feed rate and tool diameter have prominent effect on grey relational grade. The process parameters for best performance were tool diameter of 6 mm, feed rate of 1500 mm/min, D-shape geometry and step depth of 0.7 mm. The confirmation experiment results proved that there is significant improvement in the grey relational grade at optimum process settings. From this study, it can be concluded that the proposed methodology can be used for simultaneous optimization of other response variables and materials in incremental forming.

5.4 Summary

The effects of process parameters on surface roughness and manufacturing time have been discussed with a systematic experimental plan using Box-Benkhen design. The surface roughness of formed parts has been modeled using response surface methodology and different soft computing techniques such as ANN, SVR and GP. The developed models have been used for optimization using genetic algorithm. Further, the surface roughness and manufacturing time has been optimized simultaneously using multi-objective optimization algorithm NSGA-II. Another multi-objective optimization algorithm, Taguchi based grey relational analysis has been used for simultaneous optimization of formability and surface roughness. Thus, this chapter provides an opportunity to production engineer to select a set of optimum process settings to produce the part with required quality.

Chapter 6 Multi Stage Incremental Forming

The limitation over the maximum formable wall angle in single stage incremental forming can overcome by adopting multi stage forming strategy. This chapter focuses on some preliminary studies on deformation behavior of EDD steel in multi stage incremental forming in terms of thickness distribution, strains and geometric accuracy. The study has been carried by forming a conical cup with 85^0 wall angle in four stages.

6.1 Deformation analysis

Liu et al. (2013) proposed different tool path strategies to form the parts in Multi Stage Incremental Forming (MSIF). They proposed a simplified qualitative analysis to understand the deformation behavior in multistage. In ISF, the material undergoes plane strain deformation and thus thickness follows sine law. From the consistency of volume relationship, we can write

$$\varepsilon_1 + \varepsilon_2 + \varepsilon_3 = 0 \tag{6.1}$$

For plane strain condition, the above equation becomes

$$\varepsilon_1 + \varepsilon_3 = 0 \tag{6.2}$$

$$\varepsilon_1 = \ln\left(\frac{Final\ length}{Initial\ length}\right) \tag{6.3}$$

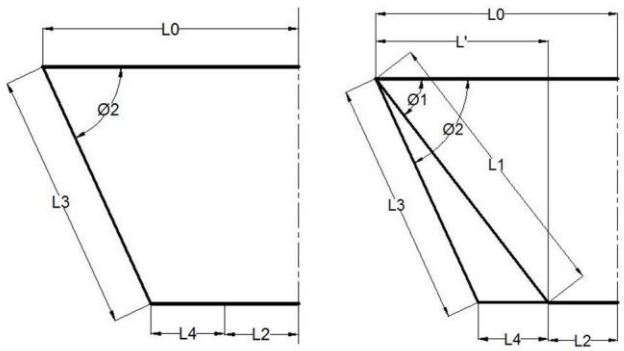

Fig. 6.1 Single stage and two stage forming process

Now the principal strains for single stage and two stage incremental forming shown in Fig. 6.1 can be written as follows. The principal strain in single stage forming is

$$\varepsilon_{1S} = \ln\left(\frac{L3}{L0 - L2 - L4}\right) \tag{6.4}$$

The principal strain in two stage forming can be written as

$$\varepsilon_{S1} = \ln\left(\frac{L1}{L0 - L2}\right) \tag{6.5}$$

$$\varepsilon_{S2} = \ln\left(\frac{L3 + L4}{L1}\right) \tag{6.6}$$

$$\varepsilon_{2s} = \varepsilon_{s1} + \varepsilon_{s2} = \ln\left(\frac{L3 + L4}{L0 - L2}\right) \tag{6.7}$$

$$\varepsilon_{2s} - \varepsilon_{1s} = \ln\left(\frac{L3L' + L4L'}{L3L' - L3L4}\right) \tag{6.8}$$

From the above relation, we can say that $\varepsilon_{2s} < \varepsilon_{1s}$ as L3>L'. In other words, thinning in two stage forming is always less than the single stage forming thus the formability of material is good in MSIF.

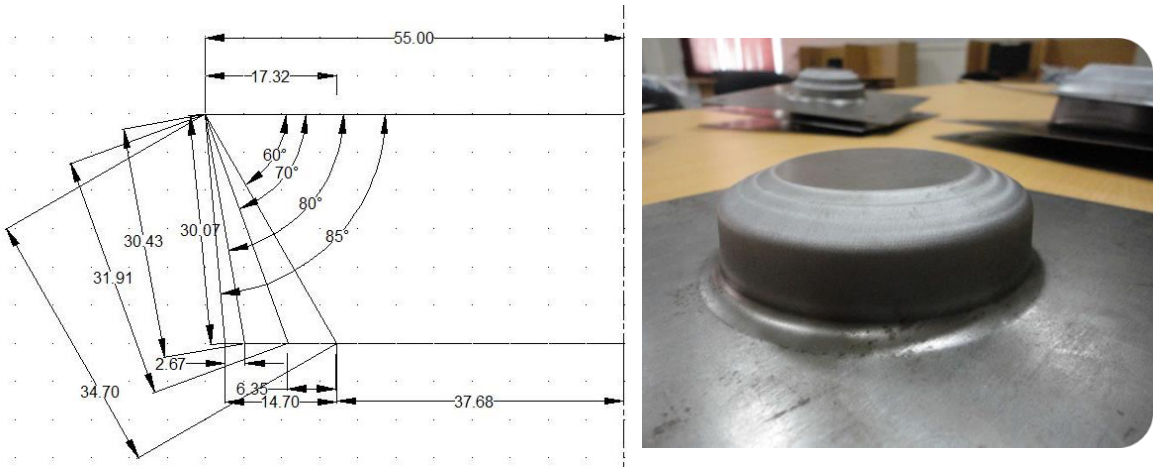

Fig. 6.2 Geometry of the cup formed in four stage

6.2 Thickness distribution and strain analysis

In the present study a conical cup with wall angle 85^0 has been formed in four stages. Initially the cup has been formed with wall angle 60^0 and has been increased in subsequent stages to 70^0, 80^0 and 85^0. In all the stages the top diameter and depth has been maintained 110 mm and 30 mm respectively. The dimensions of the cup in different stages are shown in Fig. 6.2. Thickness of the cup in each stage has been calculated considering plane strain condition and volume consistency. The result of thickness in each stage has been given in Table 6.1. In case of single stage forming thickness of the cup follows the sine law, thus the thickness of the cup with 85^0 wall angle becomes 0.087 mm. This value is very low compared to the thickness of the cup in the fourth stage of MSIF. Due to this reason it is possible to form the cups with steep wall angle in MSIF.

Table 6.1 Theoritical thickness after each stage of MSIF

	Initial length	Final length	Thickness
Stage #1	17.32	34.7	0.5
Stage #2	34.7	31.9+6.35	0.45
Stage #3	31.9	30.43+5.68	0.39
Stage #4	30.43	30.07+2.67	0.36

Finite element simulations have been performed to study the thickness distribution in each stage. The contour plots of thickness distribution in different stages are shown in Fig. 6.3. Distribution of thickness along the depth has been obtained by sectioning the cup normal to y-direction. Thickness distribution along the depth in different stages is shown in Fig. 6.4. From the Fig. 6.4 it is evident that the thickness is getting reduced in bending region and is almost constant in wall region due to constant wall angle. However, in stage three and four thickness was not constant in wall region also. In all the stages maximum thinning is observed at the bottom corners of the cup. Thus, there are more chances for the cup to fail at this location. In all the stages theoretical model is over predicting the thickness compared to finite element simulations. The deviation between theoretical model and finite element simulations is more predominant in stage 3 and 4. This could be due to the change of material flow in these stages.

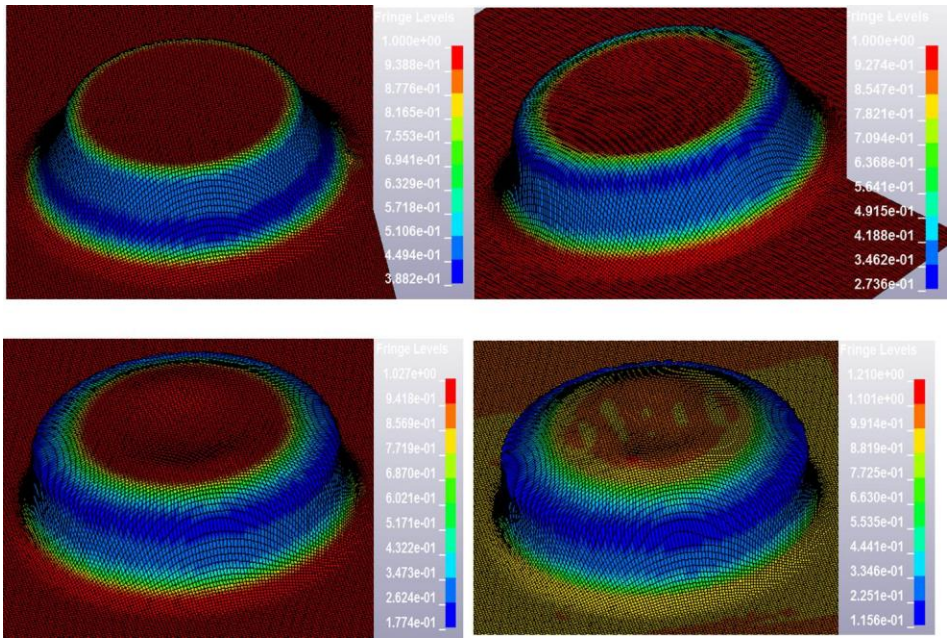

Fig. 6.3 Contour plots of thickness distribution in different stages

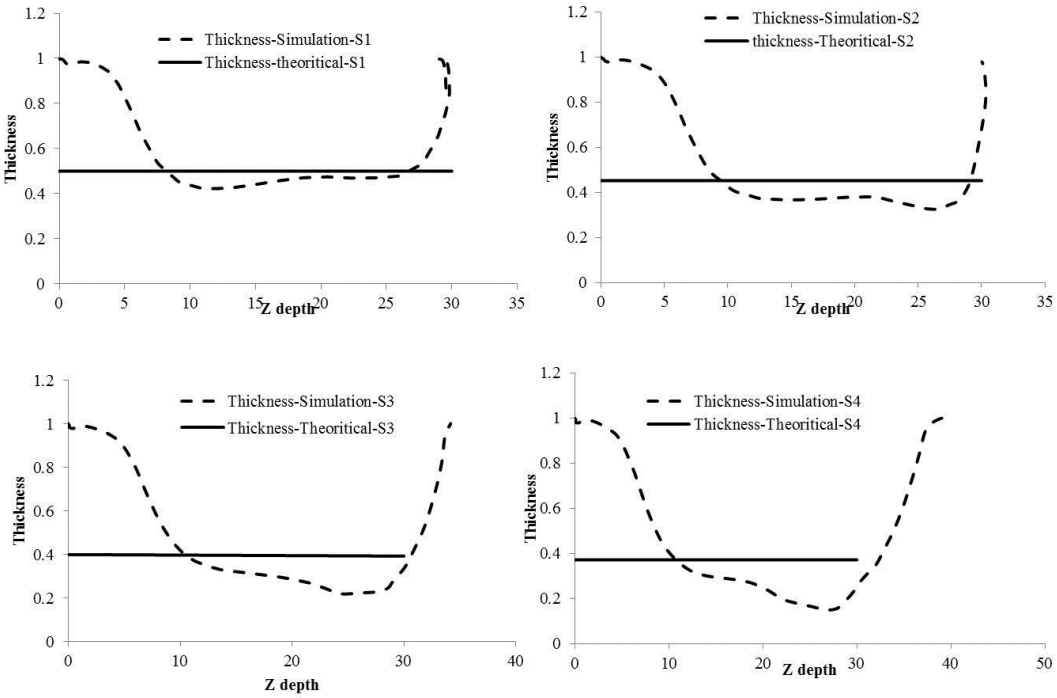

Fig. 6.4 Thickness distribution in different stages

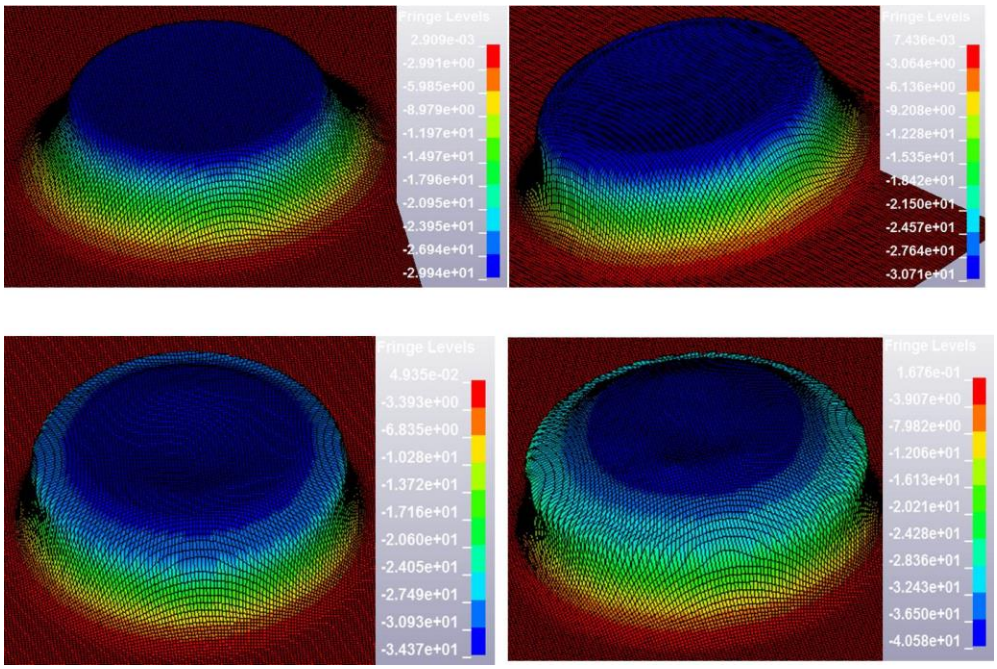

Fig. 6.5 Contour plots of z-depth in different stages

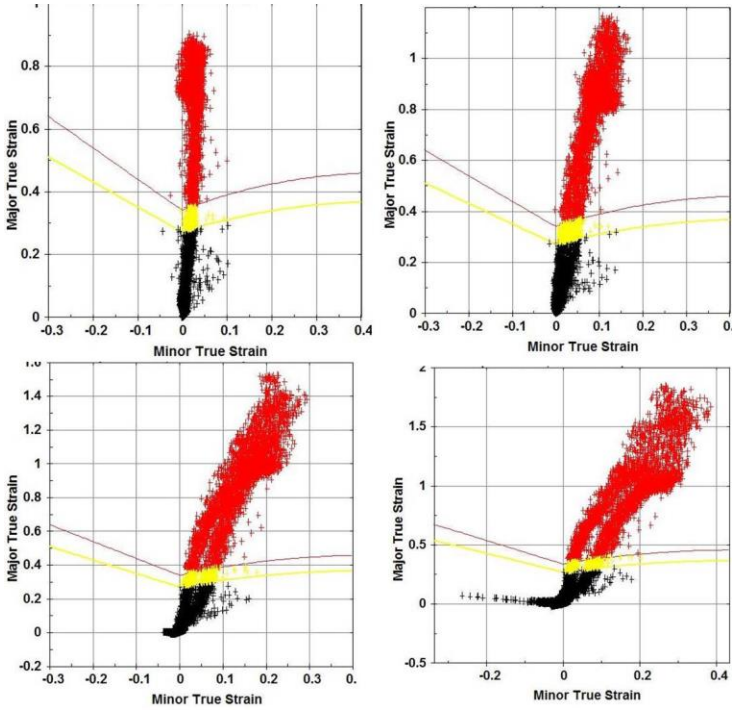

Fig. 6.6 Distribution of principal strains in different stages

The distribution of major and minor principal strains in different stages is shown in Fig. 6.6. The distribution of strains in stage one indicates that the minor strain is almost negligible. Thus the material is in plane strain condition. With the increase in number of stages the strain paths are moving towards bi-axial stretching.

6.3 Form accuracy

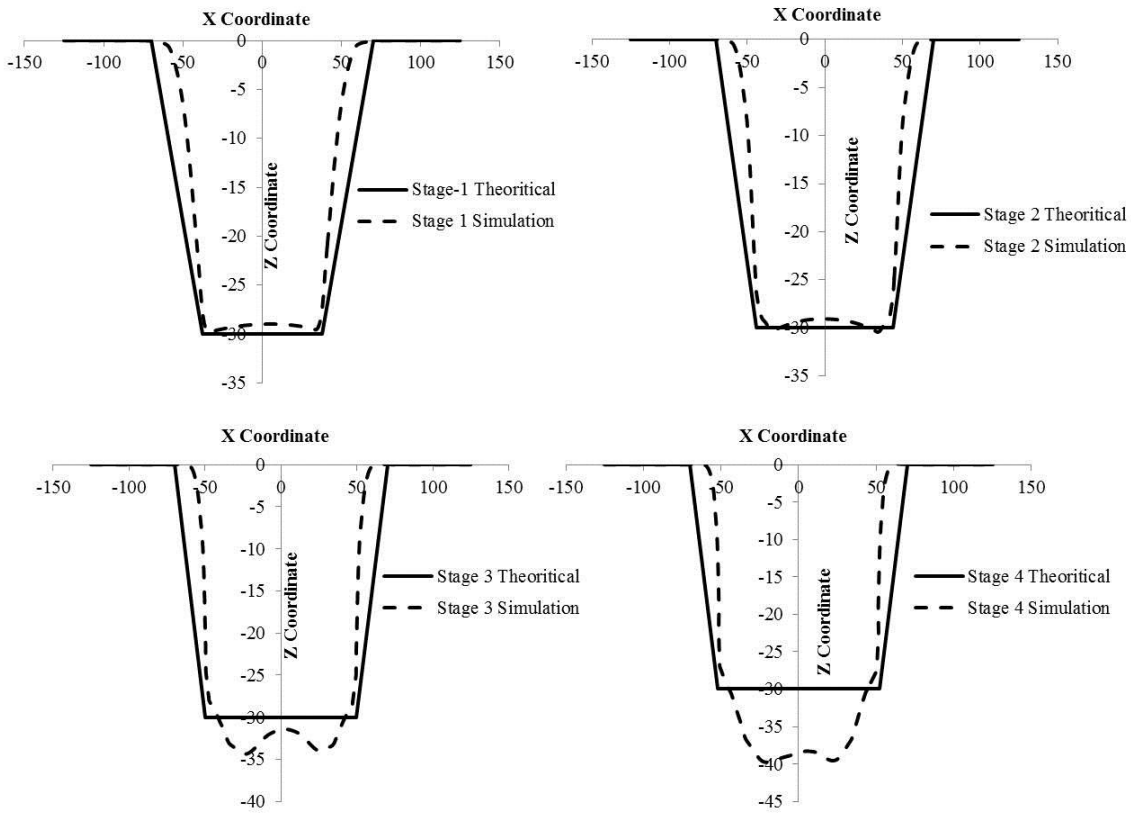

Fig. 6.7 Sectional profiles of formed cups in different stages

One of the major limitation of ISF over the other conventional forming processes is the lesser dimensional accuracy. The geometric accuracy of part formed in MSIF has been checked with FE simulations. There was a negative spring back in all stages of forming process. The spring back is more at the entry region of the backing plate. There is a pillowing effect at the bottom of the cup. The geometric inaccuracies are predominant in stage three and four. During these stages the material has been pulled downwards and the maximum depth of the cup has been exceeded the designed depth. In the fourth stage the residual potions are still more and total depth has been reached to 40 mm. This indicates that the geometric inaccuracies will become larger with the increase

in number of stages. The contour plots of deformed cups in different stages are shown in Fig. 6.5. The stepped features at the bottom of the cup can be observed in stage three and four in the Fig. 6.5. The sectional profiles obtained from FE simulations for different stages are shown in Fig. 6.7 along with theoretical profile.

6.4 Summary

The preliminary results obtained from FE simulations indicate that there is a negative spring back in all the stages of MSIF. The form in accuracies is more with increase in number of stages. Theoretical model could not predict the thickness distribution in bending region. Thickness distribution in wall region from the theoretical model is closer to simulated value. However, it is deviating more with the increase in number stages. The principal strain history reveals that the strain path is moving from plane strain to bi-axial stretching with the increase in number of stages.

Chapter 7 Conclusions and Future work

This thesis provides a detailed study on response of EDD steel in SPIF. The following conclusions are drawn from the research results presented in this thesis.

7.1 Conclusions

- The maximum wall angle that can be formed without fracture using VWACF was found to be 75 ± 2^0. VWACF have been designed with circular, elliptic, parabolic and exponential generatrices. Maximum variation in wall angle with different generatrix curves was found to be 4.6^0. This variation could be due to variation in the curvature and slope distribution of different parts.
- The limiting wall angle with VWAPF was found to be 73 ± 2^0. The reduction in wall angle with VWAPF over VWACF was due to the bi-axial stretching at the corners of the part. Further, the material can be formed without any fracture up to 75% reduction in thickness.
- The effect of process parameters on maximum wall angle has been studied through Taguchi orthogonal arrays. The study revealed that tool diameter, feed rate and step depth have negative effect on maximum wall angle. The tool diameter has maximum influence on the wall angle followed by feed rate and step depth. The optimum process parameters for maximum wall angle was found to be A1B2C1D1 (A = 6 mm, B = 1500 mm/min, C = VWACF, and D = 0.7 mm).
- Pareto ANOVA revealed that the step depth (54.1%) has major effect on grey relational grade followed by feed rate (20.9%), tool diameter (19%) and shape of the part (6%) in the simultaneous optimization of maximum wall angle and surface roughness.
- Thickness distribution obtained from numerical simulations was found to be more accurate than the values obtained from theoretical model. Theoretical model was found to be poor in predicting thickness in bending region, whereas the finite element model is good in predicting thickness both in bending and stretching regions. A correlation coefficient of above 0.99 was observed between measured and simulated thickness with different part geometries.

- The SEM analysis of the fracture surface of the incrementally formed part revealed that the fracture is predominantly ductile in nature. Thus, the ductile fracture models such as Gurson, J-C and Lamatire models can be used to model the fracture and for constructing the fracture forming limit diagram in ISF.
- Finite element studies using LS-Dyna revealed that the VWAPF have been undergoing different strain paths during incremental forming. The material on the face of the pyramid is under plane strain condition, while the material at the corners is towards bi-axial stretching.
- The quadratic model was found to be more appropriate to relate the surface roughness and manufacturing time with process parameters in ISF process of EDD steel sheets.
- Step depth and tool diameter are having a significant effect on surface roughness, while step depth, feed rate, wall angle and tool diameter are having predominant effect on manufacturing time. In case of interaction effects, AB and A^2 have major influence on surface roughness, while BC,BD,B^2,C^2 and D^2 are having significant effect on manufacturing time.
- The increase in step depth increases the surface roughness. The surface roughness value is decreasing with increase in tool diameter up to some value and again increasing with increase in diameter. The manufacturing time is decreased with increase in step depth, feed rate and tool diameter.
- Pareto front obtained from optimization can be used to select appropriate set of process parameters for better surface finish and minimum manufacturing time depending upon the requirement of process engineer. The confirmation experiments show that the results obtained from NSGA-II algorithm can be used to improve the performance of ISF process effectively.
- The surface roughness of parts formed in ISF has been modeled using ANN, SVR and GP. The error statistics reveals that the ANN and SVR techniques are having better performance over GP. Among ANN and SVR, the maximum error has occurred in ANN model. Further, the mean error in SVR was found to be less compared to ANN. Even though, the error statistics reveal that ANN and SVR have better performance than GP, the performance of GP cannot be

underestimated. The positive aspect of GP is that it produces an explicit relationship between input and output parameters, whereas, ANN and SVR both are black box methods.

- The effect of mass scaling and time scaling on numerical simulation results revealed that the punch velocity may be increased up to 40 m/s and mass scaling factor can be increased up to 10 without having any significant effect on the results. At the same time, a huge saving has been observed in terms of computational time.
- The effect of adaptive re-meshing technique in numerical simulation of ISF process revealed that the results obtained with this technique are as good as the results obtained with fine mesh. Additionally, the computational time has been reduced by 50% with adaptive re-meshing technique. Thus this technique can be used to overcome the problem of long computational time due to long tool paths associated with ISF process
- The spiral tool path can produce more uniform thinning than the profile tool path. The stress concentration is also more along the transition zone where the tool steps down from one contour to another contour in profile tool path.
- The methodology proposed to input the manufacturing tool path to finite element simulations can enhance the accuracy of the simulation results as the tool path file for simulation has been generated directly from the G-code file.

7.2 Specific Contributions to Research

Through the research presented in the preceding chapters, the following contributions have been made.

- The formability of EDD steel has been studied through systematic experimental plan and finite element simulations.
- The deformation behavior of the material in terms of stresses, strains, microstructural changes and fracture has been studied.
- The effect of process parameters on surface roughness has been studied through systematic experimental plan. Mathematical models have been developed to

predict the surface roughness as a function of process parameters using response surface methodology, ANN, SVR and GP.

- Different optimization algorithms such as genetic algorithm, NSGA-II and Taguchi based grey relational analysis have been used to optimize the process.
- A methodology has been proposed to input the manufacturing tool path directly to finite element simulations. The effect of different approaches such as mass scaling, time scaling and mesh topology on simulation results have been studied to overcome the large computational time associated with the long tool paths in ISF.
- An attempt has been made to understand the deformation behavior of the EDD steel in multi-stage incremental forming process.

7.3 Recommendations for future work

Based on the conclusion drawn in this chapter following recommendations have been made for future work.

- The future research can focus on developing the fracture forming limit diagrams and stress based forming limit diagrams for the formability analysis of different materials in ISF process.
- Future studies can be focused on studying the spring back and form accuracy of steel parts produced in multi stage incremental forming.
- There is also a need to understand the formability of difficult to form materials such as magnesium and titanium alloys at elevated temperature incremental forming.

References

Adams, D., & Jeswiet, J. (2014). A new model for contact geometry in single-point incremental forming. Proceedings of the Institution of Mechanical Engineers, Part B: Journal of Engineering Manufacture, 229(6), 982-989.

Aerens, R., Duflou, J. R., Eyckens, P., & Van Bael, A. (2009). Advances in force modelling for SPIF. International Journal of Material Forming, 2(1), 25-28.

Aerens, R., Eyckens, P., Van Bael, A., & Duflou, J. R. (2010). Force prediction for single point incremental forming deduced from experimental and FEM observations. The International Journal of Advanced Manufacturing Technology, 46(9-12), 969-982.

Ambrogio, G., Cozza, V., Filice, L., & Micari, F. (2007). An analytical model for improving precision in single point incremental forming. Journal of Materials Processing Technology, 191(1), 92-95.

Ambrogio, G., Filice, L., & Gagliardi, F. (2012). Improving industrial suitability of incremental sheet forming process. The International Journal of Advanced Manufacturing Technology, 58(9-12), 941-947.

Ambrogio, G., Filice, L., & Manco, G. L. (2008). Warm incremental forming of magnesium alloy AZ31. CIRP Annals-Manufacturing Technology, 57(1), 257-260.

Ambrogio, G., Filice, L., & Micari, F. (2006). A force measuring based strategy for failure prevention in incremental forming. Journal of Materials Processing Technology, 177(1), 413-416.

Ambrogio, G., Filice, L., De Napoli, L., & Muzzupappa, M. (2005). A simple approach for reducing profile diverting in a single point incremental forming process. Proceedings of the Institution of Mechanical Engineers, Part B: Journal of Engineering Manufacture, 219(11), 823-830.

Ashgar, J., Lingam, R., Shibin, E., & Reddy, N. V. (2014). Tool path design for enhancement of accuracy in single-point incremental forming. Proceedings of the

Institution of Mechanical Engineers, Part B: Journal of Engineering Manufacture, 228(9), 1027-1035.

Attanasio, A., Ceretti, E., Giardini, C., & Mazzoni, L. (2008). Asymmetric two points incremental forming: improving surface quality and geometric accuracy by tool path optimization. Journal of Materials Processing Technology, 197(1), 59-67.

Azaouzi, M., & Lebaal, N. (2012). Tool path optimization for single point incremental sheet forming using response surface method. Simulation Modelling Practice and Theory, 24, 49-58.

Bahloul, R., Arfa, H., & BelHadjSalah, H. (2014). A study on optimal design of process parameters in single point incremental forming of sheet metal by combining Box–Behnken design of experiments, response surface methods and genetic algorithms. The International Journal of Advanced Manufacturing Technology, 74(1-4), 163-185.

Behera, A. K., Verbert, J., Lauwers, B., & Duflou, J. R. (2013). Tool path compensation strategies for single point incremental sheet forming using multivariate adaptive regression splines. Computer-Aided Design, 45(3), 575-590.

Bhattacharya A., Jian Cao, Maneesh K., & Venkata Reddy N. (2011). Formability and surface finish studies in single point incremental forming. Journal of Manufacturing Science and Engineering, 133(6),1020-1028

Blaga, A., Bologa, O., Oleksik, V., & Breaz, R. (2011). Influence of tool path on main strains, thickness reduction and forces in single point incremental forming process. Proceedings in Manufacturing Systems, 6(4), 191-196.

Bouffioux, C., Eyckens, P., Henrard, C., Aerens, R., Van Bael, A., Sol, H., ... & Habraken, A. M. (2008). Identification of material parameters to predict Single Point Incremental Forming forces. International Journal of Material Forming, 1(1), 1147-1150.

Bouffioux, C., Lequesne, C., Vanhove, H., Duflou, J. R., Pouteau, P., Duchêne, L., & Habraken, A. M. (2011). Experimental and numerical study of an AlMgSc sheet formed by an incremental process. Journal of Materials Processing Technology, 211(11), 1684-1693.

Cao, T., Lu, B., Xu, D., Zhang, H., Chen, J., Long, H., & Cao, J. (2014). An efficient method for thickness prediction in multi-pass incremental sheet forming. The International Journal of Advanced Manufacturing Technology, 77(1-4), 469-483.

Cavaler L.C.C., Schaeffer L., Rocha A.S., Peruch F. (2010). Surface roughness in the incremental forming of AISI 304L stainless steel sheets. Far East Journal of Mechanical Engineering and Physics, 1(2), 87-98.

Çaydaş, U., & Ekici, S. (2012). Support vector machines models for surface roughness prediction in CNC turning of AISI 304 austenitic stainless steel.Journal of Intelligent Manufacturing, 23(3), 639-650.

Ceretti, E., Giardini, C. & Attanasio, A. (2004). Experimental and simulative results in sheet incremental forming on CNC machines. Journal of Materials Processing Technology, 152(2), 76–184.

Cerro, I., Maidagan, E., Arana, J., Rivero, A., & Rodriguez, P. P. (2006). Theoretical and experimental analysis of the dieless incremental sheet forming process. Journal of Materials Processing Technology, 177(1), 404-408.

Cui, Z., & Gao, L. (2010). Studies on hole-flanging process using multistage incremental forming. CIRP Journal of Manufacturing Science and Technology,2(2), 124-128.

Cui, Z., Xia, Z. C., Ren, F., Kiridena, V., & Gao, L. (2013). Modeling and validation of deformation process for incremental sheet forming. Journal of Manufacturing Processes, 15(2), 236-241.

De Bruyn R., Treurnicht N.F. (2012). An Investigation Into Lubrication Strategies For The Incremental Sheet Forming Of TI-6AL-4V. In Proceedings of the 42 nd International Conference on Computers and Industrial Engineering, Cape town, South Africa.

Dejardin, S., Thibaud, S., & Gelin, J. C. (2008). Finite element analysis and experimental investigations for improving precision in single point incremental sheet forming process. International Journal of Material Forming, 1(1), 121-124.

Dejardin, S., Thibaud, S., Gelin, J. C., & Michel, G. (2010). Experimental investigations and numerical analysis for improving knowledge of incremental sheet forming process for sheet metal parts. Journal of Materials Processing Technology, 210(2), 363-369.

Duflou, J. R., Verbert, J., Belkassem, B., Gu, J., Sol, H., Henrard, C., & Habraken, A. M. (2008). Process window enhancement for single point incremental forming through multi-step tool paths. CIRP Annals-Manufacturing Technology, 57(1), 253-256.

Duflou, J., Tunckol, Y., Szekeres, A., & Vanherck, P. (2007). Experimental study on force measurements for single point incremental forming. Journal of Materials Processing Technology, 189(1), 65-72.

Durante, M., Formisano, A., & Langella, A. (2010). Comparison between analytical and experimental roughness values of components created by incremental forming. Journal of Materials Processing Technology, 210(14), 1934-1941.

Durante, M., Formisano, A., Langella, A., & Minutolo, F. M. C. (2009). The influence of tool rotation on an incremental forming process. Journal of Materials Processing Technology, 209(9), 4621-4626.

Elford, M., Saha, P., Seong, D., Haque, M. Z., & Yoon, J. W. (2013). Benchmark 3-Incremental sheet forming. AIP Conference Proceedings, 1567(1), 227-261.

Emmens, W. C., & Van den Boogaard, A. H. (2009a). An overview of stabilizing deformation mechanisms in incremental sheet forming. Journal of Materials Processing Technology, 209(8), 3688-3695.

Emmens, W. C., Boogaard, V. D. A., & Weijde, V. D. D. (2009b). The FLC, enhanced fromavbility, and incremental sheet forming.Proceedings of the International Deep Drawing Research Group IDDRG 2009 International Conference, 773-784.

Essa, K., & Hartley, P. (2011). An assessment of various process strategies for improving precision in single point incremental forming. International journal of material forming, 4(4), 401-412.

Eyckens, P., Belkassem, B., Henrard, C., Gu, J., Sol, H., Habraken, A. M., ... & Van Houtte, P. (2011). Strain evolution in the single point incremental forming process: digital image correlation measurement and finite element prediction.International journal of material forming, 4(1), 55-71.

Fan, G., Sun, F., Meng, X., Gao, L., & Tong, G. (2010). Electric hot incremental forming of Ti-6Al-4V titanium sheet. The International Journal of Advanced Manufacturing Technology, 49(9-12), 941-947.

Filice, L., Ambrogio, G., & Micari, F. (2006). On-line control of single point incremental forming operations through punch force monitoring. CIRP annals-Manufacturing technology, 55(1), 245-248.

Filice, L., Fratini, L., & Micari, F. (2002). Analysis of material formability in incremental forming. CIRP annals-Manufacturing technology, 51(1), 199-202.

Fiorentino, A. (2013). Force-based failure criterion in incremental sheet forming.The International Journal of Advanced Manufacturing Technology, 68(1-4), 557-563.

Fratini, L., Ambrogio, G., Di Lorenzo, R., Filice, L., & Micari, F. (2004). Influence of mechanical properties of the sheet material on formability in single point incremental forming. CIRP Annals-Manufacturing Technology, 53(1), 207-210.

Gupta, A. K. (2010). Predictive modelling of turning operations using response surface methodology, artificial neural networks and support vector regression.International journal of production research, 48(3), 763-778.

Hagan, E., & Jeswiet, J. (2004). Analysis of surface roughness for parts formed by computer numerical controlled incremental forming. Proceedings of the Institution of Mechanical Engineers, Part B: Journal of Engineering Manufacture, 218(10), 1307-1312.

Ham, M., & Jeswiet, J. (2006). Single point incremental forming and the forming criteria for AA3003. CIRP Annals-Manufacturing Technology, 55(1), 241-244.

Ham, M., & Jeswiet, J. (2007). Forming limit curves in single point incremental forming. CIRP Annals-Manufacturing Technology, 56(1), 277-280.

Hamilton, K., & Jeswiet, J. (2010). Single point incremental forming at high feed rates and rotational speeds: Surface and structural consequences. CIRP Annals-Manufacturing Technology, 59(1), 311-314.

Han, F., & Mo, J. H. (2008). Numerical simulation and experimental investigation of incremental sheet forming process. Journal of Central South University of Technology, 15, 581-587.

Han, H. N., & Kim, K. H. (2003). A ductile fracture criterion in sheet metal forming process. Journal of Materials Processing Technology, 142(1), 231-238.

Henrard, C., Bouffioux, C., Eyckens, P., Sol, H., Duflou, J. R., Van Houtte, P., ... & Habraken, A. M. (2011). Forming forces in single point incremental forming: prediction by finite element simulations, validation and sensitivity.Computational mechanics, 47(5), 573-590.

Hussain, G., & Gao, L. (2007a). A novel method to test the thinning limits of sheet metals in negative incremental forming. International Journal of Machine Tools and Manufacture, 47(3), 419-435.

Hussain, G., Gao, L., & Dar, N. U. (2007b). An experimental study on some formability evaluation methods in negative incremental forming. Journal of Materials Processing Technology, 186(1), 45-53.

Hussain, G., Gao, L., & Zhang, Z. Y. (2008a). Formability evaluation of a pure titanium sheet in the cold incremental forming process. The International Journal of Advanced Manufacturing Technology, 37(9-10), 920-926.

Hussain, G., Gao, L., Hayat, N., & Dar, N. U. (2010). The formability of annealed and pre-aged AA-2024 sheets in single-point incremental forming. The International Journal of Advanced Manufacturing Technology, 46(5-8), 543-549.

Hussain, G., Gao, L., Hayat, N., & Ziran, X. (2009). A new formability indicator in single point incremental forming. Journal of Materials Processing Technology, 209(9), 4237-4242.

Hussain, G., Gao, L., Hayat, N., Cui, Z., Pang, Y. C., & Dar, N. U. (2008b). Tool and lubrication for negative incremental forming of a commercially pure titanium sheet. Journal of materials processing technology, 203(1), 193-201.

Hussain, G., Lin, G., & Hayat, N. (2011). Improving profile accuracy in SPIF process through statistical optimization of forming parameters. Journal of Mechanical Science and Technology, 25(1), 177-182.

Iseki, H. (2001). An approximate deformation analysis and FEM analysis for the incremental bulging of sheet metal using a spherical roller. Journal of Materials Processing Technology, 111(1), 150-154.

Jackson, K., & Allwood, J. (2009). The mechanics of incremental sheet forming. Journal of materials processing technology, 209(3), 1158-1174.

Jadhav, S., (2004). Basic Investigations of the Incremental Sheet Metal Forming Process on a CNC Milling Machine. Ph.D thesis, Aachen university Germany.

Jeswiet, J., & Young, D. (2005). Forming limit diagrams for single-point incremental forming of aluminium sheet. Proceedings of the Institution of Mechanical Engineers, Part B: Journal of Engineering Manufacture, 219(4), 359-364.

Jeswiet, J., Hagan, E., & Szekeres, A. (2002). Forming parameters for incremental forming of aluminium alloy sheet metal. Proceedings of the Institution of Mechanical Engineers, Part B: Journal of Engineering Manufacture, 216(10), 1367-1371.

Jeswiet, J., Micari, F., Hirt, G., Bramley, A., Duflou, J., & Allwood, J. (2005). Asymmetric single point incremental forming of sheet metal. CIRP Annals-Manufacturing Technology, 54(2), 88-114.

Ji, Y. H., & Park, J. J. (2008). Incremental forming of free surface with magnesium alloy AZ31 sheet at warm temperatures. Transactions of nonferrous metals society of China, 18, s165-s169

Jie, L., Jianhua, M., & Shuhuai, H. (2004). Sheet metal dieless forming and its tool path generation based on STL files. The International Journal of Advanced Manufacturing Technology, 23(9-10), 696-699.

Jie, L., Jianhua, M., & Shuhuai, H. (2004). Sheet metal dieless forming and its tool path generation based on STL files. The International Journal of Advanced Manufacturing Technology, 23(9-10), 696-699.

Junchao, L., Junjian, S., & Bin, W. (2013). A multipass incremental sheet forming strategy of a car taillight bracket. The International Journal of Advanced Manufacturing Technology, 69(9-12), 2229-2236.

Kalpakjian, S., & Schmid, S.R. (2009). Manufacturing processes for engineering materials. Pearson education, Inc. India.

Khan, Z. A., Siddiquee, A. N., & Sheikh, M. H. (2012). Selection of optimal condition for finishing of centreless-cylindrical ground parts using grey relational and principal component analyses. International Journal of Materials and Product Technology, 43(1-4), 2-21.

Kim, T. J., & Yang, D. Y. (2000). Improvement of formability for the incremental sheet metal forming process. International Journal of Mechanical Sciences, 42(7), 1271-1286.

Kim, Y. H., & Park, J. J. (2002). Effect of process parameters on formability in incremental forming of sheet metal. Journal of materials processing technology,130, 42-46.

Kök, M., Kanca, E., & Eyercioğlu, Ö. (2011). Prediction of surface roughness in abrasive waterjet machining of particle reinforced MMCs using genetic expression programming. The International Journal of Advanced Manufacturing Technology, 55(9-12), 955-968.

Koza, J. R. (Ed.). (1999). Genetic programming III: Darwinian invention and problem solving (Vol. 3). Morgan Kaufmann.

Kuram, E., & Ozcelik, B. (2013). Multi-objective optimization using Taguchi based grey relational analysis for micro-milling of Al 7075 material with ball nose end mill. Measurement, 46(6), 1849-1864.

Le Van Sy. 2009. Modeling of single point incremental forming process for metal and polymeric sheet. Ph.D thesis, University of padua, Padova.

Li, J., Geng, P., & Shen, J. (2013). Numerical simulation and experimental investigation of multistage incremental sheet forming. The International Journal of Advanced Manufacturing Technology, 68(9-12), 2637-2644.

Li, J., Hu, J., Pan, J., & Geng, P. (2012a). Thickness distribution and design of a multi-stage process for sheet metal incremental forming. The International Journal of Advanced Manufacturing Technology, 62(9-12), 981-988.

Li, M., Zhang, L. C., Mo, J. H., & Lu, Y. (2012b). Tool-path generation for sheet metal incremental forming based on STL model with defects. The International Journal of Advanced Manufacturing Technology, 63(5-8), 535-547.

Li, Y., Liu, Z., Daniel, W. J. T., & Meehan, P. A. (2014b). Simulation and Experimental Observations of Effect of Different Contact Interfaces on the Incremental Sheet Forming Process. Materials and Manufacturing Processes,29(2), 121-128.

Li, Y., Liu, Z., Lu, H., Daniel, W. B., Liu, S., & Meehan, P. A. (2014). Efficient force prediction for incremental sheet forming and experimental validation. The International Journal of Advanced Manufacturing Technology, 73(1-4), 571-587.

Lingam, R., Bansal, a. & Reddy, N. V. (2015). Analytical prediction of formed geometry in multi-stage single point incremental forming. International Journal of Material Forming. (In Press).

Liu, Z., Daniel, W. J., Li, Y., Liu, S., & Meehan, P. A. (2014a). Multi-pass deformation design for incremental sheet forming: analytical modeling, finite element analysis and experimental validation. Journal of Materials Processing Technology, 214(3), 620-634.

Liu, Z., Li, Y., & Meehan, P. A. (2013). Vertical wall formation and material flow control for incremental sheet forming by revisiting multistage deformation path strategies. Materials and manufacturing processes, 28(5), 562-571.

Liu, Z., Li, Y., & Meehan, P. A. (2014b). Tool path strategies and deformation analysis in multi-pass incremental sheet forming process. The International Journal of Advanced Manufacturing Technology, 75(1-4), 395-409.

Lu, B., Chen, J., Ou, H., & Cao, J. (2013). Feature-based tool path generation approach for incremental sheet forming process. Journal of Materials Processing Technology, 213(7), 1221-1233.

Lu, B., Fang, Y., Xu, D. K., Chen, J., Ou, H., Moser, N. H., & Cao, J. (2014). Mechanism investigation of friction-related effects in single point incremental forming using a developed oblique roller-ball tool. International Journal of Machine Tools and Manufacture, 85, 14-29.

Ma, L. W., & Mo, J. H. (2008). Three-dimensional finite element method simulation of sheet metal single-point incremental forming and the deformation pattern analysis. Proceedings of the Institution of Mechanical Engineers, Part B: Journal of Engineering Manufacture, 222(3), 373-380.

Malhotra, R., Bhattacharya, A., Kumar, A., Reddy, N. V., & Cao, J. (2011a). A new methodology for multi-pass single point incremental forming with mixed tool paths. CIRP Annals-Manufacturing Technology, 60(1), 323-326.

Malhotra, R., Cao, J., Beltran, M., Xu, D., Magargee, J., Kiridena, V., & Xia, Z. C. (2012a). Accumulative-DSIF strategy for enhancing process capabilities in incremental forming. CIRP Annals-Manufacturing Technology, 61(1), 251-254.

Malhotra, R., Cao, J., Ren, F., Kiridena, V., Xia, Z. C., & Reddy, N. V. (2011b). Improvement of geometric accuracy in incremental forming by using a squeezing tool path strategy with two forming tools. Journal of Manufacturing Science and Engineering, 133(6), 061019.

Malhotra, R., Reddy, N. V., & Cao, J. (2010). Automatic 3D spiral tool path generation for single point incremental forming. Journal of manufacturing science and engineering, 132(6), 061003.

Malhotra, R., Xue, L., Belytschko, T., & Cao, J. (2012b). Mechanics of fracture in single point incremental forming. Journal of Materials Processing Technology, 212(7), 1573-1590.

Manco, L., Filice, L., & Ambrogio, G. (2011). Analysis of the thickness distribution varying tool trajectory in single-point incremental forming.Proceedings of the

Institution of Mechanical Engineers, Part B: Journal of Engineering Manufacture, 225(3), 348-356.

Martins, P. A. F., Bay, N., Skjødt, M., & Silva, M. B. (2008). Theory of single point incremental forming. CIRP Annals-Manufacturing Technology, 57(1), 247-252.

Meier, H., Buff, B., Laurischkat, R., & Smukala, V. (2009). Increasing the part accuracy in dieless robot-based incremental sheet metal forming. CIRP Annals-Manufacturing Technology, 58(1), 233-238.

Micari, F., Ambrogio, G. (2004). A common shape for conductingincremental forming tests. 1st Incremental FormingWorkshop. University of Saarbrucken.

Micari, F., Ambrogio, G., & Filice, L. (2007). Shape and dimensional accuracy in single point incremental forming: state of the art and future trends. Journal of Materials Processing Technology, 191(1), 390-395

Minutolo, F. C., Durante, M., Formisano, A., & Langella, A. (2007). Evaluation of the maximum slope angle of simple geometries carried out by incremental forming process. Journal of Materials Processing Technology, 194(1), 145-150.

Nguyen, D. T., Park, J. G., Lee, H. J., & Kim, Y. S. (2010). Finite element method study of incremental sheet forming for complex shape and its improvement. Proceedings of the Institution of Mechanical Engineers, Part B: Journal of Engineering Manufacture, 224(6), 913-924.

Pa, N. M. N., Sarhan, A. A. D., & Shukor, M. H. A. (2012). Optimizing the cutting parameters for better surface quality in 2.5 D cutting utilizing titanium coated carbide ball end mill. International Journal of Precision Engineering and Manufacturing, 13(12), 2097-2102.

Paniti, I., & Somló, J. (2014). Novel Incremental Sheet Forming System with Tool-Path Calculation Approach. Acta Polytechnica Hungarica, 11(7), 43-60.

Park, J. J., & Kim, Y. H. (2003). Fundamental studies on the incremental sheet metal forming technique. Journal of Materials Processing Technology, 140(1), 447-453.

Parrella, F. (2007). Online support vector regression. Master's Thesis, Department of Information Science, University of Genoa, Italy.

Pérez-Santiago, R., Bagudanch, I., & García-Romeu, M. L. (2011). Force modeling in single point incremental forming of variable wall angle components. In Key Engineering Materials,473, 833-840.

Petek, A., Kuzman, K., & Kopac, J. (2009a). Deformations and forces analysis of single point incremental sheet metal forming. Archives of Materials science and Engineering, 35(2), 35-42.

Petek, A., Kuzman, K., & Suhač, B. (2009b). Autonomous on-line system for fracture identification at incremental sheet forming. CIRP Annals-Manufacturing Technology, 58(1), 283-286.

Pohlak, M., 2007. Rapid protyping of sheet metal components with incremental sheet forming technolgy. Ph.D thesis, Tallinn university of technology, Estonia.

Radu, C., Tampu, C., Cristea, I., & Chirita, B. (2013). The effect of residual stresses on the accuracy of parts processed by SPIF. Materials and Manufacturing Processes, 28(5), 572-576.

Rao, R. V. (2010). Advanced modeling and optimization of manufacturing processes: international research and development. Springer Science & Business Media.

Rattanachan K., Chungchoo C. (2010). The Effect of The Single Point tooling Radius to Roughness of DIN 1 . 0037 Steel Formed Workpiece in Incremental Forming Process. The 24th Conference of the Mechanical Engineering Network of Thailand. AMM-25.

Rauch, M., Hascoet, J. Y., Hamann, J. C., & Plenel, Y. (2009). Tool path programming optimization for incremental sheet forming applications.Computer-Aided Design, 41(12), 877-885.

Ren, F., Cui, Z., Xia, Z. C., Slavik, T., Zhang, L., & Zhu, X. (2010). Process Modeling of Freeform Incremental Forming Using LS-DYNA®. In 11th International LS-DYNA Users Conference of Metal Forming.

Salman, Ö., & Kayacan, M. C. (2008). Evolutionary programming method for modeling the EDM parameters for roughness. journal of materials processing technology, 200(1), 347-355.

Sarraji, W. K., Hussain, J., & Ren, W. X. (2012). Experimental investigations on forming time in negative incremental sheet metal forming process. Materials and Manufacturing Processes, 27(5), 499-506.

Sena, J. I. V., de Sousa, R. A., & Valente, R. A. F. (2010). Single point incremental forming simulation with an enhanced assumed strain solid-shell finite element formulation. International Journal of Material Forming, 3(1), 963-966.

Seong, D. Y., Haque, M. Z., Kim, J. B., Stoughton, T. B., & Yoon, J. W. (2014). Suppression of necking in incremental sheet forming. International Journal of Solids and Structures, 51(15), 2840-2849.

Setti, F., Bini, R., Lunardelli, M., Bosetti, P., Bruschi, S., & De Cecco, M. (2012). Shape measurement system for single point incremental forming (SPIF) manufacts by using trinocular vision and random pattern. Measurement science and technology, 23(11), 115402.

Shi, X., Hussain, G., Zha, G., Wu, M., & Kong, F. (2014). Study on formability of vertical parts formed by multi-stage incremental forming. The International Journal of Advanced Manufacturing Technology, 75(5-8), 1049-1053.

Shim, M. S., & Park, J. J. (2001). The formability of aluminum sheet in incremental forming. Journal of Materials Processing Technology, 113(1), 654-658.

Silva, M. B., Skjødt, M., Atkins, A. G., Bay, N., & Martins, P. A. F. (2008). Single-point incremental forming and formability—failure diagrams', The Journal of Strain Analysis for Engineering Design, 43(1), 15-35.

Silva, M. B., Skjoedt, M., Bay, N., & Martins, P. A. F. (2009). Formalibity in multistage single point incremental forming. In 7th EUROMECH Solid Mechanics Conference, Lisbon Portugal.

Singh, S. K., Mahesh, K., Kumar, A., & Swathi, M. (2010). Understanding formability of extra-deep drawing steel at elevated temperature using finite element simulation. Materials & Design, 31(9), 4478-4484.

Skjødt, M., Bay, N., Endelt, B., & Ingarao, G. (2008). Multi stage strategies for single point incremental forming of a cup. International Journal of Material Forming, 1(1), 1199-1202.

Skjødt, M., Hancock, M. H., & Bay, N. (2007). Creating helical tool paths for single point incremental forming. Key Engineering Materials, 344, 583-590.

Tanaka, S., Nakamura, T., Hayakawa, K., Nakamura, H., & Motomura, K. (2008). Experimental and numerical investigations on negative springback in incremental sheet metal forming. Metal forming, 1, 55-62.

Vapnik, V. (2000). The nature of statistical learning theory. Springer Science & Business Media.

Watzeels, K., Tunckol, Y., Henrard, C., Gu, J., Sol, H., Duflou, J., & Habraken, A. (2005). Experimental validation of the finite element simulation of the first stroke in single point incremental forming. In 8th ESAFORM Conference on Material Forming (pp. 703-706). The publishing House of the Romanian Academy.

Wei, H., Chen, W., & Gao, L. (2011). Springback Investigation on Sheet Metal Incremental Formed Parts. World Academy of Science, Engineering and Technology, 55, 285-289.

Wen, K. L., Chang, T. C., & You, M. L. (1998). The grey entropy and its application in weighting analysis. In Systems, Man, and Cybernetics,2,1842-1844.

Xu, D., Malhotra, R., Reddy, N. V., Chen, J., & Cao, J. (2012). Analytical prediction of stepped feature generation in multi-pass single point incremental forming. Journal of Manufacturing Processes, 14(4), 487-494.

Yamashita, M., Gotoh, M., & Atsumi, S. Y. (2008). Numerical simulation of incremental forming of sheet metal. Journal of materials processing technology,199(1), 163-172.

Young, D., & Jeswiet, J. (2004). Wall thickness variations in single-point incremental forming. Proceedings of the Institution of Mechanical Engineers, Part B: Journal of Engineering Manufacture, 218(11), 1453-1459.

Zhang, C., Xiao, H., & Yu, D. (2013). Negative incremental forming of sheet based on interval model of hydraulic bulging analysis. Rev. Adv. Mater. Sci, 33, 360-366.

Zhang, G., Patuwo, B. E., & Hu, M. Y. (1998). Forecasting with artificial neural networks: The state of the art. International journal of forecasting, 14(1), 35-62.

Appendix

Sample Part program for incremental forming

O0075	N140X24.825Y-46.596Z-0.935
G0 G91 G28 Z0.	N145X25.758Y-46.081Z-0.94
G90 G54 G17 G40	N150X26.69Y-45.553Z-0.936
G0 X0 Y0 Z10.	N155X27.622Y-44.995Z-0.935
S300 M3	N160X28.55Y-44.405Z-0.94
X4.917Y-52.563	N165X29.487Y-43.794Z-0.936
Z3.0	-------
N55G1Z-0.939F375.	-------
N60X5.944Y-52.462Z-0.936F750.	--------
N65X7.576Y-52.249Z-0.937	--------
N70X8.275Y-52.14Z-0.941	N104865X-0.344Y-12.804Z-70.173
N75X9.907Y-51.858Z-0.937	N104870X0.346Y-12.803Z-70.179
N85X13.17Y-51.127Z-0.936	N104875X1.038Y-12.764Z-70.185
N90X14.103Y-50.874Z-0.939	N104880X1.211Y-12.747Z-70.186
N115X20.163Y-48.794Z-0.936	G0Z25.0
N120X21.156Y-48.367Z-0.939	M30
N130X22.96Y-47.537Z-0.94	%

Generatrices used for modeling VWACF and VWAPF parts

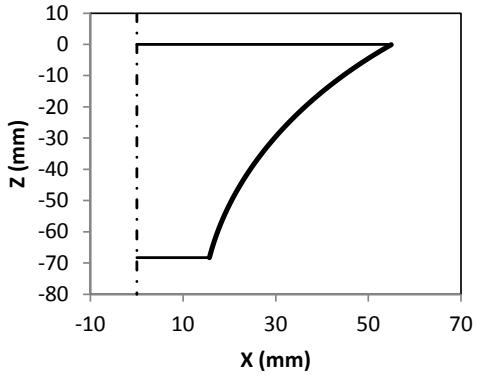

(a)

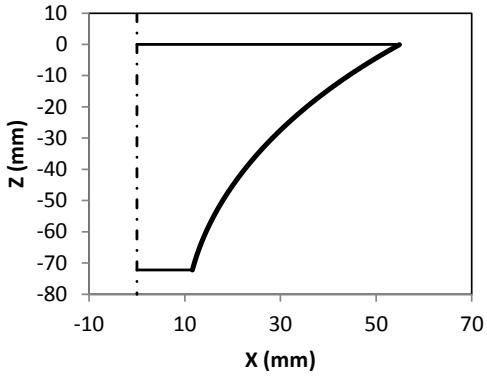

(b)

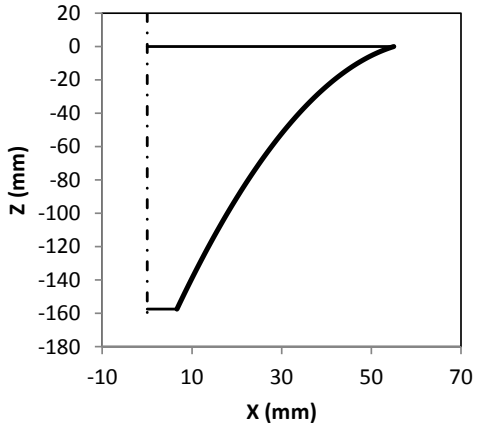

(c)

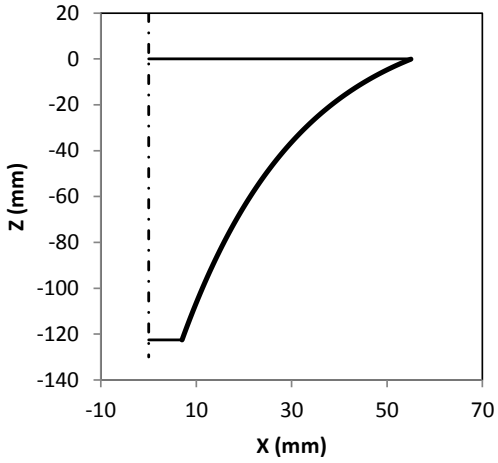

(d)

Optimum process settings from NSGA-II

S.no	A	B	C	D	RA	T	S.no	A	B	C	D	RA	T
1	12.31	0.28	35.01	1098.51	0.7105	18.23	51	11.75	0.25	35.10	1098.65	0.6718	22.39
2	11.85	0.23	35.04	1096.86	0.6512	24.85	52	11.45	0.19	35.15	1098.88	0.5895	35.35
3	11.28	0.16	35.00	1098.97	0.5352	47.43	53	11.43	0.18	35.24	1098.20	0.5695	39.64
4	12.04	0.26	35.10	1097.90	0.6818	21.03	54	11.93	0.23	35.06	1097.90	0.6459	25.70
5	11.33	0.16	35.19	1098.89	0.5379	47.04	55	11.12	0.16	35.16	1098.32	0.5313	48.64
6	11.43	0.18	35.10	1097.35	0.5606	41.59	56	11.32	0.18	35.05	1098.93	0.5584	41.87
7	11.18	0.15	35.15	1096.81	0.5167	52.53	57	11.71	0.23	35.17	1098.31	0.6443	25.94
8	11.72	0.23	35.11	1097.87	0.6431	26.08	58	11.91	0.23	35.16	1097.87	0.6499	25.13
9	11.54	0.20	35.14	1097.28	0.6058	32.29	59	12.06	0.25	35.14	1098.85	0.6679	22.74
10	12.61	0.29	35.06	1099.82	0.7257	17.29	60	11.09	0.15	35.27	1099.92	0.5122	53.70
11	11.78	0.22	35.00	1099.37	0.6255	28.72	61	11.33	0.16	35.18	1098.69	0.5258	50.35
12	11.29	0.17	35.19	1098.16	0.5493	44.19	62	11.34	0.17	35.13	1097.66	0.5461	44.97
13	11.48	0.20	35.01	1099.03	0.5930	34.52	63	11.14	0.16	35.22	1098.29	0.5258	50.09
14	12.19	0.28	35.07	1098.31	0.7074	18.52	64	11.50	0.21	35.11	1098.20	0.6236	29.30
15	11.11	0.15	35.28	1098.38	0.5129	53.61	65	12.01	0.29	35.13	1097.57	0.7160	18.10
16	11.20	0.15	35.19	1097.50	0.5148	53.14	66	11.31	0.16	35.15	1098.72	0.5306	48.93
17	11.81	0.26	35.17	1098.43	0.6813	21.33	67	11.29	0.19	35.11	1097.74	0.5765	38.11
18	11.91	0.25	35.06	1099.02	0.6765	21.63	68	11.37	0.19	35.19	1098.46	0.5860	36.17
19	11.16	0.16	35.23	1096.33	0.5327	48.42	69	11.39	0.19	35.10	1098.86	0.5793	37.39
20	11.82	0.24	35.10	1097.47	0.6616	23.52	70	11.20	0.16	35.13	1099.00	0.5382	46.79
21	11.39	0.15	35.11	1097.85	0.5211	51.93	71	11.37	0.15	35.10	1097.39	0.5195	52.30
22	11.25	0.17	35.20	1099.34	0.5415	46.04	72	12.02	0.24	35.05	1097.98	0.6573	24.11
23	11.66	0.20	35.10	1099.61	0.6035	32.67	73	12.14	0.27	35.08	1098.99	0.6999	19.17
24	11.27	0.15	35.14	1097.65	0.5218	51.24	74	11.30	0.16	35.05	1097.11	0.5347	47.75
25	11.75	0.22	35.05	1097.85	0.6279	28.38	75	11.36	0.19	35.10	1096.61	0.5843	36.47
26	11.77	0.22	35.09	1098.39	0.6356	27.16	76	11.41	0.18	35.16	1098.24	0.5708	39.27
27	12.09	0.25	35.12	1097.41	0.6699	22.53	77	11.33	0.19	35.07	1098.84	0.5806	37.15
28	12.29	0.29	35.00	1099.44	0.7171	17.70	78	11.86	0.25	35.13	1098.45	0.6754	21.86
29	12.18	0.27	35.02	1096.81	0.6910	20.04	79	11.26	0.16	35.20	1097.47	0.5366	47.36
30	11.22	0.15	35.19	1098.06	0.5160	52.80	80	11.37	0.17	35.09	1098.11	0.5564	42.44
31	11.32	0.18	35.17	1099.69	0.5668	40.12	81	11.54	0.20	35.13	1098.03	0.5955	34.19
32	12.78	0.30	35.09	1099.95	0.7336	17.01	82	12.00	0.26	35.17	1097.16	0.6794	21.36
33	11.49	0.18	35.05	1097.70	0.5720	39.01	83	11.68	0.23	35.11	1098.83	0.6418	26.28
34	11.16	0.16	35.18	1097.40	0.5290	49.24	84	11.51	0.19	35.11	1098.27	0.5779	37.77
35	11.54	0.22	35.14	1098.35	0.6321	27.94	85	11.41	0.18	35.14	1096.31	0.5736	38.70
36	11.47	0.19	35.16	1099.55	0.5823	36.79	86	11.71	0.22	35.10	1098.18	0.6322	27.70
37	11.94	0.24	35.14	1098.37	0.6534	24.63	87	11.51	0.19	35.28	1098.79	0.5787	37.73
38	11.45	0.21	35.18	1097.79	0.6215	29.81	88	12.04	0.27	35.03	1097.75	0.6970	19.48
39	11.93	0.24	35.09	1098.26	0.6634	23.22	89	11.44	0.17	35.21	1098.98	0.5557	42.86
40	12.67	0.29	35.07	1099.78	0.7244	17.53	90	11.48	0.18	35.12	1096.93	0.5684	39.88
41	11.41	0.18	35.09	1098.32	0.5748	38.31	91	11.53	0.19	35.12	1098.29	0.5821	36.89
42	11.57	0.20	35.09	1098.38	0.6072	31.94	92	11.54	0.21	35.07	1099.73	0.6092	31.54
43	11.24	0.16	35.02	1096.67	0.5334	47.97	93	11.18	0.16	35.10	1099.56	0.5228	50.69
44	11.45	0.20	35.22	1097.47	0.5953	34.34	94	12.06	0.26	35.05	1098.89	0.6846	20.67
45	11.30	0.16	35.13	1098.74	0.5392	46.62	95	11.60	0.20	35.01	1098.38	0.6072	31.87
46	11.44	0.18	35.18	1098.08	0.5619	41.35	96	11.32	0.17	35.23	1097.58	0.5576	42.32
47	11.22	0.16	35.19	1099.17	0.5272	49.68	97	12.03	0.27	35.07	1097.33	0.6939	19.80
48	12.03	0.24	35.08	1098.35	0.6650	23.05	98	13.00	0.30	35.00	1099.85	0.7420	17.00
49	11.29	0.18	35.12	1098.58	0.5629	40.97	99	11.45	0.19	35.15	1098.88	0.5904	35.16
50	12.06	0.26	35.05	1098.63	0.6839	20.75	100	12.06	0.26	35.05	1098.63	0.6839	20.75

List of Publications and Presentations

Kurra, S., & Regalla, S. P. (2014). Experimental and numerical studies on formability of extra-deep drawing steel in incremental sheet metal forming. Journal of Materials Research and Technology, 3(2), 158-171.

Kurra, S., Bagade, S. D., & Regalla, S. P. (2014). Deformation Behavior of Extra Deep Drawing Steel in Single Point Incremental Forming. Materials and Manufacturing Processes, (In Press).

Kurra, S., Nasih, H.R., Regalla, S.P., Gupta, A.K. (2015). Parametric study and multi-objective optimization in single-point incremental forming of extra deep drawing steel sheets. Proceedings of the Institution of Mechanical Engineers, Part B: Journal of Engineering Manufacture, (In Press)

Kurra, S., Nasih, H.R., Regalla, S.P., Gupta, A.K. (2015). Modeling and optimization of surface roughness in single point incremental forming process.Journal of Materials Research and Technology, (In Press)

Kurra, S., & Regalla, S. P. (2015). Multi-objective optimization of single point incremental sheet forming using Taguchi based grey relational analysis.Int. J. Materials Engineering Innovation, (in Press).

Kurra, S., & Regalla, S. P. (2012). Simulation of forces and strains in single point incremental forming process.Int. Journal of Machining and forming technologies, 6(2), 79-98.

Suresh, K., Khan, A., & Regalla, S. P. (2013). Tool Path Definition for Numerical Simulation of Single Point Incremental Forming. Procedia Engineering, 64, 536-545.

Surech, K., & Regalla, S. P. (2014). Effect of Time Scaling and Mass Scaling in Numerical Simulation of Incremental Forming. Applied Mechanics and Materials,612,105-110).

Suresh, K., & Regalla, S. P. (2014). Analysis of Formability in Single Point Incremental Forming Using Finite Element Simulations. Procedia Materials Science, 6, 430-435.

Suresh, K., & Regalla, S. P. (2014). Effect of Mesh Parameters in Finite Element Simulation of Single Point Incremental Sheet Forming Process.Procedia Materials Science, 6, 376-382.

Suresh, K., & Regalla, S. P. (2014). Formability of extra deep drawn steel in single point incremental forming.AIP Conference Proceedings 1567 (1), 856-859.

Suresh, K., Regalla, S.P., Anudeep A.V.V.N., Suri S.S.M. (2012). Effect of Tool path on Thinning In Negative Incremental Forming Process. 4th International and 24th AIMTDR Conference, Jadavpur University, Kolkata, Dec 14-16, 2012

Suresh, K., & Regalla, S. P. (2012). Modeling and Simulation of Asymmetric Incremental Sheet Metal Forming: A Review. Proceedings of the International Conference on Materials Processing and Characterization, March 8-10, 2012, GRIET, Hyderabad, India, pp. 25-30

Suresh, K., & Regalla, S. P., Rogelio Pérez-Santiago. (2014). Study on Influence of Process parameters in Incremental Forming using Finite Element Simulations and Taguhi Orthogonal Arrays. Advances in Materials & Processing Technology Conference, Nov. 17-20, 2014, Dubai, United Arab Emirates.

Suresh, K., & Regalla, S. P. (2015). Digital fabrication in sheet metal forming : Incremental forming. International symposium on digital fabrication, March. 2-3, 2015, IIT Hyderabad, Hyderabad.

Brief Biography of the Candidate

Suresh Kurra is a lecturer at Birla Institute of Technology and Science Pilani, Hyderabad Campus, India. He obtained his Master degree in Production engineering from the Indian Institute of Technology Delhi, India, in 2005. He worked on wear modeling of ceramic tools in hardturing in his masters project. His major research interests are incremental forming, modeling and optimization of manufacturing processes and finite element studies in manufacturing.

Brief Biography of the Supervisor

Dr. Srinivasa Prakash Regalla obtained his PhD in 1998 on *Evaluation of Boundary Friction under Sub-surface Plastic Deformation for Metal Forming Processes* from IIT Delhi. He obtained his M.Tech. in 1992 with specialization of Manufacturing science/Mechanical Engineering from IIT Kanpur, where he carried out his thesis work on finite element analysis of steady state cold rolling of strain hardening material. He obtained his B.Tech. in 1990 in Mechanical Engineering from Kakatiya University, Warangal. He has 20 years of research experience, which includes 17 years of teaching and brief industrial experience. He worked in the Manufacturing Systems Integration Division (MSID) at the NIST, Gaithersburg, Maryland, USA in 1998 as a Guest Researcher, during which he carried out research in the engineering design technologies related to national advanced manufacturing test bed (NAMT). He authored around 50 research papers in reputed journals and conference proceedings and 2 textbooks on design and manufacturing. His current research interests are Sheet metal forming, 3D printing and additive manufacturing, medical device design and manufacturing, micro-forming, product design, MEMS, CAD/CAM, tribology.